Founded 1925

Incorporated
by Royal Charter 1961

To promote the advancement of radio, electronics and kindred subjects by the exchange of information in these branches of engineering

Volume 46 No. 4

April 1976

The Radio and Electronic Engineer

The Journal of the Institution of Electronic and Radio Engineers

THE GOLDEN JUBILEE CONVENTION

'Electronics in Society'

THIS summer the Institution's Convention in Cambridge will be a further event commemorating our fiftieth anniversary. The University of Cambridge has been the host to five previous IERE conventions or conferences since 1951 when the Television Engineering session of the Festival of Britain Convention was held at King's College and in the Cavendish Laboratory. These same parts of the University will be the main centres this year and as in 1951 a Clerk Maxwell Memorial Lecture will be presented. Five of the nine Lectures will then have been given in the Laboratory founded by Maxwell and in the lecture theatre now bearing his name, which is particularly appropriate because of his place in science as the propounder of the theory on which modern radio engineering has been based. Dr. H. B. G. Casimir's work as a solid-state physicist and as head of the famous Philips Research Laboratory in Eindhoven will enable him to make a valuable contribution to the range of subjects initiated by Professor G. W. O. Howe twenty-five years ago.

But whilst it is proper that in discussing a Convention to mark an historical anniversary we should look back over the years, by far the major part of the programme will deal very much with the present and, indeed, with the future. The impact of the applications of electronics on society has of course always been a fact, albeit perhaps only half realized. One may instance the role played by the communications engineer ever since the inventions of the telegraph, of the telephone, of radio and of television, and consider how different all our lives today would have been without them. None of these applications is standing still, nor are such other developments as the computer, navigational aids, and industrial and medical electronics. Hence the twenty papers that are to be presented in the six main sessions will endeavour to get to the heart of the matter and spell out where, in the judgment of the authors, electronics is going and just what effect the work of the engineer will have on society. For we must recognize that it is the engineer who, in modern parlance, is the interface between the scientific research worker and the rest of mankind.

Two sessions may perhaps be cited from the programme on page 203 as typifying the importance of looking at what the electronic engineer can do today—Cognitive Science and Signal Processing, and Medical Electronics, and papers in these sessions reveal fascinating possibilities for the future. These and the other sessions are primarily looking at things very much from the engineer's point of view. An innovation for an IERE convention is that keynote addresses will be given by speakers who are able to discuss the problems and possibilities of electronics in its relationship to society from a wide vantage point. Taken together, these two approaches should stimulate well-informed discussion.

Institution Conventions and Conferences have usually had a single fairly well defined theme and its relation to a particular member's interests has therefore been clear: some would feel it to be highly relevant, others would not. This Golden Jubilee Convention, however, has a wide ranging approach to the profession of electronic and radio engineering which must give it a universal relevance to *all* engineers. The broader view which it will give to those taking part will surely be of the utmost value in enabling them to relate their own branches of electronics *to* society.

Contributors to this issue

Mr. Peter W. Fry read chemistry at the University of Oxford and received the B.A. degree in 1961 and the M.A. and B.Sc. degrees in 1964. In 1963 he also received the H.N.C. in electrical engineering at Oxford College of Technology.

Mr. Fry then joined the Plessey Company at the Allen Clark Research Centre, Towcester, where he worked on new metallization techniques for silicon devices, and from 1965 undertook the first stages of the company's photodetector array work. In 1966, he transferred to the Research Laboratory of the Automation Group of Plessey at Poole, where he was responsible for the development of transducers and instrumentation techniques. Three years later he helped to found Integrated Photomatrix Ltd., where he is Technical Director responsible for circuit development.

Dr. M. Tomlinson graduated in electronic engineering from Birmingham University in 1967 and for the next three years was a research student at Loughborough University working on high speed data transmission over telephone lines. This culminated in the award of a Ph.D. and in 1975 he was appointed a Principal Engineer at Plessey Telecommunications Research at Taplow Court. Last year Dr. Tomlinson joined the Signals Research and Development Establishment at Christchurch (now the Royal Signals and Radar Establishment) as a Senior Scientific Officer.

He has published several papers in the fields of adaptive equalizers, f.s.k. shaping filter design, and digital filtering, and holds several patents in these and associated subjects. His current interests include multi-channel digital processing, maximum likelihood(m.a.p.)diversity reception, and computer aided telecommunication system design.

Mr. M. V. Bennett (Graduate 1976) began his career with International Computers and Tabulators Ltd., and studied electronic, radio and power engineering at Croydon and Wimbledon Colleges of Technology. Following completion of his apprenticeship with ICT in 1962 he joined the Research and Development Laboratories of ICT Engineering and worked on the development of ferrite core storage systems and magnetic character recognition. This was followed by two years with Louis Newmark Ltd., working on the design of helicopter flight control systems for pre-programmed flight and manoeuvre procedures. In 1965 Mr. Bennett joined Marconi-Elliott Avionics Ltd., Basildon Essex and he is now a senior principal engineer engaged on the design and development of advanced electro-optical systems for commercial and military applications.

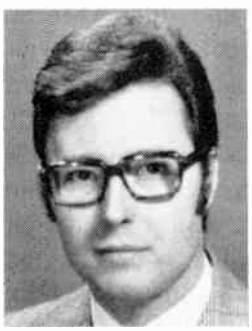

Dr. Renato De Mori gained a doctorate in electronic engineering from the Politecnico di Torino, Turin, where he has been an Associate Professor since 1971.

For several years he was involved in the design of specialized hardware for signal processing but recently his interests have been in speech data reduction, speech perception and recognition. The main results of his work in this field to date were presented in papers at the IFIP World Congress 1974, at the World Congress on Cybernetics 1975, and at the Joint International Conference on Artificial Intelligence at Tbilisi, USSR, in 1975.

Dr. De Mori was a lecturer at an Advanced Summer Institute on Pattern Recognition sponsored by Purdue University, Indiana, USA, in September 1975.

Dr. J. K. Stevenson (Member 1974) is a Lecturer in the Department of Electrical and Electronic Engineering at the Polytechnic of the South Bank, London. A graduate of the University of London, he obtained his doctorate following work at Queen Mary College and before going to his present appointment in 1973 he was with the General Electric Company, initially at the Hirst Research Centre and subsequently with Marconi Space and Defence Systems. His main research interests are in circuit theory and he has contributed several papers to the Institution's Journal on this subject over the past three years.

UDC 621.3.049.774: 621.383.51

Applications of self-scanned integrated photodiode arrays

P. W. FRY, M.A., B.Sc., M.Inst.P., C.Eng., M.I.E.E.*

SUMMARY

The development of self-scanned photodiode arrays is traced briefly, and a comparison made between their properties and those of the vidicon tube.

The theory of their operation is explained, showing how charge integration is used to obtain high responsivity, and the various scanning methods used to read out the signal from linear and two-dimensional arrays are described.

The optical and electrical characteristics of arrays are discussed, together with the main limiting factors affecting array performance. The main application areas are presented, first for linear and then for two-dimensional arrays. These areas include industrial gauging and inspection, optical character recognition, facsimile, guidance systems and television imaging.

*Integrated Photomatrix Ltd., The Grove Trading Estate, Dorchester, Dorset.

1 Introduction

The possibility of forming image sensors from arrays of silicon photodiodes on a single silicon chip has been recognized for many years, probably since the inception of integrated circuit technology some fifteen years ago. It was quickly apparent that the array size was limited, not by the number of diodes that could be included on the silicon, but by the number of output leads necessary to form connexions to these diodes. To circumvent this problem, it was necessary to scan the diodes, that is, to multiplex them in to a single output lead by means of switching circuitry on the same integrated chip. A second problem was that of detecting the minute photocurrents produced by the necessarily very small diodes. The technique of charge integration had been used in the Vidicon for some years, and it was pointed out by G. P. Weckler in 1965 that this technique could be used with photodiode arrays, the switching being achieved by m.o.s. transistors.[1] The one step necessary to complete the picture was now to include a shift register on an integrated circuit with the diodes and m.o.s.t.s to perform the serial multiplexing function. The first fully self-scanned arrays using this technique were announced in 1967.[2]

It may be asked what practical purpose was behind this field of development, since fairly adequate image scanners were already available in the form of vidicon tubes and the like. The answer lies in two properties of integrated circuit arrays, not shared by electron-scanned tubes, which were early recognized as fundamental characteristics of such arrays; first, their infra-red sensitivity which, combined with the possibility of light weight and freedom from 'burn out', gave promise for military surveillance systems; second, their lack of retention of previous images, which enabled completely new information to be read out at each scan of the array. This latter property was essential to the new application of optical character recognition being developed at the same period.[8] Since those early developments a further unique property of such arrays has been recognized and made use of; the high positional accuracy (better than 1 μm) of each diode, which makes gauging systems possible. The present status of development of these serially multiplexed arrays includes lines of diodes over 25 mm long, consisting of up to 1024 photodiodes and associated circuitry; and two-dimensional arrays up to 4096 (64 × 64) diodes.[3]

Theoretical studies indicate that two-dimensional arrays of up to two or three hundred diodes on a side can be made by this technique, whilst in the USA arrays of this complexity have already been demonstrated using the comparable technique of charge-coupling.[4]

2 The Operation of Self-scanned Photodiode Arrays

2.1 Light Integration

In a scanned array the silicon photodiode is operated in the light integration mode, whereby the self-capacitance of the diode is charged to a negative potential, thus reverse-biasing the photodiode, via an m.o.s. transistor acting as a switch. When this transistor is turned off the

photodiode capacitance sees an extremely high impedance, the decay of charge on it being determined by carriers produced by the incident light falling on the photodiode. Without any light falling on the diode, there is still a small rate of decay of charge due to the leakage current of the diode; this limits the minimum light level at which the technique may be used. Figure 1 shows this basic array element. The typical responsivity of the photodiode operated in the light integration mode is 25 V s^{-1} μW^{-1} cm^2, i.e. the bias decay would be 25 mV in an integration period of 1 ms for an incident light level of 1 $\mu W cm^2$ (tungsten filament at 2870 K). The charge loss associated with this voltage decay is proportional to the area of the diode, whose capacitance is typically 3 nF cm^{-2}.

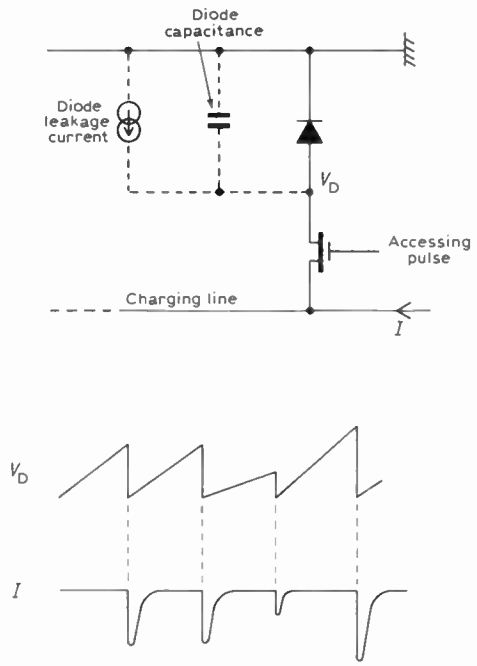

Fig. 1. Basic photodiode array element.

2.2 Linear Arrays

The point-to-point signal across an array consists of the amount of charge lost by each individual diode; this can be sampled either by restoring the initial condition and monitoring the quantity of charge required to do so (recharge sampling) or by looking at the actual level to which the voltage across each diode has decayed (voltage sampling). The time between samples is called the integration period.

The sequential switching process which is necessary for interrogating the diodes is universally achieved by the use of shift registers. A pulse appearing at one end of a shift register can be clocked through at high speed, opening and closing diode sampling switches as it goes.

Three elements of an array operating in the recharge sampling mode are shown in Fig. 2. A pulse passed through the shift register charges each diode to the reference voltage applied to the output line. After an interval equal to the integration time, another pulse goes through the register, the diode is again recharged to the

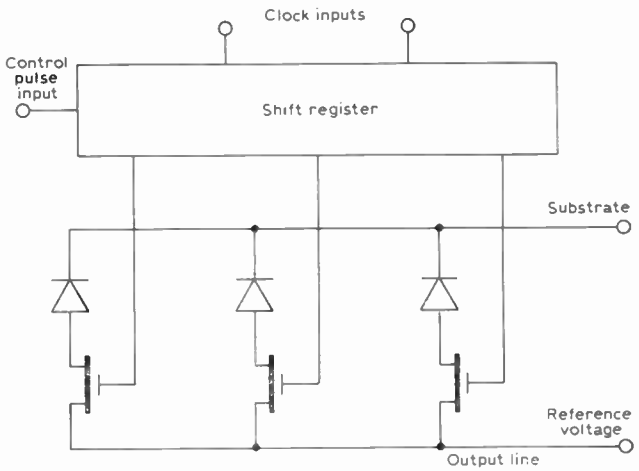

Fig. 2. Recharge-sampled array.

reference voltage, and the amount of charge required to reinstate the original voltage appears as a current pulse on the output line. Charge amplification, together with complex integration and sample-and-hold functions are necessary to produce the more familiar boxcar waveform output from the current pulse signal. The simplicity of the array structure employed in the recharge mode is offset by the extra complexity of signal processing necessary, but a bonus is gained in superior performance (particularly at high multiplexing rates (up to 5 MHz)) responsivity matching and signal/noise ratio as compared to the simpler voltage-sampling mode.

Figure 3 shows three elements of an array for voltage sampled operation. Each element now contains two extra m.o.s. transistors. A pulse propagated through the m.o.s. shift register appears sequentially at lines n, $n+1$, $n+2$, and the photodiode capacitances are charged to a negative potential. The diodes then begin to discharge at a rate dependent on the incident illuminance. After one integration period, a pulse reappears at line n. At this point it turns on m.o.s. switch TR3 and allows current to flow through TR2, TR3 and the external load resistor. The magnitude of this current is controlled by the voltage on the gate of the amplifying transistor TR2, this voltage being dependent on the degree of discharge of the photodiode. Having sampled the voltage on the diode, the pulse moves on to $n+1$ where it recharges diode n as before and at the same time samples the voltage on diode $n+1$.

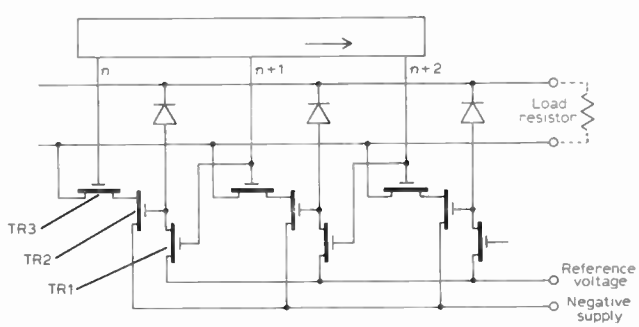

Fig. 3. Voltage-sampled array.

This scanning method involves the minimum of external circuitry and is very suitable for looking at high contrast images at moderate (up to 1 MHz) scanning rates. This includes the majority of industrial applications involving the detection of flaws or edges.

Linear self-scanned arrays are available in lengths from 16 diodes on 0·01 mm (0·004 in) pitch to 1024 diodes on 0·025 mm (0·001 in) pitch.

2.3 Two-dimensional Arrays

The recharge-sampling method described above has also been extended to two dimensional arrays by various switching schemes. Those currently in use are shown in Fig. 4. In Fig. 4(a), the two m.o.s.t.s operate together so that TR1 conducts only when both X and Y scanning signals are present. In Fig. 4(b) charge from a complete line of diodes is first distributed on to the column lines, which are then scanned as if they were a line-array. The latter scheme has the advantage of using only one m.o.s.t. per photodiode, together with no contact between silicon and metallization compared with two in the former case. This in turn leads to a smaller array element size (60–75 μm) and more efficient utilization of photosensitive area.[9] The layout of an element of this array is shown in Fig. 5.

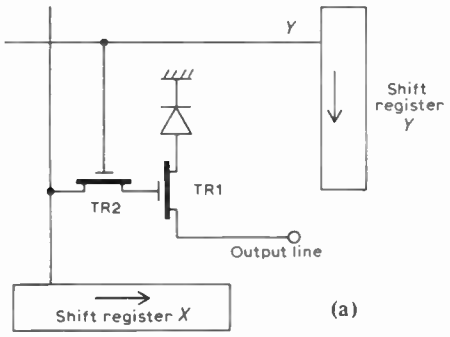

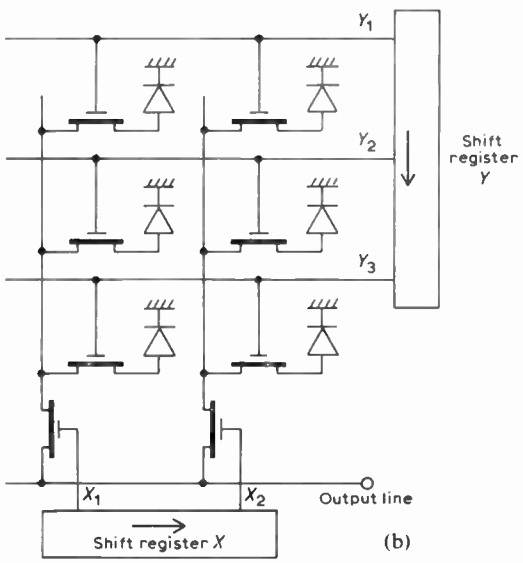

Fig. 4. Methods of diode access in 2-dimensional arrays.

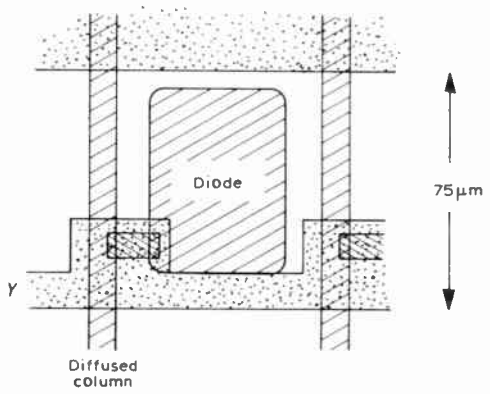

Fig. 5. Layout of element shown in Fig. 4(b).

This small, simple, high-yield structure has been achieved only at the expense of speed limitations inherent in the diffused column. The method which has been developed to overcome this is illustrated in Fig. 6, and operates as follows.

As soon as a line scan is complete, the column shift register is clocked, and switches a new line of diodes on to their column lines, which at this point in time are fully charged to a potential V_R. A period now elapses before the line scan is recommenced, during which the F signal switches on m.o.s.t.s connecting each column to each capacitor C. This period may be termed the 'line-flyback' period since it occurs between each line-scan. It is made sufficiently long (a few microseconds) to ensure that the charge loss on the diode is distributed between the diode capacitance, the column line capacitance, and capacitor C. At the end of this fly-back period, signal F turns off the m.o.s.t.s, isolating capacitors C from the column lines and diodes. The line scan now occurs, sampling the charge losses on capacitors C, which are in proportion to the original diode charge-losses. By making C roughly equal to the column line capacitance, about half the original signal is held on C;

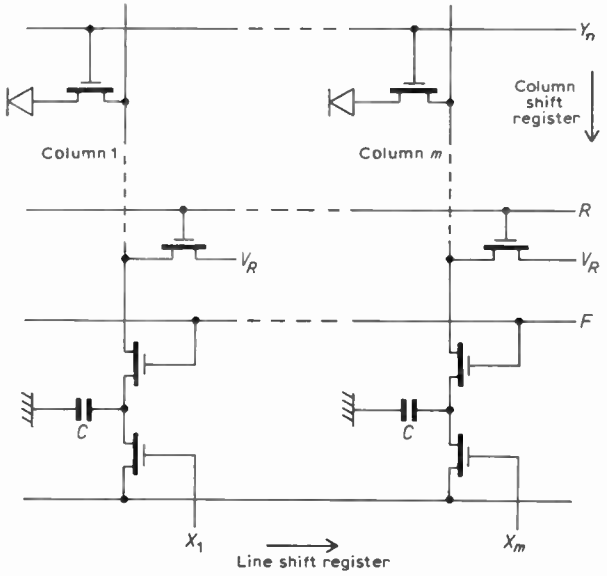

Fig. 6. Circuit of 2-dimensional array scanning method.

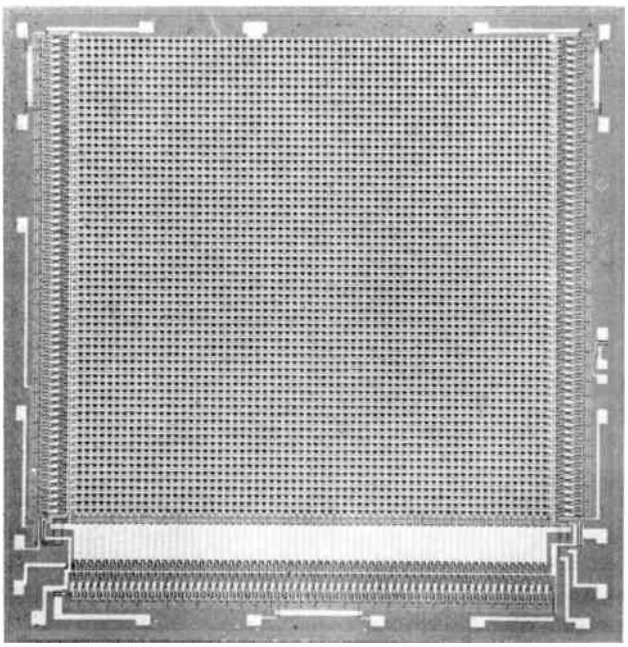

Fig. 7. A 64 × 64 scanned array.

this is thought to be about the optimum proportion. Whilst the line scan proceeds, signal R causes the column lines and diodes to be recharged to V_R, so that when the column shift register finally isolates the diodes they commence integrating the light, whilst the column lines are charged to V_R, ready for the next flyback period.

Using the principles described, 64 × 64 scanned photodiode arrays are available with a pitch of 75 μm, giving a total array size of 4·8 mm square on a silicon chip 6·2 mm square. Around the array are spaced the shift registers and the output capacitors with their associated m.o.s. switches. A photograph of this array is shown in Fig. 7.

3 Characteristics of Photodiode Arrays

3.1 Geometry

Photolithography, as developed for integrated circuit technology, allows the fabrication of arrays that have element size and pitch small enough to be comparable with electron beam scanned tubes, yet accurately defined in space to limits better than ±1 μm. Diode pitches are in the range 0·025 mm (0·001 in) to 0·125 mm (0·005 in).

3.2 Dynamic Range

The operation of arrays in the charge storage mode allows a wide dynamic range in the same sense as that of ordinary photography, where a compensation for a low light level is obtained by increasing the exposure time. The analogy with photographic film is quite close, in that both sensors have a saturation level, a fog level, and give a specific signal for a specific exposure where that exposure can be arrived at by varying combinations of intensity and time.

The absolute limits of operation are set at high irradiance levels by the maximum multiplexing rate of the array, and at low irradiance by the rate of self-decay of diode charge. This is due to thermal leakage, or dark current. With a low-intensity image and increasing integration time, part of the observed video signal results from this leakage current until, in the limit, saturation level can be reached through dark current alone. Cooling the array below ambient can extend the dynamic range since leakage current falls by approximately a factor of two for every 8 degC drop in temperature.

Between the two extremes there is a linear operating range of three to six orders of magnitude, according to array length and diode size. For any fixed integration period the dynamic range is typically 100 : 1 in recharge sampling, governed by the ratio of noise level to saturation. Maximum multiplexing rates for currently available arrays are in the region of 4–10 MHz and maximum integration times range from 2–80 ms.

3.3 Responsivity

The output of an individual diode is either a voltage, or a charge in picocoulombs. The input power is customarily given as an irradiance in $\mu W\,cm^{-2}$ from a source of stated spectral distribution. Responsivities are therefore quoted in units of $Vs^{-1}\,\mu W^{-1}\,cm^2$ or $pCs^{-1}\,\mu W^{-1}\,cm^2$. Sometimes the latter is expressed in the equivalent form of $pA\,\mu W^{-1}\,cm^2$.

Calculation of the signal that will be obtained in any particular situation involves manipulating two parameters—integration time and irradiance level. If the diode responsivity is $R\,(pCs^{-1}\,\mu W^{-1}\,cm^2)$ and the integration time is T (s), an irradiance of $W\,(\mu W\,cm^{-2})$ will give a resultant signal charge of RWT (pC).

Manufacturer's data will give saturation charge along with R, from which the signal level can be estimated as a percentage of saturation. A similar calculation can be performed in the voltage sampling mode. In absolute terms, the video output signal at saturation is in the 1–10 V range or the 1–20 pC range.

The responsivity R is invariably quoted radiometrically for a tungsten lamp running at colour temperature of 2870 K. For this source, typical values of R vary from $10\,pCs^{-1}\,\mu W^{-1}\,cm^2$ for diodes on 0·1 mm pitch to $1\,pCs^{-1}\,\mu W^{-1}\,cm^2$ for diodes on 0·025 mm pitch. To deduce the responsivity to other sources or to obtain the equivalent photometric quantities has always proved a headache with spectrally selective detectors such as silicon, since it involves numerical integration using the source and detector spectral curves. Table 1 presents a selection of conversion factors for various common light sources when they are used with a typical silicon detector.

3.4 Noise Considerations

Photodiode arrays are subject to a number of noise sources not found in other forms of detector. These are generally grouped together under the heading 'fixed pattern noise' (f.p.n.), so called because it is stationary with respect to the array, and it arises from the discrete nature of the sensing elements and the sampling methods used to extract the video signal.

Each element of the array has associated with it several parameters which exhibit small deviations from

nominal value due to the variability of materials and processing. Since the functioning of integrated circuit devices is essentially geometry-dependent, photo-lithographic errors and mask misalignment are one source of variations. Additionally, device parameters are affected by any inhomogeneity of the monocrystalline silicon substrate material. The result of these small variations is twofold:

(i) There is a corresponding variation in the desired output signal (apparent responsivity fluctuations from diode to diode).

(ii) A random contribution is added to the switching transients which appear on the video output.

The effect of these sources of f.p.n. is to produce an output video waveform which exhibits a stationary noise structure even when the array is uniformly illuminated (or in the dark). Noise arising from switching spikes is signal independent, observable under dark conditions, and is typically $\pm 0{\cdot}5\%$ of the saturation level in recharge sampling or $\pm 3\%$ in voltage sampling. Noise arising from those sources which produce apparent responsivity variations is signal dependent and has typical values of $\pm 5\%$ of signal at 50% saturation. These two distinct forms of noise are commonly quoted separately in specifications.

Since f.p.n. is of constant form it is possible in principle to remove it by suitably processing the video output. Both additive and multiplicative variations may be cancelled using two digital store read-only memories programmed with pre-determined correction factors and clocked in synchronism with the array. At the expense of introducing extra complexity the memories may be programmed automatically from dark and light scans.

3.5 Low Light Level Operation

Thermal leakage current has already been mentioned as the limiting factor in determining the minimum irradiance at which arrays can operate. It is not fundamentally a noise mechanism since the primary effect is to progressively decrease the available signal swing—or video window—with increasing integration time. However, noise is associated with it: this arises from random variations in leakage current from diode to diode.

The minimum irradiance depends on the signal/dark current ratio that can be tolerated. The signal charge has previously been given as:

$$RWT \text{ (pC)}.$$

The dark current equivalent charge is:

$$I_d T \text{ (pC)}.$$

The signal/leakage ratio is therefore:

$$RW/I_d$$

which is independent of integration time. Taking typical values:

$$I_d = 35 \text{ pA}$$
$$R = 10 \text{ pA } \mu\text{W}^{-1} \text{ cm}^2.$$

For a signal/leakage ratio of 1:

$$W = I_d/R = 3{\cdot}5 \ \mu\text{W cm}^{-2}.$$

This figure is often termed the dark-current equivalent power. Cooling the array from an ambient of 22°C to −5°C would reduce this figure to about $0{\cdot}35 \ \mu\text{W cm}^{-2}$.

Table 1. Spectral conversion factors for silicon detectors

Source	A Watts Conversion Factors	B Lumens Conversion Factors
2500K tungsten	0·7	0·10
2870K tungsten	1	0·05
3200K tungsten	1·3	0·038
Sunlight	1·7	0·019
Overcast daylight	1·6	0·017
White fluorescent tube	2·4	0·007
Low pressure sodium	3	0·0057
High intensity neon	3	0·025
GaAs/P solid state lamp	3·1	0·034
GaAs solid state lamp	3·2	∞
Helium-neon laser	3·1	0·019

To obtain equivalent watts of 2870K tungsten multiply source watts by column A factor or source lumens by column B factor.

3.6 Spectral Response

Photo-diode arrays have a spectral response broadly similar to other silicon photo-detectors (Fig. 8), covering a useful range in the visible and near infra-red.

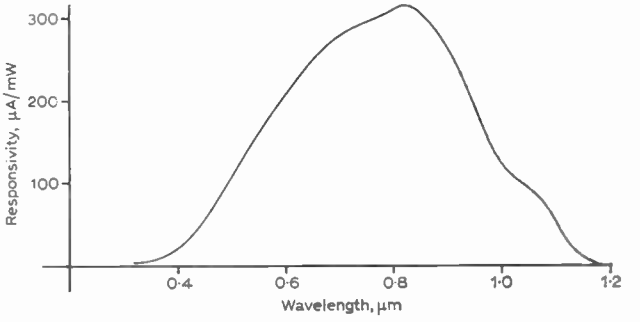

Fig. 8. Typical silicon photodiode spectral response.

3.7 Image Quality

The video output obtained from a self-scanned array is the result of a spatial sampling process in which, for a stationary optical image, each diode delivers a signal proportional to the integrated irradiance over the diode area.

Sampling theory indicates that the maximum spatial frequency unambiguously detectable by an array is one half the frequency corresponding to the reciprocal diode pitch, e.g. 5 cycles mm^{-1} for a 0·1 mm pitch.

The presence of higher spatial frequencies will cause spurious modulation to appear in the output sampled intensity distribution: a phenomenon known as 'aliasing'.

Apart from the limitations imposed by sampling, there is one additional source of image blur contributed by the array which is known as 'crosstalk'. This is an effect

resulting from residual photo-sensitivity outside the normal diode area and manifests itself as an apparent sideways signal 'leakage'. If, for example, an intensity step function is imaged on the array to fall between two diodes, there will be a small decrease in signal amplitude on the first illuminated diode and a corresponding increase on the adjacent obscured diode. The effect is small (at about 5%) with diodes on 0·1 mm centres but increases in magnitude with decreasing pitch.

4 Application of Linear Arrays

Applications for photodiode arrays can be broadly classified as: industrial dimension gauging and flaw detection; optical character recognition; facsimile; aerospace guidance systems; and imaging for television, surveillance etc.

The advantages of the broad silicon spectral response are evident in the wide range of radiation sources with which it may be coupled. In industrial applications the infra-red response of silicon arrays will often permit imaging using the self-radiation of hot bodies such as steel or glass in situations where the provision of external illumination is an inconvenience. The lowest temperatures that will produce useful signals are in the region of 600°C–700°C. Large aperture refracting optical systems are often used for image formation, and it is important in such cases to check that their aberration correction is adequately maintained in the near infra-red.

4.1 Dimensional Gauging

The monitoring of mechanical dimensions constitutes, perhaps, the most diverse range of applications of linear arrays in industry. Provided that an optical image of the required dimension can be obtained suitably scaled in size to the array, a fast non-contacting measuring system is readily achieved. Thus, any part which can be optically imaged on to an array can be gauged by this technique, either as an on-line monitoring function, as in the case of steel, glass, etc., or as a piece-part inspection facility

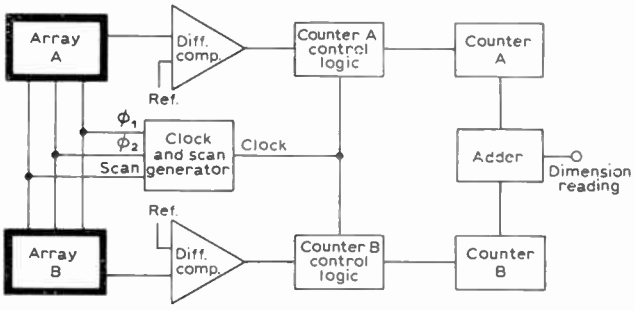

Fig. 9. Block diagram of steel rod measurement head.

where the parts are fed by a mechanical handling system through the gauging head and then sorted according to measured size.

Inspection systems utilizing photodiode arrays generally involve customer engineering and this makes such specialized systems relatively expensive, the final cost depending upon the length of array or arrays employed and the total complexity of the system. The use of such a system must be economically viable, and the application of self-scanned arrays in the field of dimension monitoring becomes justifiable in cases where a high degree of inspection reliability is involved, e.g. mass-produced items such as certain automotive parts, or products where the cost of scrap or material processing is relatively high.

Complex gauging systems have been developed in which a small process computer has been employed. One example of this type of system is a hot steel rod gauging system employing several separate optical heads at different locations in the mill, each feeding measurement data to the process computer for analysis and recording. Figure 9 shows the block diagram of the basic measurement head and Fig. 10 shows one such measurement head where the two arrays can clearly be seen. The essence of the technique is to digitally count the total number of diodes obscured on the two arrays.[10]

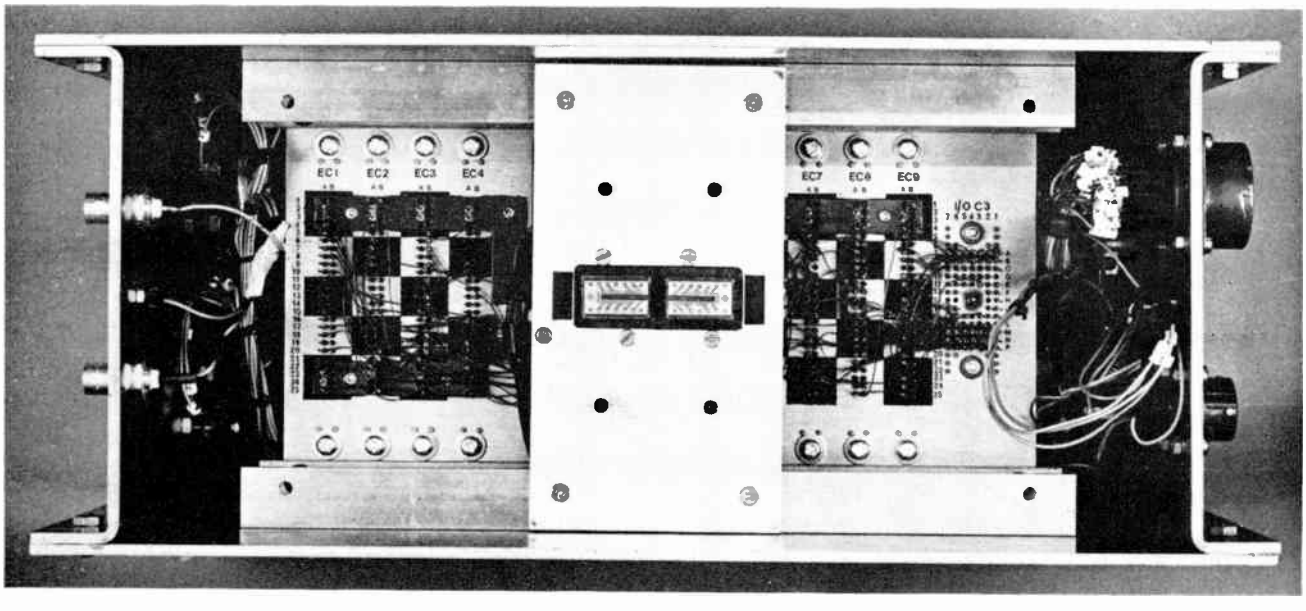

Fig. 10. Photograph of steel rod measurement head.

Another similar example is the use of two separate line-scan cameras for monitoring railway track gauge. In this case the edge of the track is illuminated by a high intensity light source and the worn surface of the rail produces an optical contrast against the remainder of the rail, suitable for imaging on to a photodiode array. Again, the total number of diodes obscured is digitally counted and the date fed to the computer to analyse and record variations in track gauge.

Particular advantages of self-scanned arrays in the above type of gauging system are: non-contacting measurement, high accuracy and repeatability, digital signal processing, on-line capability and fast response time. An additional advantage in the case of such width measurement systems is that lateral movement does not produce any measurement errors, as the total number of diodes obscured does not vary with lateral motion until the optical edge reaches the end of the array. In fact where a computer is employed the lateral movement of the object may be used to advantage to increase the accuracy or resolution of measurement. This is achieved by taking a large number of readings which, due to the fluctuation of the object, will have a statistical spread. The readings are integrated by the computer to give an increase in measurement accuracy dependent on the total number of readings analysed. The technique has been successfully used to improve accuracy by a factor of 100 over the basic optical accuracy.

Another method of increasing the resolution of such a measurement system, which has been demonstrated to give an inherent resolution of better than one-tenth of a diode pitch, involves the use of special analogue processing circuitry to find the 'centre of gravity' of the imaged edge. This technique makes use of the information present in the analogue output levels of diodes in the region of the edge.[6]

Dimension gauging techniques are widely used in on-line monitoring of hot glass, colour printing registration using reference marks and hole area measurement. There are clearly many other potential applications in on-line measurement and gauging and automatic sorting of piece-parts.

4.2 Flaw Detection and Industrial Inspection

Flaw detection is a problem in many manufacturing industries, particularly where a high volume of piece-parts is involved or where material is produced in a continuous strip at a high rate. In both cases the use of self-scanned linear arrays for automatic inspection offers obvious advantages. Figure 11 illustrates the basic system required for on-line detection of flaws, e.g. pinholes, in such materials as emulsion-coated tape or film. In this case, the material is illuminated from below so that pinhole flaws will have a high transmission of light giving a high contrast against the emulsion coating. On many other materials such as sheet metal, it is necessary to use a reflexion system in order to detect surface blemishes.

Consider an example of film which is coated with an emulsion as a 50 cm wide web prior to further expensive processing. It is necessary to identify sections of the web which contain flaws as small as 1 mm, and this may be achieved using an array camera system as illustrated in Fig. 12. The array length required to resolve small pinholes is not as great as would first seem apparent. This is due to the high transmission of light through even a tiny flaw and also to the fact that it is not important accurately to locate the position of such flaws but merely to identify the zones of the web in which flaws occur. In order to detect flaws down to 1 mm diameter across the 50 cm wide web, a camera employing an array of 100 photodiodes is adequate. The lens used is a 16 mm cine lens $f/1{\cdot}9$ of 25 mm focal length and, to give the correct magnification and resolution, the camera is located 120 cm above the web. To discriminate flaws the video output is connected to a voltage comparator.

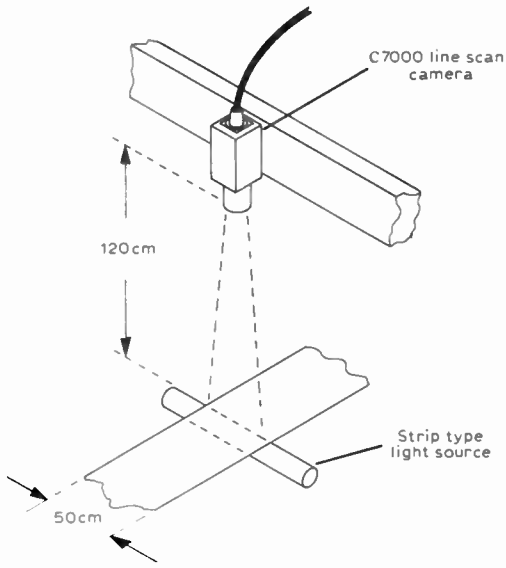

Fig. 11. Basic flaw-detection system.

The clock pulses and the start-of-scan pulse are utilized to identify the location of flaws in zones across the web by means of simple logic. Footage information is produced from a separate sensor which may be a pick-off from the mechanical drive. The output of the logic can conveniently drive a printer to give a print-out of the location of flaws in terms of zones and footage, thus permitting sections with flaws to be removed prior to any further processing. Another useful technique in flaw detection of separate items is to scan simultaneously two items, nominally identical, with separate cameras and to compare electronically the video output. If a flaw appears on one of the items then a difference signal will result.

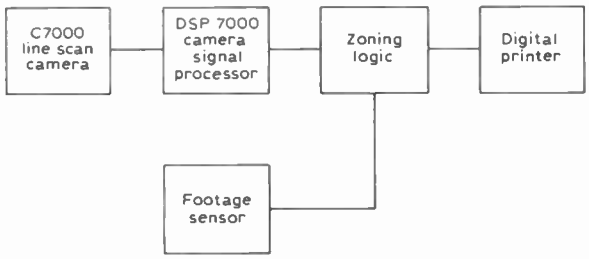

Fig. 12. Camera system for detecting flaws in emulsion-coated film.

Assuming that the position of flaws is random then the probability of getting two items with identical flaws is remote. If the manufacturing process is such that there is a likelihood of repetitive flaws occurring, then a master item having no flaws must be used for the comparison. In each case, of course, the alignment of the two cameras must be precise. This technique is currently being used for the detection of flaws in banknotes, and can also be employed for the automatic inspection of items such as plastic or rubber mouldings where the quantities involved are very large and the use of visual inspection techniques would otherwise necessitate the employment of many trained operators.

4.3 Optical Character Recognition

O.c.r. is a field where the highest scan rates are required and it provided one of the earliest spurs to the development of self-scanned arrays. In principle it is a straightforward application of linear arrays to the reading of printed characters moving at high velocity. A slightly unorthodox scanning technique is coming into use to obtain maximum multiplexing rates, in which the array is accessed in blocks which are scanned in parallel. For example, a single 256-element array is divided electrically into four separate segments so that it operates as four 64-element arrays placed end-to-end but driven in parallel. The scrambled video signal is correctly sequenced in the subsequent processing so that the output of the four sections scanned at 5 MHz is equivalent to a single 256-element line scanned at 20 MHz. The use of linear arrays in this application presupposes that the characters being read are scanned mechanically, at a fairly uniform rate, past the reading head. In cases where this is not possible a two-dimensional array becomes essential.

4.4 Facsimile

Facsimile is an application requiring many more picture-lines than o.c.r. but a much lower operating rate, limited by the data transmission capacity of telephone lines. In general, only two grey levels need to be transmitted, but these may be close together if the original document is faint. The use of arrays in facsimile scanning is in an early stage and has become practical with the advent of 1024 element sensors. A problem which is common to o.c.r. and facsimile applications, and indeed to certain inspection systems as well, is posed by the infra-red transparency of many of the printing inks, ball-point and felt-tip pens in everyday use. The preponderance of infra-red over visible response of a silicon array causes contrast to be lost, and even causes images to disappear in extreme cases. The infra-red response of the array must be largely removed, for instance by means of a filter if tungsten light is used, or else by the use of a lamp with low infra-red output. For the best facsimile reproduction a close match to a photopic eye response is required. This can be achieved by filtering, at the expense of a ten-fold reduction in response to normal tungsten light (2870 K).

4.5 Satellite Attitude Monitors

Several linear array systems have been designed for attitude measurement in satellites; a 100-diode array is, for example, presently in orbit on *Miranda*, (X4), supplying information on the distribution of sunlight reflexion (albedo) from the earth, and on the satellite angular position as measured by horizon and 'terminator' observations.[5] Further arrays for sun-angle measurement are planned for *UK6*.

The 'centre of gravity' computing system, described under Section 4.1, was in fact developed for use in fine resolution sun-angle measurement in a satellite sensor.[6]

5 Applications of Two-dimensional Arrays

Although a two-dimensional array is in many respects similar to a vidicon or other camera tube, its chief applications lie in areas where its properties differ from those of the latter. As we noted earlier, these properties are:

(i) Compactness of both imager and drive circuitry (no e.h.t. supply).

(ii) High positional accuracy and stability.

(iii) No image retention.

(iv) No burn-out; indefinite life.

(v) Infra-red sensitivity.

5.1 Area Gauging

Electronic processing of two-dimensional images of objects such as small piece-parts or machined holes can yield information about the dimensions and area of such objects. In its simplest form this processing involves a count of obscured (or exposed) diodes over the complete field within which the object lies. More sophisticated processing can determine all the major dimensions of an image if certain assumptions about its shape can be made. The image itself could in principle be detected by a linear array, past which the image is swept by either a rotating mirror or by movement of the object itself. Such methods introduce their own scale inaccuracies and non-linearities, however, which can be removed by the use of a two-dimensional array.

In the leather industry, for instance, it is necessary to assess the areas of individual irregularly-shaped pieces of leather for valuation purposes, and also to assess how many shapes of a particular type can be obtained from each piece. These assessments have to be done on a large scale, and automatic inspection of the leather is therefore employed, using a two-dimensional array built into a 'camera' unit. For simple area measurement the number of obscured diodes is counted in a digital counter; this count is then either used directly or multiplied, by a factor dependent on the optical system used, in a calculator circuit to give the area in terms of a chosen unit.

More extensive processing of the signal is required to assess the number of standard shapes obtainable from a piece, and signal processing of this type normally involves the use of a computer, with appropriate interfacing between it and the video output of the array.

5.2 Flaw Detection

The use of two-dimensional, as opposed to linear, arrays in gauging and flaw detection systems extends

their capability to cases where movement of the image across the array is either non-existent or irregular.

Large numbers of small holes in the perimeter of a turbine wheel casting have to be inspected for size and for freedom from flaws or dirt. On a manual basis this is a long and laborious task, which becomes fast and simple when a camera containing a two-dimensional array is set up to examine the holes as they pass, whilst the wheel is rotated by hand.

Float glass, as manufactured, contains random flaws which must be eliminated when the manufactured sheets are cut to size against specific customer orders. The output from a two-dimensional array provides information from which a computer can calculate the most economical cutting schedule to fulfil current orders.

Inspection of the bases of milk and beer bottles after washing, to detect remaining dirt, cannot readily be done with a linear array owing to the necessity of ignoring the area surrounding the disk-shaped area being examined. A two-dimensional array is therefore used, the output being taken as valid only when a bottle reaches a specific point on a conveyor directly over the array and optical system. To complete the system, a read-only memory defines which diode outputs are to be ignored to transform the square area observed by the basic array to a circular effective area. This system is illustrated in Fig. 13. An alternative system uses a specially-designed array with a circular sensitive area.

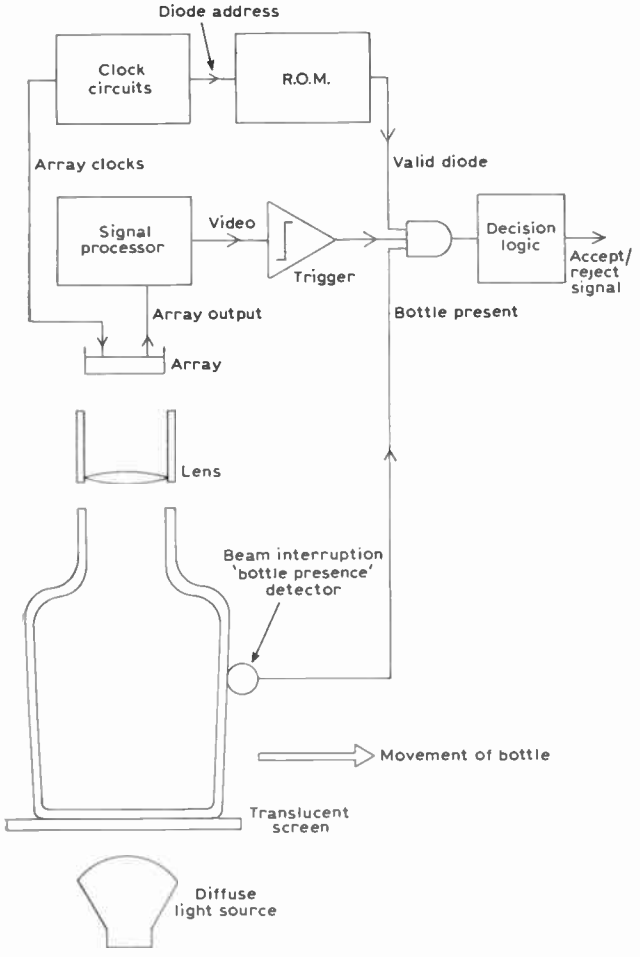

Fig. 13. Bottle-base inspection system.

5.3 Pattern and Character Recognition

There are many fields of pattern recognition where the image cannot easily be scanned past the reading head in any regular manner; two-dimensional arrays are then used. Examples are: the automatic recognition of blood cells in medical screening, where large numbers of skilled personnel are otherwise required to carry out the microscopic examination of thousands of blood smears; the recognition of pieceparts in an automatic assembly operation, routing them according to a program defined by computer control; and character recognition of 'point-of-sale' information on tickets affixed to supermarket goods, using a hand-held 'wand' to scan the ticket.

This last application, which is being introduced into supermarket chains to both automate the check-out or 'point-of-sale' and to enable simultaneous stock control, promises to be a major market for small two-dimensional arrays in the future. The goods themselves, when packaged, are coded with a label showing, in a code at once recognizable by automatic character recognition and the human eye, the type of goods and the weight. At the check-out, the operator passes a hand-held 'wand' over the label. This 'wand' contains an illumination source, a fibre-optic or standard optical system, and a photodetector array of around 14×40 elements. The code is read by the wand, and passed to a central computer which 'looks-up' the cost of the item per unit weight, calculates its price, adds up the customer's bill which is presented at the cash desk, and adjusts stock level records.[11]

5.4 Guidance Systems

A two-dimensional array has the advantage over the more common four-quadrant detector used in guidance systems, in that it supplies accurate positional information of a light-emitting or illuminated target in off-axis as well as on-axis positions. More precise control of corrective action is therefore possible. Besides their use in defence systems, space guidance applications have been proposed in which a rocket or satellite is stabilized in two dimensions at any chosen angle to the Sun, Moon, or Earth horizon.

The 'centre-of-gravity' calculation mentioned in Section 4.1 is also applicable to two-dimensional operation and can extend the positional resolution and accuracy of arrays by more than a factor 10 in each dimension.

In this method, the classical centre-of-gravity formula

$$\bar{X} = \frac{\sum_x (X \sum_y I)}{\sum_x (\sum_y I)}; \qquad \bar{Y} = \frac{\sum_y (Y \sum_x I)}{\sum_y (\sum_x I)}$$

is calculated, where I is the output level derived from a diode at position X, Y. The summation is normally carried out only over a limited portion of the array around a region of high illumination. This minimizes the effect of fixed-pattern and random noise on the calculation by eliminating areas of negligible signal level.

The calculations shown above can, in fact, be performed using a combination of two arrays with cylindrical optics at right angles to each other, but the summations $\sum_y I$ and $\sum_x I$, which are then done by blurring the image at right angles to each array, must of necessity then include the whole row or column.

5.5 Television Imaging

Imaging, with the resolution currently achieved by vidicons, plumbicons etc. has long been the dream of the array researcher. The obvious appeal of market volume (if low prices can be achieved) is backed up by the expected improvement in longevity. Of particular interest to colour camera manufacturers is the promise of an imaging system with faultless dimensional stability and a greatly enhanced responsivity stability over present systems. The long hours spent at present trimming the balance and registration of colour images will certainly be a thing of the past when such arrays are achieved in production quantity.

In the meantime, however, the dimensional stability, reliability and long life of silicon imagers offset their limited resolution for such applications as industrial surveillance ('burglar alarms'), whilst the infra-red sensitivity enables invisible infra-red floodlighting to be used in military surveillance schemes. The ruggedness and light weight achievable with solid-state arrays, with their simple, low voltage supply requirements, are of value in portable equipment of this type.

5.6 Blind Aids

One particularly interesting application which has been developed over a long period at Stanford University, California, is closely allied to facsimile and o.c.r. A small two-dimensional array (24 × 6) in a portable imager is moved by hand, by the blind user, over any normal printed script. The image picked up, consisting of a letter or so at a time, is translated point-by-point to an array of piezoelectrically vibrated pins. By touching the array of pins the user perceives a tactile image identical to the visual one seen by the array. With practice, these tactile images can be readily recognized.[7]

6 Conclusions

The linear scanned photodiode array has, since its introduction five years ago, found use in many fields of imaging where dimensional stability, compactness, ease of use or high speed are required. The newly available two-dimensional systems show promise of extending their use into similar fields, and also into areas previously the preserve of the vacuum-tube imager.

References

1. Weckler, G. P., 'Operation of p–n junction photodetectors in a photon flux integrating mode', *IEEE J. Solid State Circuits*, SC-2, No. 3, pp. 65–73, September 1967.
2. Noble, P. J. W., 'Development and potential of optoelectronic techniques', *Component Technology*, 2, No. 8, pp. 23–8, December 1967.
3. Integrated Photomatrix Ltd. Information sheets Nos. PX148 and PX146, October 1974.
4. Rodgers, R. L., 'Charge-coupled imager for 525-line television', IEEE Intercon Digest, 1974.
5. 'Miranda—X4, In-orbit Performance Assessment Report', Hawker Siddeley Dynamics, Stevenage, 1974.
6. 'Techniques for using Analogue Information in Photodiode Array Sensors', Ministry of Defence Contract No. K/GW 31a/100. Final Report 1974.
7. Brugler, J. S., Meindl, J. D., Plummer, J. D., Salsbury, P. S. and Young, W. T., 'Integrated electronics for a reading aid for the blind', *IEEE J. Solid State Circuits*, SC-4, No. 6, pp. 304–12, December 1969.
8. Bell, H. A., 'Survey: optical character recognition', *Systems Technology*, 2, No. 2, pp. 32–7, 1967.
9. Fry, P. W., 'A self-scanned 64 × 64 photodiode array'. Proc. Second European Electro-Optics Markets and Technology Conference, Montreux, pp. 295–301. (International Publishing Corporation, London 1974).
10. Antonsson, L., Malmgren, N., Redlund, G. and Ringborg, B., 'A new system for on-line gauge control in rod and bar mills', *Scandinavian J. Metallurgy*, 4, pp. 59–64, 1975.
11. 'British company readies photodiode array for mark reading and medical imaging', *Electronics*, 47, No. 5, p. 2E, 7th March 1974.

Manuscript first received by the Institution on 6th March 1975 and in revised form on 3rd July 1975. (Paper No. 1710/CC 245).

UDC 621.372.54/5:621.376.2/4:621.394.9

The specification and design of filters for amplitude and phase modulated data transmission systems

M. TOMLINSON, B.Sc., Ph.D., C.Eng., M.I.E.E.*

Based on a paper presented at the IERE Colloquium on Signal Processing in Communications Systems held in London on 29th October 1974.

SUMMARY

A baseband pre-envelope model is used to define the important performance parameters of amplitude, and phase modulation of digital transmission systems as far as the system's filters are concerned. Typical figures are given of these parameters and a filter specification is drawn up. Theoretical characteristics are derived which optimize the performance parameters and form target responses for practical filters. A simple example is given of this method. A low-pass prototype shaping filter and a phase equalizer is obtained which meets the typical specification.

* *Formerly with Plessey Telecommunications Research, Ltd., Taplow Court, Taplow, Maidenhead SL6 0ER; now at Royal Signals and Radar Establishment, Christchurch, Dorset BH23 4JB.*

1 Introduction

Since the aim of pulse transmission is to transmit and detect each pulse individually, it was first thought that the pulses had to be sufficiently short so that the tails of one pulse have completely decayed before the arrival of the next pulse. Apart from requiring a large bandwidth for a given data rate, this philosophy meant that the filters in the transmission system had to have as flat a frequency response as possible over the signal bandwidth and cut off as soon as possible outside this bandwidth so as to reject noise and interference. This led to the requirement that filters be only transparent to the signal and not to the noise; consequently filter specifications were in terms of passband ripple, stopband rejection and noise bandwidth.

Nyquist[1], from his study of sampling, was one of the first people to realize that the interference between pulses need only be restricted at one time-instant per pulse. He then proposed pulse shapes which were designed to overlap with oscillatory tails, yet could be sampled at one instant per pulse where there was no inter-symbol interference. The advantage of Nyquist's techniques over the previous methods was that much less bandwidth was required for the same data rate, thus paving the way for more efficient use of the available spectrum. Since Nyquist, many more pulse shapes have been published which have zero intersymbol interference culminating in the paper by Gibby and Smith[2] which gives the relationship between the magnitude and phase response of a waveform which has zero intersymbol interference. Since only one relationship has to be satisfied they were able to show that there are an infinite number of flat and shaped amplitude responses, and non-linear and linear phase responses which, taken together, have the property of defining a waveform with zero intersymbol interference.

With the increased congestion of the radio spectrum, the interference from other transmitters becomes a problem and the quantity of stray spectral energy radiated by a transmitter has to be controlled by bandlimiting at the transmitter. In addition, the quantity of spurious spectral energy received has to be controlled by bandlimiting at the receiver. The spectral interference at the transmitter has been termed the electromagnetic compatibility (e.m.c.), and the rejection of spurious transmissions at the receiver has been termed the adjacent channel rejection (a.c.r.). Both of these parameters are now of importance.

Following bandlimiting at the transmitter and receiver together with the Nyquist concept of detection by sampling, attention was turned towards organizing the transmitter and receiver spectral shaping so that the signal power at the sampling instant is as high a proportion of the transmitter power as is possible. When no other kinds of interference have been eliminated by bandlimiting, the interference that remains is the thermal, usually white, Gaussian noise which must be minimized at the sampling instant. The conflicting requirements of minimum noise power and maximum signal power lead to a requirement for the ratio of the two powers, i.e. the s.n.r., to be maximized at the sampling instant.

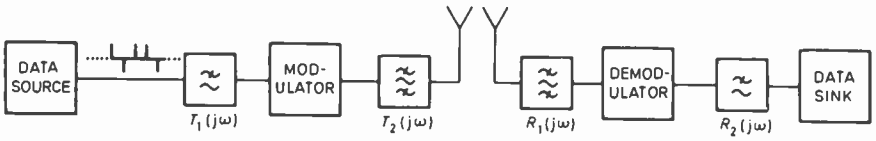

Fig. 1. Model of the frequency shaping in the communication system.

In this way, we are led to the present-day performance specification of several parameters which are controlled by the spectral shapes at transmitter and receiver. Since the spectral shaping is primarily done by the transmitter and receiver filters, these filters have to be designed so that the best possible practical performance of the digital system may be achieved.

2 Definition of System Model for the Different Modulation Methods

2.1 The Basic Pre-envelope Baseband Model

In order to optimize the performance of the digital system it is necessary to derive a model of the communication system which shows the primary components which affect the performance and yet leaves out the secondary components which only affect the performance in a small way. Although this could be termed a somewhat idealized and impracticable view of a system, it does enable targets to be formulated and comparisons to be made against ideal, though realizable, systems. Furthermore, many recently developed communication systems, such as satellite systems, have performances very close to the ideal theoretical limit.

A model of the frequency shaping in the system is shown in Fig. 1. All the bandpass filtering in the transmitter is considered as a single bandpass filter $T_2(j\omega)$ and all the low-pass filtering prior to modulation is lumped into the filter $T_1(j\omega)$. This is not far from the practical situation where, for design convenience, several noise or power limiting filters are deliberately designed with bandwidths several times that of the shaping filters so that they may be safely ignored. In this case the frequency shaping is effectively done by a single filter. It should be noted that the pulse shape of the data source usually affects the frequency response of the transmitter so that its pre-distortion effect on the spectrum is lumped into $T_1(j\omega)$; the data source is considered as a series of multi-level impulses as shown in Fig. 1.

When the significant bandwidth of a modulated signal is less than twice the carrier frequency, then it may be represented by its complex envelope known as the pre-envelope which is an equivalent baseband representation. Any bandpass signal (no matter how it is derived) may be represented mathematically as $i(t)\cos\omega_c t - q(t)\sin\omega_c t$, where ω_c is the carrier angular frequency and $i(t)$, $q(t)$ are usually called the in-phase and quadrature components of the modulating signal, respectively. Expanding trigonometrically:

$$\begin{aligned} i(t)\cos\omega_c t - q(t)\sin\omega_c t &= [i(t)+jq(t)]\tfrac{1}{2}\exp(j\omega_c t) + \\ &\quad + [i(t)-jq(t)]\tfrac{1}{2}\exp(-j\omega_c t) \\ &= \text{Real Part}\,[i(t)+jq(t)]\exp(j\omega_c t). \end{aligned}$$

The significant aspect of this expansion is that the bandpass signal is completely represented by the complex baseband signal $i(t)+jq(t)$ (the pre-envelope) and that furthermore, the operations of modulation and bandpass filtering may be determined from simple, equivalent baseband operations. If the Fourier transform of $i(t)\cos\omega_c t - q(t)\sin\omega_c t$ is $R(f)$, where the transform operation is represented by $\Rightarrow$, then:

$$R(f) \Rightarrow i(t)\cos\omega_c t - q(t)\sin\omega_c t$$

and

$$A(f) \Rightarrow i(t) \text{ and } B(f) \Rightarrow q(t)$$

then

$$R(f) = A(f-f_c) + jB(f-f_c) \text{ for positive } f.$$

Therefore, the equivalent baseband spectrum is merely obtained from the shifted bandpass spectrum.

An important implication is that all filters, whether bandpass or low pass, may be represented by their complex or real impulse responses respectively. The impulse response of two bandpass filters in cascade is given simply by the convolution of their respective impulse responses. For example, if the first filter has an impulse response $a(t)+jb(t)$ and the second filter has an impulse response $c(t)+jd(t)$, then the two in cascade have an impulse response:

$$\begin{aligned} &[a(t)+jb(t)] * [c(t)+jd(t)] \\ &\quad = [a(t)*c(t) - b(t)*d(t)] + j[b(t)*c(t) + a(t)*d(t)] \end{aligned}$$

where $*$ represents convolution.

The expression may be denoted $e(t)+jf(t)$ for brevity; it will be noticed that this has exactly the same form as either of the two filters. Thus, the whole system, whether phase or amplitude modulated, may be modelled at baseband: although this baseband signal is complex unlike practical signals.

The above is another way of stating that only the frequency-shifted positive frequency response needs to be taken into account when calculating the effects of the bandpass component parts of the system such as i.f. filters, modulated baseband signals, etc. Of course, both positive and negative frequency responses of the low-pass components are taken into account, as these are not frequency shifted but remain unchanged in the pre-envelope model. (Their impulse responses are purely real.)

2.2 System Model for Amplitude Modulation

In digital transmission via amplitude modulation the received signal is of the form

$$i(t)\cos\omega_c t - q(t)\sin\omega_c t$$

where the signals $i(t)$ and $q(t)$ take on discrete values at integral multiples of the data symbol period T, e.g.

$i(nT)$, $q(nT) = \pm 1$'s, the total number of complex values or levels per symbol is four and the transmitted data rate is $2/T$ bits/s. With the pre-envelope model the received signal is $i(t)+jq(t)$: the system model is shown in Fig. 2. The data source produces a complex stream of impulses $s(t)$ as shown. The modulator and demodulator together with bandpass and low-pass filters are lumped together as the complex frequency response $T(f)$ and $R(f)$. If $s(t) \Rightarrow S(f)$, then

$$S(f).T(f).R(f) \Rightarrow i(t)+jq(t).$$

If a system has ideal performance for four levels then it will have ideal performance for any number of levels, since the system is linear.

2.3 System Model for Phase Modulation

A phase modulated signal is represented by

$$A \cos(\omega_c t + \phi(t))$$

where $\phi(t)$ is the signal modulating the phase of the cosinusoidal signal $A \cos \omega_c t$. By trigonometry,

$$A \cos[\omega_c t + \phi(t)] = A \cos \phi(t) \cos \omega_c t - A \sin \phi(t) \sin \omega_c t$$

which is of the same form as

$$i(t) \cos \omega_c t - q(t) \sin \omega_c t.$$

In fact, if the phase $\phi(t)$ takes on four discrete values at integral multiples of symbol period T, then $i(t)$ and $q(t)$ take on one of two discrete levels each, as shown in Fig. 2. Thus the two systems are equivalent. There are some phase-modulation systems which may not be modelled by the filter model of Fig. 2, unless the responses $T(f)$ and $R(f)$ are allowed to be time varying. However, as these systems require more bandwidth, (the bandwidth of a time varying $T(f)$ is greater than that of a fixed $T(f)$), they are not likely to be employed in future systems. Thus the pre-envelope of Fig. 2 applies for phase modulation systems as well as amplitude modulation systems.

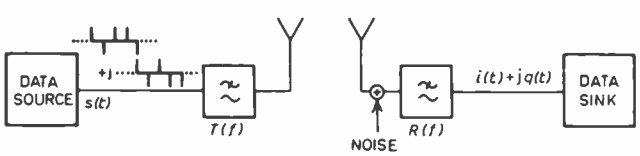

Fig. 2. Pre-envelope model of a four-level amplitude modulation system.

3 Definition of Performance Parameters

3.1 Introduction

When a random stream of data is transmitted through a communication system the performance is measured in terms of the average error rate, which is a function of the instantaneous ratio of signal power to Gaussian noise power at each sampling point, every symbol period. The distinction is made between the interference, which is deterministic, and the Gaussian noise which is, practically speaking, non-deterministic. Interference, such as intersymbol interference, is thought of as a reduction in the margin against the thermal Gaussian noise. In order to minimize the error rate, the interference from all sources must therefore be minimized and taken into account in the filter design. The following parameters describe the different forms of interference possible.

- i.s.i. interference between symbols
- a.c.r. interference received out of band from neighbouring frequency channels
- e.m.c. interference transmitted in-band from neighbouring transmitters
- c.c.i. co-channel interference which affects only certain kinds of amplitude modulation systems
- p.o.i. pulse overshoot interference, which is the intersymbol interference at time constants other than sample instants and is only of importance for systems which have sensitive timing recovery circuits.

Having accounted for the interference, the remaining parameter of interest is the s.n.r., which defines the proportion of signal power relative to the noise power (removing all interference) of the transmitted signal power which appears at the sampling point for each symbol.

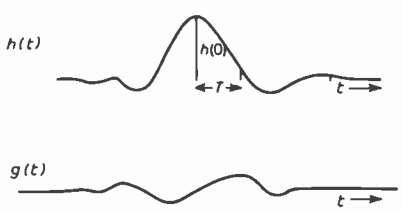

Fig. 3. A typical impulse response of the amplitude modulation model.

3.2 Definition of Interference Parameters

It has already been shown that all the modulation methods may be described using only the pre-envelope model shown in Fig. 2, and it follows that the performance parameters may be described using this model. Figure 3 shows the overall response of the model of Fig. 2, when a single real impulse is transmitted; the response is denoted $h(t)+jg(t)$. The sample corresponding to the data (the single impulse) is $h(0)$; the interference terms are $h(nT)$, where n is an integer not equal to zero. The intersymbol interference is defined as the sum of the magnitude of these terms normalized by $h(0)$. Thus i.s.i. is defined as:

$$\sum_{\substack{n=-\infty \\ n\neq 0}}^{\infty} \frac{|h(nT)|}{h(0)} \times 100\%. \qquad (1)$$

Of course the time reference (denoted above as $t = 0$) is completely arbitrary and would normally be chosen as the time which gives least i.s.i.

The above definition refers to two-phase p.m. where the response $g(t)$ can be separated from $h(t)$ by the demodulator; this is not true in the case of amplitude modulation using envelope detection, or four-phase p.m. where the co-channel interference defined as:

$$\text{c.c.i.} = \sum_{n=-\infty}^{\infty} \frac{|g(nT)|}{h(0)} \times 100\% \qquad (2)$$

will interfere with the wanted signal. Usually, it is

convenient to lump the co-channel interference in with the intersymbol interference where appropriate and obtain different definitions for the i.s.i. for the different modulation methods; these definitions are listed in Table 1.

Table 1

Definitions of i.s.i. for various systems

AMPLITUDE MODULATION, VESTIGIAL SIDEBAND, SINGLE SIDEBAND, TWO-PHASE P.M.
$\text{i.s.i.} = \sum_{\substack{n=-\infty \\ n\neq 0}}^{\infty} \frac{\lvert h(nT)\rvert}{h(0)} \times 100\%$
QUADRATURE AMPLITUDE MODULATION, FOUR-PHASE P.M. ENVELOPE DETECTION A.M.
$\text{i.s.i.} = \sum_{\substack{n=-\infty \\ n\neq 0}}^{\infty} \frac{\lvert h(nT)\rvert + \lvert g(nT)\rvert}{\sqrt{h^2(0)+g^2(0)}} \times 100\%$

Although i.s.i. and c.c.i. need only be restricted at sampling instants, the interference such as a.c.r. comes from adjacent transmitters which are not time-synchronized, with the consequence that the interference must be restricted at all time instants. The interferences a.c.r. and e.m.c. are treated very similarly and have the following definitions:

$$\text{a.c.r.} \leqslant -10_{\log 10}\lvert R(f)\rvert^2, \quad \lvert f\rvert \geqslant f_0 \tag{3}$$

$$\text{e.m.c.} \leqslant -10_{\log 10}\lvert T(f)\rvert^2, \quad \lvert f\rvert \geqslant f_0 \tag{4}$$

f_0 is usually taken as the frequency equal to the symbol rate, $1/T$.

From the sampling theorem[3] the pulse overshoot interference, p.o.i., may be represented by samples spaced every $T/2$, since the received signal has a bandwidth of at the most $1/T$. P.o.i. is defined in similar fashion to i.s.i.; the overshoot interference for two-phase p.m. is given below:

$$\text{p.o.i.} = \sum_{\substack{n=-\infty \\ n\neq 0}}^{\infty} \frac{\lvert h(nT/2)\rvert}{h(0)} \times 100\%. \tag{5}$$

For the class of modulation methods including quadrature amplitude modulation, four-phase p.m. etc., the definition is again similar to that of i.s.i.:

$$\text{p.o.i.} = \sum_{\substack{n=-\infty \\ n\neq 0}}^{\infty} \frac{\lvert h(nT/2)\rvert + \lvert g(nT/2)\rvert}{\sqrt{h^2(0)+g^2(0)}} \times 100\%. \tag{6}$$

The signal power at the sampling instant (assuming unity resistors) is $\lvert h(0)\rvert^2$ which is given by the Fourier transform of $T(f).R(f)$:

$$\lvert h(0)\rvert^2 = \left[\int_{-\infty}^{\infty} T(f).R(f).e^{j\omega t_0}\,df\right]^2 \tag{7}$$

t_0 is the time instant corresponding to the best time to sample the received waveform. If the noise spectral density is N_0 watts/Hz, the double-sided noise spectral density, and is valid for positive and negative frequencies, then the noise power at the output of the receiver is

$$N_0 \int_{-\infty}^{\infty} \lvert R(f)\rvert^2\,df.$$

The noise appears at the input to the receiver as shown in Fig. 2. Thus the s.n.r. is given by:

$$\frac{\left[\int_{-\infty}^{\infty} T(f).R(f).e^{j\omega t_0}df\right]^2}{N_0.\int_{-\infty}^{\infty}\lvert R(f)\rvert^2\,df}. \tag{8}$$

In order that filter deficiencies are not compensated by merely increasing the transmitter power, a parameter termed s.n.d., the s.n.r. degradation is derived. Multiplying top and bottom of the expression above by the energy transmitted for each pulse E_b, and noting that

$$E_b = \int_{-\infty}^{\infty}\lvert T(f)\rvert^2\,df$$

$$\text{s.n.r.} = \frac{\left[\int_{-\infty}^{\infty} T(f).R(f).e^{j\omega t_0}df\right]^2}{\int_{-\infty}^{\infty}\lvert T(f)\rvert^2\,df.\int_{-\infty}^{\infty}\lvert R(f)\rvert^2\,df}.\frac{E_b}{N_0} \tag{9}$$

$$= \text{s.n.d.}\cdot\frac{E_b}{N_0}. \tag{10}$$

The important aspect of this is that the maximum value of s.n.d. is unity, and it is entirely a function of the spectral shapes of transmitter and receiver. Thus s.n.d. is defined by:

$$\text{s.n.d.} = \frac{\left[\int_{-\infty}^{\infty} T(f).R(f).e^{j\omega t_0}\,df\right]^2}{\int_{-\infty}^{\infty}\lvert T(f)\rvert^2\,df.\int_{-\infty}^{\infty}\lvert R(f)\rvert^2\,df} \tag{11}$$

4 Derivation of Filter Specifications

4.1 Introductory Comments

As the parameters affecting the error rate have been now defined, it is a relatively straightforward procedure to write a specification for filters which will give good performance in a digital system. To complete the specification the conventional parameters such as terminating impedances, etc. must be included. The following data should be considered as part of the specification, where applicable, for bandpass and low-pass filters:

Method of modulation
Symbol rate
Intermediate frequency
Terminating impedances
Insertion loss at midband
Maximum input signal

Since design margins must be allowed it is important to know how the parameters may be typically traded off against each other. It is shown later that the major parameters of i.s.i., a.c.r., e.m.c. and s.n.d. may be optimized independently and are only prevented from reaching the theoretical, limiting values by the small effects of practical filters. (The limiting values are listed in Table 2.)

4.2 The Specification

A specification with typical design margins is shown in Table 3. As this refers to the complete transmitter and receiver response, it is necessary to take into account any fixed filters, or time domain shaping, when designing a particular filter. In addition, the receiver i.f. filter cannot be designed on its own, but must take the transmitter filters into account. The transmitter and receiver filters are normally designed together and except for a few simple cases, computer-aided design is almost mandatory.

As one result of this form of specification, some parameters such as i.s.i. and s.n.d. have quite deep implications and can virtually specify uniquely the whole of the system filtering.

Table 2

Limiting values of the performance parameters

i.s.i.	0%
c.c.i.	0%
p.o.i.	0%
e.m.c.	∞ dB
a.c.r.	∞ dB
s.n.d.	0 dB

Table 3

Typical specifications for a receiver/transmitter filter pair

RECEIVER I.F. FILTER	
modulation method	a.m.
symbol rate	8 k symbols/second
intermediate frequency	40 MHz
terminating impedances	600 Ω
insertion loss at midband	<2 dB
maximum input signal	100 mV
i.s.i.	<10%
c.c.i.	included in i.s.i.
p.o.i.	not applicable
a.c.r.	40 dB
s.n.d.	<0·4 dB
TRANSMITTER LOW-PASS FILTER	
modulation method	a.m.
symbol rate	8 k symbols/second
terminating impedances	600 Ω
insertion loss at d.c.	<0·5 dB
maximum input signal	1 V
i.s.i.	<10%
c.c.i.	included in i.s.i.
p.o.i.	not applicable
e.m.c.	30 dB
s.n.d.	<0·4 dB

Note.—The parameters i.s.i., c.c.i., p.o.i. and s.n.d. are identical by necessity since they are a measure of both receiver and transmitter filters.

5 Classes of Frequency Responses That Meet the Specifications

5.1 Introduction

Before attempting to design practical filters that would meet a typical specification that follows the lines laid down in the previous chapter, it is necessary to determine the classes of transmitted and received characteristics (albeit theoretical) that will meet the specification. If this is not done it will be necessary to design the transmitter and receiver filters simultaneously with the handicap that the relationship between the poles and zeros of the filters and the performance parameters is an extremely complicated non-linear function and even well beyond present-day computer-aided design techniques. Determining a class of acceptable frequency responses instead of a single response avoids the risk of overdesign and specification with the consequence, for example, that a 12th-order filter is used instead of a 4th-order filter. The pre-envelope models are used to derive the classes of frequency responses acceptable for the a.m./p.m. family of modulation methods.

5.2 The Derivation

The major problem of translating the specification into a filter design is that the parameters i.s.i., c.c.i. and p.o.i. are described in the time domain, whilst the remaining performance parameters are defined in the frequency domain. Although the Fourier transform may be used to determine the effect of one domain upon the other, optimization of the filter to meet the specification requires that the time domain parameters be expressed in the frequency domain. Even though Nyquist gave some frequency responses that possessed zero i.s.i. it was not until the extensions to his theory first derived by Gibby and Smith[2] that the constraints of i.s.i. could be linked to the frequency domain: when the frequency response at the detectors is denoted by $W(f)$ where $W(f) = T(f).R(f)$, the pre-envelope spectrum, the complex time domain response at intervals nT (where n is an integer and T the symbol period) is given by

$$W(nT) = \int_{-\frac{1}{2}T}^{\frac{1}{2}T} X(f).e^{j\omega nT}df \qquad (12)$$

where

$$X(f) = \sum_{k=-\infty}^{\infty} W(f+k/T). \qquad (13)$$

When the i.s.i. is zero, $W(nT) = 0$ for $n \neq 0$, and as equation (12) is the complex Fourier series expansion of $X(f)$, zero i.s.i. implies that $X(f)$ is merely equal to a complex constant for all f, namely

$$X(f) = C_1 + jC_2. \qquad (14)$$

Consequently for zero intersymbol interference, (12) becomes

$$\sum_{k=-\infty}^{\infty} W(f+k/T) = C_1 + jC_2. \qquad (15)$$

This expression may be simplified further, since in practice any demodulating phase ϕ may be used, and $W(f)$ becomes $W(f).e^{j\phi}$. Substituting in (15) gives

Table 4

f	$\frac{-1}{T}$	$\frac{-3}{4T}$	$\frac{-1}{2T}$	$\frac{-1}{4T}$	0	$\frac{1}{4T}$	$\frac{1}{2T}$	$\frac{3}{4T}$	$\frac{1}{T}$
$W(f)$ [real component]	0	−0·27	0·6	1·71	2	2·27	1·4	0·29	0
$W(f)$ [imaginary component]	0	−j0·141	j0·2	−j0·141	0	j0·141	−j0·2	j0·141	0

$$(C_1+jC_2)e^{j\phi} = (C_1+jC_2)(\cos\phi + j\sin\phi).$$

This becomes a real constant C when

$$jC_2\cos\phi + jC_1\sin\phi = 0,$$

i.e. $\tan\phi = -C_2/C_1$. As the phase, ϕ may be arbitrary, (15) may be simplified to

$$\sum_{k=-\infty}^{\infty} W(f+k/T) = C. \qquad (16)$$

With the constraints of e.m.c. and a.c.r. imposed upon $T(f)$ and $R(f)$, $W(+1)/T$ is typically −80 dB down relative to mid-band. These figures correspond to values of 0·0001+j0·0001 which may be safely ignored in the summation of (16). Consequently, so far as practical communication systems are concerned (16) simplifies to

$$W(f-1/T)+W(f)+W(f+1/T) = C. \qquad (17)$$

As an example, Fig. 4 shows the real and imaginary parts of a complex time response. It is apparent that there is no i.s.i. or c.c.i. The corresponding frequency response is obtained via the Fourier transform and is shown plotted in Fig. 5. Although it is not obvious from the diagram, the frequency response obeys the relation (17), as the real and imaginary components tabulated in Table 4 show:

$$W\left(\frac{-3}{4T}\right)+W\left(\frac{1}{4T}\right)+W\left(\frac{5}{4T}\right)$$
$$= 0{\cdot}27-j0{\cdot}141+2{\cdot}27+j0{\cdot}141+0 = 2$$

also,

$$W\left(\frac{-1}{2T}\right)+W\left(\frac{1}{2T}\right) = 0{\cdot}6+j0{\cdot}2+1{\cdot}4-j0{\cdot}2 = 2$$

and

$$W\left(\frac{-1}{4T}\right)+W\left(\frac{3}{4T}\right) = 1{\cdot}71-j0{\cdot}141+0{\cdot}29+j0{\cdot}141 = 2.$$

The relationship is satisfied and the constant C of this example equals 2. The complex frequency response can be equivalently expressed in terms of magnitude and phase, and these responses are plotted in Fig. 6. For interest and to correspond to practice, a linear phase/frequency characteristic has been added to the phase corresponding to a delay of the time response by T. Clearly, a delay does not change the shape of the time response and any slope of the phase/frequency characteristic may be used.

The appearance of this single complex pulse at radio frequency is shown in Fig. 7. Since both real and imaginary time components of the pre-envelope model are zero at intervals T apart, the envelope of the r.f. signal,

$$g(t).\cos\omega_c t - h(t).\sin\omega_c t = \sqrt{g^2(t)+h^2(t)}.\cos(\omega_c t+\phi(t))$$

and is correspondingly zero at these instants.

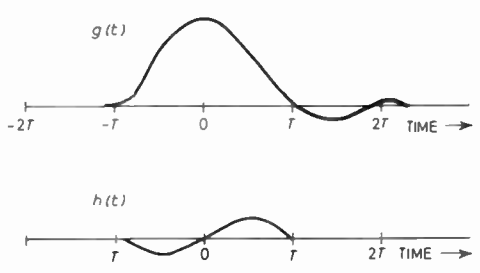

Fig. 4. Real and imaginary time responses.

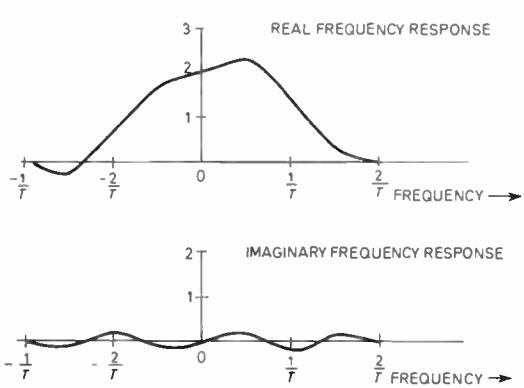

Fig. 5. Frequency response corresponding to the time response of Fig. 4.

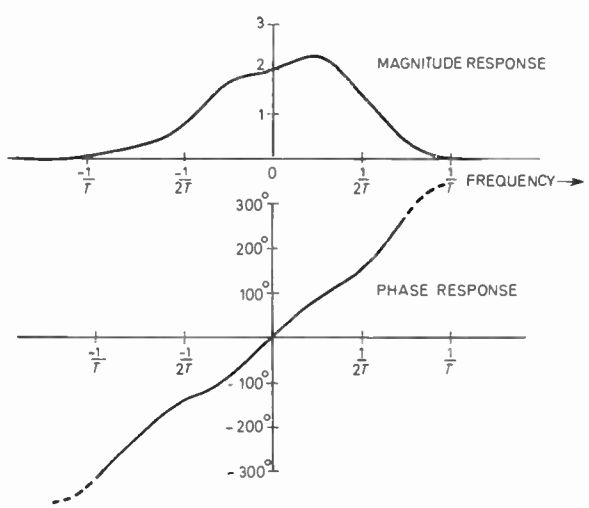

Fig. 6. Magnitude and phase response (including delay).

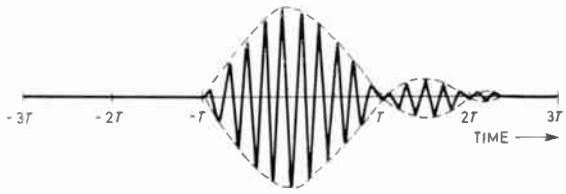

Fig. 7. The r.f. pulse response.

The conditions for zero i.s.i. can now be imposed in the frequency domain by using equation (17). An interesting corollary of this equation is that if the response $W(f)$ does not have zero i.s.i. due to an additional distorting network, say $R_2(j\omega)$ and an equalizer is to be used, say $R_3(j\omega)$ to compensate for $R_2(j\omega)$, then $R_3(j\omega)$ does not have to have the inverse response $1/R_2(j\omega)$, as might be thought, since a distortion in the frequency band $W(-1/T)$ to $W(0)$ may be compensated for in the frequency band $W(0)$ to $W(-1/T)$, or any band of bandwidth $1/T$. If the signal bandwidth is generous, say two or three times $1/T$, then designing an equalizer to give zero i.s.i. would be relatively easy. On the other hand if $W(f)$ is of small bandwidth, say $1{\cdot}5/T$, with

$$W(f) = 0 \quad \text{for} \quad |f| > \frac{3}{4T},$$

then (17) reduces to

$$W(f) = C \quad \text{for} \quad \frac{-3}{8T} \leqslant f \leqslant \frac{3}{8T}$$

and it follows that $W(f)$ is purely real, and has a phase response of zero. Again, since a delay does not change the result, this means in practice that the only frequency responses of this bandwidth with zero i.s.i. have linear phase over the bandwidth $3/4T$ about the centre frequency, and also have a flat magnitude response.

The signal/noise ratio degradation was defined in equation (11) and the minimum value may be found by several methods[3]. The solution is that

$$R(f) = T^*(f)e^{-j\omega t_0} \tag{18}$$

where * represents the complex conjugate, and this is the well-known matched filter result of detection theory and it follows from (18) that

$$|R(f)| = |T(f)|. \tag{19}$$

Substituting in (11) and noting that

$$T(f).T^*(f) = |T(f)|^2,$$

the minimum value of s.n.d. is found to be unity.

It is not often noticed that this result has some interesting implications for the overall response, $W(f) = R(f).T(f)$. Since

$$W(f) = T(f).T^*(f).e^{-j\omega t_0},$$

it follows that

$$W(f) = |T(f)|^2.e^{-j\omega t_0}. \tag{20}$$

The aspect of importance is that $W(f)$ is now linear phase with the obvious corollary that any characteristic $W(f)$ which has non-linear phase must have a signal/noise ratio degradation.

When equation (20) is expressed in terms of the complex frequency response, and the delay is removed (now the phase is zero), $W(f)$ has zero imaginary components and positive, real components. Assuming that s.n.d. has been minimized and that the response $W(f)$ is only significant in a $2/T$ bandwidth due to typical a.c.r./e.m.c. values, (17) becomes:

$$\left.\begin{aligned} &|T(f)|^2 + |T(f \pm 1/T)|^2 = C \\ &|T(f)|^2 = C - |T(f \pm 1/T)|^2 \\ &\text{which from (19) is equivalent to} \\ &|R(f)|^2 = C - |R(f \pm 1/T)|^2 \end{aligned}\right\} \tag{21}$$

This relationship is known as the property of skew-symmetry, and two examples of it are given in Figs. 8 and 9. The first example is a typical bandpass characteristic whilst the second example being a low-pass filter characteristic has even symmetry about zero and thus has odd symmetry about $T(f \pm 1/2T)$. These responses give optimum values for s.n.d., i.s.i., c.c.i., a.c.r. and e.m.c. provided the phase response of $W(f)$ satisfies (20).

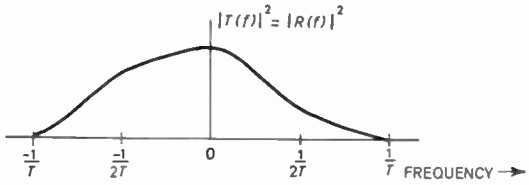

Fig. 8. Typical characteristic that has optimum values for s.n.d., i.s.i., c.c.i., e.m.c. and a.c.r.

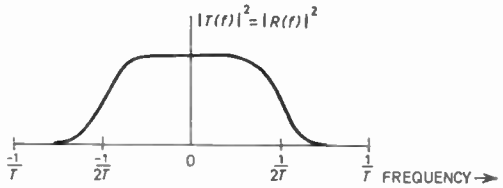

Fig. 9. A typical baseband characteristic.

What has been shown is that there is a class of theoretical characteristics of $|T(f)|$ and $|R(f)|$ given by the relationship (21). (Remembering that the magnitude squared uniquely defines the magnitude.) This class of characteristics gives optimum values for i.s.i., c.c.i., s.n.d., and of course a.c.r. and e.m.c., as these have already been assumed, and forms a suitable target for realizable filter responses. The transmitted and received characteristics can now be designed one at a time using equations (20) and (21) and need not be designed simultaneously as may have been thought initially.

6 Realization of Practical Filters

6.1 A Simple Example

There are several methods by which the above theoretical results may be turned into practical filter designs. If computer-aided optimization procedures are available then the poles and zeros, or filter component values, may be iteratively adjusted to optimize the time-frequency

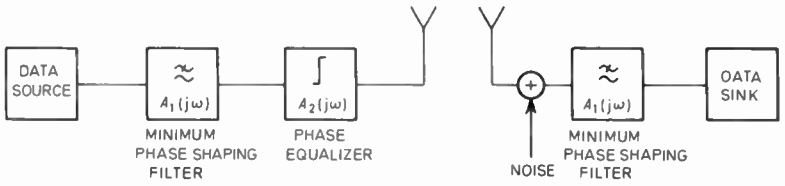

Fig. 10. Pre-envelope model showing the positions of the filters.

response to produce, directly, optimum low-pass or band-pass filters. In the following example, a simpler approach is taken, using the following assumptions:

(1) The only spectral shaping is done by a single low-pass transmitter filter and a single i.f. band-pass receiver filter.

(2) The ratio of bandwidth to i.f. is sufficiently low that the usual band-pass transformation of a low-pass prototype produces negligible distortion. Thus the pre-envelope of the band-pass filter's frequency response is identical to the prototype low-pass filter's impulse response.

(3) The i.f. filter is to be realized as a crystal filter and may only be obtained from a prototype low-pass filter which has a monotonic magnitude response. The i.f. filter is obtained by conventional transformations of the low-pass filter.

(4) The low-pass filter and i.f. filter are minimum phase and are only used to shape the magnitude response since a phase equalizer network is used at the transmitter to control the phase response of the overall response $W(f)$.

With these assumptions, the pre-envelope model becomes that shown in Fig. 10 where the realizable filter responses $A_1(j\omega)$, $A_2(j\omega)$ replace the theoretical characteristics $T(f)$, $R(f)$: $A_1(j\omega)$ is the minimum phase prototype low-pass filter and $A_2(j\omega)$ is the phase equalizer.

6.2 Design of the Prototype Low-Pass Filter $A_1(j\omega)$

Since the phase equalizer $A_2(j\omega)$ has a flat magnitude response, and as the same magnitude shaping filter $A_1(j\omega)$ is to be used at both transmitter and receiver, the first condition, (19), for optimum s.n.d. is satisfied. When the network $A_2(j\omega)$ is such that the overall response has linear phase, then the last condition for optimum s.n.d. is satisfied and both relationships (18) and (20) hold.

The design problem reduces to finding a filter characteristic which satisfies the zero i.s.i. conditions of (16) where $W(f)$ is equivalent to $|A_1(j\omega)|^2$, (the simpler relation (21) may be used when there is sufficient attenuation of the frequency $1/T$), and yet possesses sufficient stop-band attenuation to meet the a.c.r. and e.m.c. specifications. The approach that has been taken is to find characteristics for a given order of filter which have the maximum attenuation at $1/T$ for a given i.s.i.

A paper which has been published by P. G. Halpern describes monotonic low-pass filters having optimum stop-band attenuation for a given order of filter.[4] It is shown that any low-pass monotonic filter may be represented by a sum of orthogonal Jacobi polynomials $U(i)$ of increasing order weighted by a set of coefficients; if the transfer function $|H(j\omega)|$ is $1/(1+L_n(\omega)^2)$ then

$$L_n(\omega)^2 = \int_0^{\omega} x \left(\sum_{i=1}^{\frac{1}{2}n} C_{2i-1} . U_{2i-1} \right)^2 \mathrm{d}x$$

U_{2i-1} are the Jacobi polynomials and C_{2i-1} are the coefficients. The orthogonal polynomials have the property that the stop-band attenuation is indicated by the size of the highest order coefficient C_{n-1}. The bigger C_{n-1} the more stop-band attenuation: if C_{n-1} is fixed, then the bigger C_{n-3}, the more attenuation and so on. Rakovich and Litovski[5] have successfully used these polynomials to obtain a least squares approximation to a maximally flat response, which is flatter than a Butterworth filter in the normalized range $0{\cdot}6 < \omega < 1$ and has a greater stop-band attenuation. The success of the approach suggests the idea of small i.s.i. filters specified by a set of Halpern coefficients; the resulting filters are termed 'Halcoff' filters.

The error function $E_{\text{i.s.i.}}$ below is approximately proportional to the i.s.i. and is simple to calculate as it need only be evaluated at a few frequency points:

$$E_{\text{i.s.i.}} = \int_{-\pi/T}^{\pi/T} \frac{\left| C - \sum_{k=-\infty}^{\infty} \left| A_1\left(j\omega + \frac{j2\pi k}{T}\right) \right|^2}{\frac{2\pi C}{T}} \mathrm{d}\omega$$

where C is the constant of equation (21).

Table 5 tabulates the Halpern coefficients for a 6th-order filter; the attenuation in dB at $1/T$; and the corresponding values found for $E_{\text{i.s.i.}}$ expressed as a percentage.

Table 5

C_5	C_3	C_1	Attn.(dB)	$E_{\text{i.s.i.}}$%
1	0	0	52·7	16
0·95	0·296	0·098	52·4	11·4
0·9	0·435	0	52·1	8·8
0·9	0·194	0·389	51·9	13·2
0·85	0·526	0	51·7	7·35
0·85	0·5	0·166	51·68	7·28
0·85	0·44	0·288	51·64	7·95
0·85	0·372	0·37	51·6	9·1
0·8	0·6	0	51·25	6·39
0·8	0·57	0·19	51·24	5·9
0·8	0·5	0·328	51·19	6·34

A plot of $E_{i.s.i.}$ against stop-band attenuation reveals that it is an oscillating function whose minimum values approach zero as the attenuation is reduced. The true i.s.i. was calculated at these local minima points assuming linear phase and the filter design selected at the first acceptable value of i.s.i. The filter obtained has an attenuation of 47·6 dB and i.s.i. of 1·5% with component values corresponding to those shown in Fig. 11 for a data rate of 10 kbauds. The magnitude squared response is found to have the skew symmetry property of equation (21) as expected.

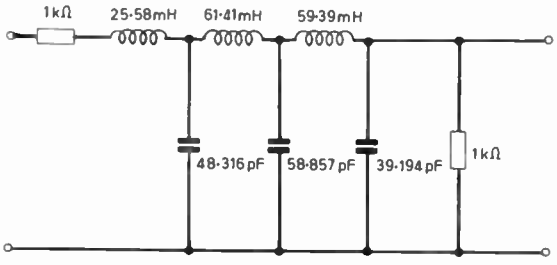

(a) The Halcoff low-pass transmitter shaping filter.

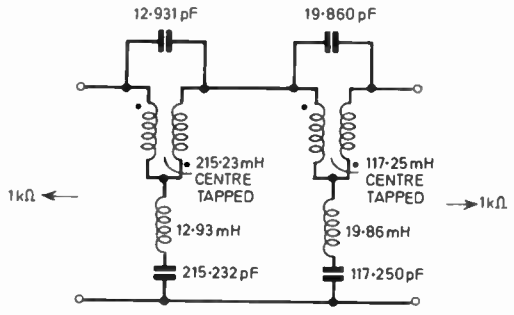

(b) Phase equalizer for the Halcoff filter.

Fig. 11.

6.3 Design of the Phase Equalizer $A_2(j\omega)$

The task of the phase equalizer is to make the overall phase response linear, and as this correspoinds to flat group delay, conventional group delay equalizer design methods may be used to determine a suitable design. The particularly sharp cut-off of the Halcoff filter results in severe group delay distortion and a 4th-order equalizer was found necessary to reduce the i.s.i. to an acceptable 15%. The overall s.n.d. was found to be less than 0·1 dB. The equalizer design is shown in Fig. 11.

7 Conclusions

A baseband model has been given of amplitude and phase modulation systems. Using the model, the performance parameters of importance were defined and a typical filter specification was drawn up. Classes of frequency characteristics were derived which optimize all of the performance parameters except the pulse overshoot interference parameter, with the intention that these frequency characteristics would be used as targets for practical filters. One example was given of the way the theoretical results would be used to derive practical shaping filters.

Further work will be done to utilize the theoretical results in a computer-aided optimization program so as to take more account of practical difficulties such as geometric distortions due to bandpass transformations and the existence of fixed filters at transmitter and receiver. Future theoretical results are hoped to be derived which will include the control of the pulse overshoot interference.

8 Acknowledgments

The author would like to express his gratitude to his colleagues in the Filter Division of Plessey Telecommunications Research, especially to A. J. L. Muir, A. E. Methiwalla and L. B. D. Ellis, and also to W. J. Cullyer of R.S.R.E. The work has been carried out with the support of the Procurement Executive, Ministry of Defence, sponsored by CVD.

9 References

1. Nyquist, H., 'Certain topics in telegraph transmission theory', *Trans. Amer. Inst. Elect. Engrs*, **47**, pp. 617–44, April 1928.
2. Gibby, R. A. and Smith, J. W., 'Some extensions of Nyquist's telegraph theory', *Bell Syst. Tech. J.*, **44**, pp. 1487–1510, September 1965.
3. Schwartz, M., Bennett, W. R. and Stein, S., 'Communication Systems and Techniques' (McGraw-Hill, New York, 1966).
4. Halpern, P. G., 'Optimum monotonic low pass filters', *IEEE Trans. on Circuit Theory*, CT-16, pp. 240–1, May 1969.
5. Rakovich, B. D. and Litovski, V. B., 'Least squares monotonic low pass filters with sharp cut-off', *Electronics Letters*, 9, No. 4, pp. 75–6, February 1973.

Manuscript received by the Institution on 4th February 1975. (Paper No. 1711/CC 246).

UDC 621.373.121.11–758.747: 621.3.011.716

The effect of water migration on oscillator stability

M. V. BENNETT (Graduate)*

SUMMARY

During the development of a stable free-running oscillator an unusual frequency drift phenomena was observed. When investigated, the drift was found to be due to the molecular migration of water to and from the oscillator. Although the drift observed is emphasized by the frequency of oscillation and the temperature ranges involved, it is believed that the findings of this work are applicable to the stability of any circuit or component used in an a.c. application.

To overcome the water migration effect, the oscillator was dried and sealed, and from this work it is postulated that free-running oscillators with extremely good long-term stabilities are possible.

* *Marconi-Elliott Avionic Systems Ltd., Electro-Optical Systems Division, Christopher Martin Road, Basildon, Essex SS 14 3EL.*

1 Introduction

A requirement arose for a family of oscillators operating in 300 to 500 MHz region with a stability of $\pm 0{\cdot}06\%$ over a period of six years, and an operational temperature range of $-30°C$ to $+90°C$. For reasons not detailed here crystals could not be used, thus it was proposed that a Clapp oscillator[1] (Fig. 1) in an oven operating at 95°C (to overcome temperature/frequency problems) would satisfy the requirement.

Initially the requirement appeared to be adequately fulfilled by this design, but later it was found that the frequency stability requirement was not being met. The failure became evident in two discrete phases.

(a) During the 'burn in' tests employed in the manufacture of the oscillator, it was noted that an exponential increase in frequency occurred. It was assumed that this effect was due to the 'ageing' and 'settling down' of the components and the test was doing the 'job' that was intended. To overcome this frequency drift phenomenon, the length of 'burn in' time was extended until all oscillators stabilized at their high frequency.

(b) Later it was found that oscillators which had been set after 'burn in' and stored for some months, were markedly low in frequency at switch-on. It was further found that if the oscillator was run again for long periods, the frequency moved upwards until the original setting was approached again.

Analysis of a batch of oscillators showed that, although all oscillators exhibited this reversible characteristic, the difference between the start and finish frequencies and the rate of the drift was considerably different from oscillator to oscillator.

It was assumed that the variation seen was due to a slow reversible change in the tuned circuit, but a systematic check on all components did not reveal what such a change could be.

At this stage, frequency drifts were being observed for which there appeared to be no known explanation. A review of papers on the stability of free-running oscillators did not reveal a similar pattern, and no reports of a Clapp oscillator exhibiting such characteristics were found. However, a paper by Lea[2] published in 1945 was found, which reported that unusual frequency drifts had been observed when water vapour was condensed on to an oscillator.

2 Improvements in Frequency Stability by Drying and Sealing

The possibility of water vapour being responsible for the frequency drifts could explain many of the features seen, and a series of trials were carried out, where the oscillators were vacuum dried at 60°C for 24 hours and then hermetically sealed in cans in a similar manner to crystals.

The above simple process gave an immediate improvement in frequency stability, and although the general characteristics of frequency drift were still being observed, it had been reduced by approximately an order, this

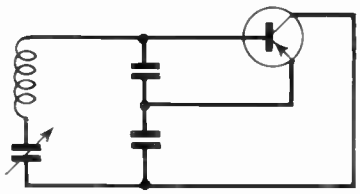

Fig. 1. Basic Clapp oscillator circuit.

being adequate to ensure that the requirement would be satisfied.

To maintain the dried oscillator in a dry condition three methods of sealing were evaluated: solder sealing, total epoxy resin encapsulation, and a fillet of epoxy resin around the lid of the existing oven can.

Two methods of drying were also evaluated, high temperature vacuum baking and high temperature gas flow drying. It was found that for the same period of drying, the bake/gas flow method was more effective in removing water from the oscillator assembly, but the capital plant and precise controls required for this technique make it a highly specialist operation.

A solder-sealed unit filled with dry gas after vacuum baking was adopted as the most suitable technique as a production process.

The standards maintained during this process were as follows:

(a) Leak rate in oven oscillator seal, less than 10^{-8} $cm^3\ s^{-1}\ atm^{-1}$.

(b) Dryness level during vacuum bake, less than 1 part in 10^6 of water vapour (at 100°C) in vacuum.

(c) Dryness level of gas within sealed oscillator oven (after one year of storage) less than 200 parts in 10^6 of water vapour at 20°C.

Figure 2 indicates the frequency stability of oscillators made to these standards. These oscillators were stored in an environmental chamber which simulated an accelerated storage factor of 10. Thus the results for the solder-sealed units are a prediction on a 20-year basis.

From the results obtained it was evident that the high oven temperature employed was baking out water from the oscillator and in the unsealed case this water was free to return back to the oscillator once the oven was switched off. It is equally evident that migration of water molecules will occur at any time when changes in humidity and temperature occur, thus all electronic components or assemblies are susceptible to these changes and the rate of change is determined by the encapsulation techniques employed.[3,4,5]

Two interesting aspects now need answering:

(a) Why do water molecules affect the stability of an oscillator?

(b) Is it possible to improve the long-term stability of a Clapp oscillator to approach the stability of a crystal oscillator?

The next Section will attempt to give an answer to these questions.

3 The Effect of Water Molecules in a High Frequency Oscillator

In 1910 Debye[6] produced a theory to explain why certain materials had physical properties which were not in keeping with their atomic weights or placings in the atomic tables. These materials were said to have polar molecules, and water is one of these such materials.

In a polar molecule the charge pattern is not balanced, thus the molecule appears to have polarity like a magnet. If these molecules are placed in an electric field, then they will align themselves within this field; if the field is reversed then complete re-alignment will take place. The time in which this re-alignment can take place is short, but finite, and as the frequency of the electric field reversals is increased, then greater frictional and inertial losses occur within the polar molecule until one passes beyond the resonant frequency of the molecule.

Relating the polar molecule and water migration phenomena to an oscillator operating in the 300 to 500

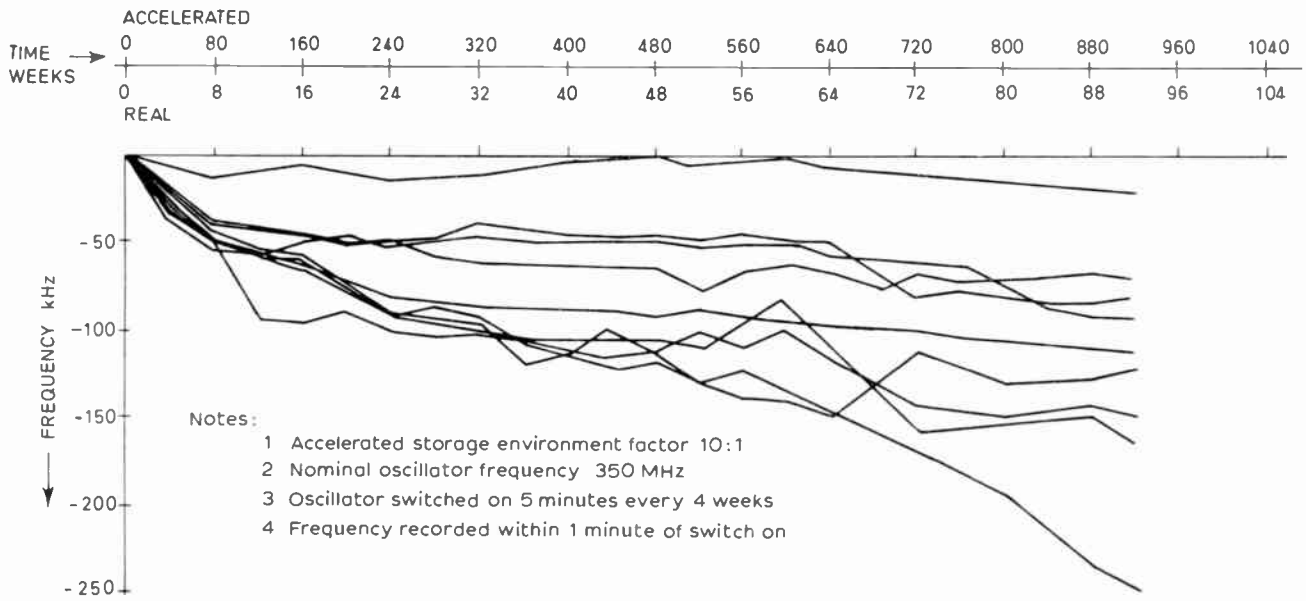

Fig. 2. Normalized frequency drift of solder-sealed units for a random sample of processed oscillators.

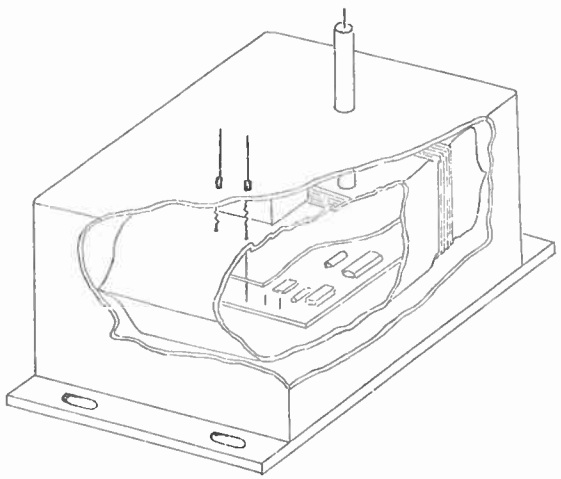

Fig. 3. Cut-away section of oscillator assembly.

MHz region, the dielectric losses in the tuned circuit and sustaining amplifier must all be influenced to some degree by the energy absorption effect.[7]

If an oscillator is operating at a given frequency and the number of water molecules are reduced, then the following effects are seen:

(a) The effective values of the tuned circuit change (lower losses, higher Q, lower 'resistive' element at resonant frequency, thus higher resonant frequency).

(b) The input/output impedances of the sustaining amplifier change (lower 'resistive' losses).

(c) The phase shift of the sustaining amplifier change (due to reduced 'resistive' losses).

(d) If the harmonic content of the oscillator decreases, this would enhance the effects listed above because the energy absorbed by the polar molecules will be decreased.

If the number of water molecules is increased, then the reverse of (a), (b) and (c) would occur.

4 Conclusions

It can be seen that the long-term frequency stability of a free-running oscillator can be improved by reducing the migration of water molecules to and from the oscillator. This is a well-established phenomenon associated with quartz crystal oscillators but not previously applied to free-running oscillators.

It is suggested that an oscillator processed and constructed to the following concepts will achieve a good long-term frequency stability.

(a) A Clapp oscillator followed by a buffer amplifier.

(b) All components and the mounting substrate must be constructed of intrinsically stable materials (e.g. gold, stainless steel, ceramic), to be capable of withstanding prolonged drying and exposure to temperatures of 400°C (to overcome the critical pressure/temperature of water).

(c) The electronic assembly should be mounted within a leak-free evacuated enclosure, and the total assembly maintained at a constant temperature by means of an oven.

(d) An additional refinement would be to enclose the above complete assembly within a second leak-free envelope.

An assembly using these criteria is shown in Fig. 3.

5 Acknowledgments

Appreciation is expressed to the following organizations for their assistance and support: Royal Aircraft Establishment at Farnborough, Microwave Associates Limited, Hirst Research Centre. Also to colleagues from Marconi-Elliott Avionic Systems Limited and G.E.C.-Marconi Electronics Limited.

6 References and Bibliography

1. Clapp, J. K., 'An inductance-capacitance oscillator of unusual frequency stability', *Proc. Inst. Radio Engrs*, **36**, pp. 356–8, March 1948.
2. Lea, N., 'Notes on the stability of LC oscillators', *Proc. Instn Elect. Engrs*, **92**, Part III, pp. 261–79, December 1945.
3. Kubota, Y., Uetake, T. and Saito, T., 'Properties of epoxy resin as an encapsulating material', *Rev. Elect. Commun. Lab.*, **19**, No. 9–10, pp. 1026–37, September–October 1971.
4. Kobayashi, M., 'Humidity influence on capacitance stability', *Rev. Elect. Commun. Lab.*, **19**, No. 9–10, pp. 994–1006, September-October 1971.
5. Sullivan, N. J., 'Experimental investigation of humidity effects in LC oscillators', Department of Supply, Australian Defence Scientific Service, Aeronautical Research Laboratories Flight Note 46, June 1971.
6. Debye, P., 'Polar Molecules' (Dover Reprint, New York).
7. McIntosh, R. L., 'Dielectric Behaviour of Physically Absorbed Gases' (Marcel Dekker, New York, 1966).

Armstrong, J. H., Blomster, P. R. and Hokanson, J. L., 'Ageing characteristics of quartz crystal resonators', 20th Annual Symposium on Frequency Control, 1966. (US Army Electronics Laboratories, Fort Monmouth, N.J.).

Byrne, R. J. and Reynolds, R. L., 'Design and performance of a new series of gold welded crystal unit enclosures', 18th Annual Symposium on Frequency Control, 1964. (US Army Electronics Laboratories, Fort Monmouth, N.J.)

Eisenburg, B. R., 'Frequency stability of a Clapp VCO', *IEEE Trans. on Instrumentation and Measurements*, **IM-18**, pp. 221–4, No. 3, September 1969.

Hartshorn, L., 'Experimental electricity and magnetism', Reports on Progress in Physics, Vol. 3 (Institute of Physics, London, 1936).

Hasted, J. B., 'Water—a Comprehensive Treatise' (ed. F. Franks), Vol. 1, Chapter 7. (Plenum Press, 1972).

Sykes, R. A., Smith, W. L. and Spencer, W. J., 'Performance of precision quartz-crystal controlled frequency generators', *IRE Trans. on Instrumentation*, **I-11**, No. 3–4, pp. 243–7, December 1962.

Vigoureux, P., 'Ageing phenomena of quartz elements', Chap. 10, 'Quartz Vibrators and their Application' (H.M.S.O., London, 1948).

Warner, A. W., Fraser, D. B. and Stockbridge, C. E., 'Fundamental studies of ageing in quartz resonators', *IEEE Trans. on Sonics and Ultrasonics*, **SU-12**, pp. 52–9, June 1965.

Manuscript first received by the Institution on 9th December 1974 and in final form on 21st May 1975. (Short Contribution No. 176/CC 247).

UDC 621.372.54:621.374

Cellular structures for implementing recursive and non-recursive digital filters

RENATO DE MORI, Ph.D.*

SUMMARY

Some cellular arrays for implementing digital filters as iterative assemblies of equal modules are introduced. The main advantage of these structures, which can be sequential or combinational, is that there is a large overlapping between the execution of the multiplications required to compute an output sample. In this way the time for a multiplication gives only an additive contribution to the total time needed for obtaining an output sample thus improving on the solutions previously presented.

* *Istituto di Elettrotecnica Generale, Politecnico di Torino, Corso Duca degli Abruzzi 24, 10129 Torino, Italy.*

1 Introduction

The rapid development of large-scale integration capabilities has made feasible the hardware implementation of digital filters. In a recent paper,[7] existing solutions have been reviewed, and the design proposed by Jackson *et al.*[1] to implement the second-order digital recursion is considered the most efficient way to solve that problem. Furthermore, it is emphasized that the efficiency of this solution represents a vast improvement over the conventional computer type structures.

Typical applications of hardware digital filters are in the communication and control area. While in the former total delay in processing is not critical, in the latter, total delay in processing affects stability margins in closed-loop operations.[7]

Another typical application of hardware digital filters is real-time signal processing of acoustic waveforms. Recent methods, introduced for speech recognition systems[8] and applicable to similar problems like speech data reduction and speaker identification, require the extraction of formants from digital spectrograms.

The computation of digital spectrograms as well as some processing of speech in order to classify sounds into broad classes can be performed by digital filtering. In this case, filters with considerable numbers of poles (>10) are required and the accuracy of the spectrograms depends on the number of filters.

A single filter can be multiplexed to obtain all the spectral samples between two time samples of the waveform. The processing speed is very important in such cases.

The speed depends mainly on the arithmetic unit of the filter; this unit is generally the slowest and most expensive component. This aspect is considered by Bass *et al.*[9], where multiplier architecture for digital filters is proposed.

This paper presents a different approach to the implementation of digital filters based mostly on logic-in-memory cellular arrays. Recursive and non-recursive filters are considered here for which sequential and combinational solutions are presented. Number representation is assumed to be that of 2's complement binary fractions; this implies some advantages, the most important of which is that an end-carry or overflow occurring during the computation of an intermediate result does not affect the exactitude of the final output.[1,4]

A linear digital filter is characterized by a pulsed transfer function of the form:

$$H(z) = \frac{\sum_{n=0}^{M} a_n z^{-n}}{\sum_{n=0}^{M} b_n z^{-n}} \qquad (1)$$

and this corresponds to the following linear difference equation relating to the input samples $x(nT)$ and the output samples $y(nT)$ as follows:

$$\sum_{k=0}^{M} b_k y(nT-kT) = \sum_{k=0}^{M} a_k x(nT-kT).$$

Assuming $b_0 = 1$ and defining the auxiliary variables:

$$w(nT) = x(nT) - \sum_{i=1}^{M} b_i w(nT - iT),$$

$$\mu_k(nT) = \mu_{k-1}(nT) + (-b_{M-2k+1})w[(n-M+2k-1)\times T] + (-b_{M-2k+2})w[(n-M+2k-2)T], \quad (2)$$

$$\lambda_k(nT) = \lambda_{k-1}(nT) + a_{M-2k+1}w[(n-M+2k-1)\times T] + a_{M-2k+2}w[(n-M+2k-2)T],$$

$$k = 1, 2, \ldots, L; \quad L = M/2,$$

with the following initial conditions:

$$\mu_0(nT) = x(nT)$$
$$\lambda_0(nT) = a_0 w(nT), \quad (3)$$

enables the required system output at any time constant to be obtained recursively as:

$$w(nT) = \mu_L(nT)$$
$$y(nT) = \lambda_L(nT) = \sum_{i=0}^{M} a_i w(nT - iT), \quad (4)$$

The recursive solution of equations (2), (3) and (4) can be effected by means of an arithmetic module (a.m.) of the form shown in Fig. 1, which may be combined to realize equation (1) in the manner shown in Fig. 2. Cascade and parallel realizations can be similarly implemented, and the object of this paper is to show

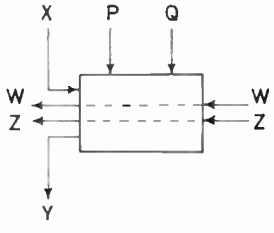

Fig. 1. Arithmetic module symbol.

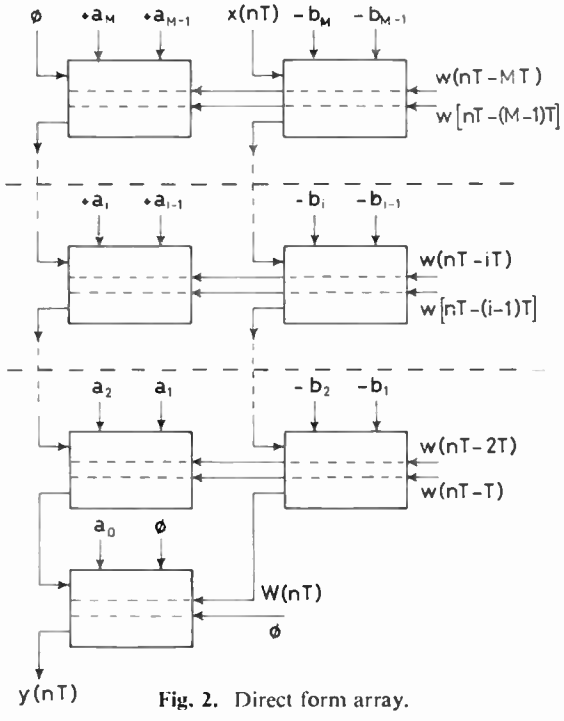

Fig. 2. Direct form array.

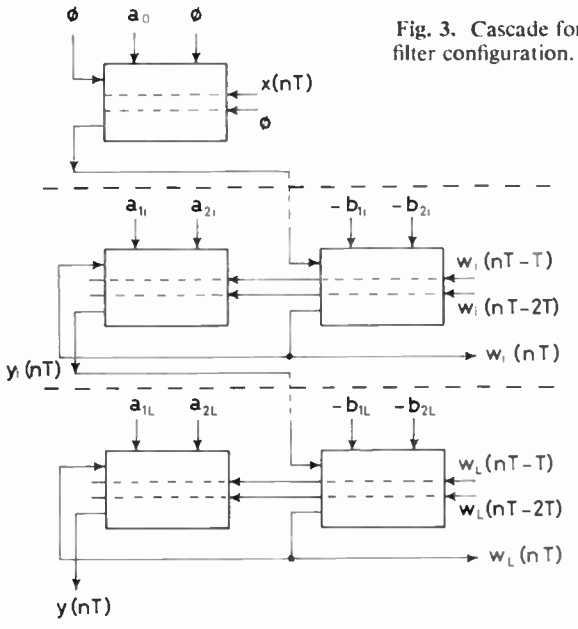

Fig. 3. Cascade form filter configuration.

that this cellular approach gives rise to significantly faster hardware realizations than have hitherto been achieved. Figures 3 and 4 show the implementations of the cascade and parallel forms corresponding to the following transfer functions:

$$H(z) = a_0 \prod_{i=1}^{L} \frac{a_{2i}z^{-2} + a_{1i}z^{-1} + 1}{b_{2i}z^{-2} + b_{1i}z^{-1} + 1}$$

$$H(z) = g_0 + \sum_{i=1}^{L} \frac{g_{1i}z^{-1} + g_{0i}}{d_{2i}z^{-2} + d_{1i}z^{-1} + 1}.$$

2 Arithmetic Module Sequential Implementation

A sequential a.m. can be implemented with the cellular iterative array depicted in Fig. 5.

Coefficients are represented as sign-magnitude binary fractions where the sign bit is the integer part (0 is for +; 1 is for −), while variables are 2's complement fractions.

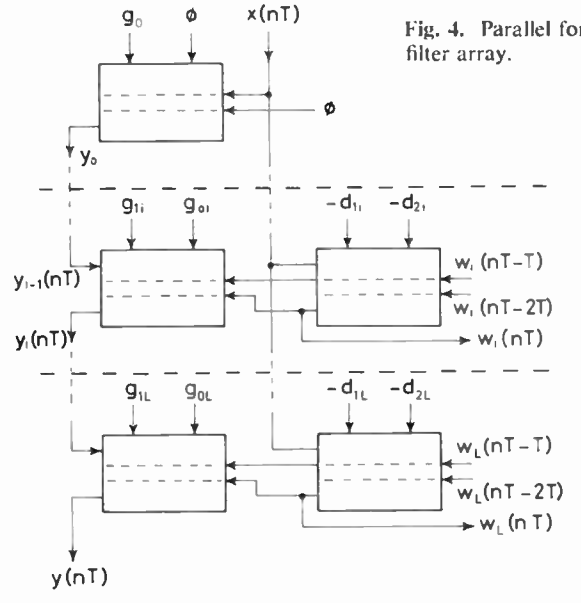

Fig. 4. Parallel form filter array.

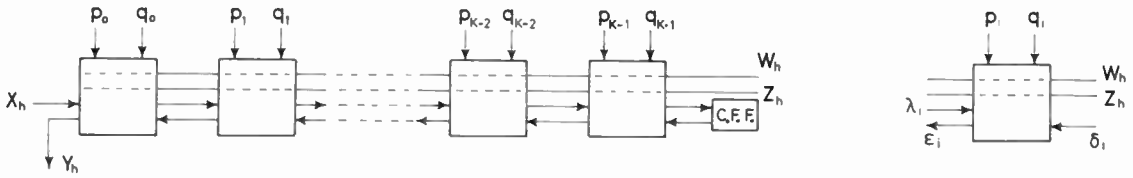

Fig. 5. Sequential a.m. iterative array.

Let $|P|$ and $|Q|$ be the magnitude of two coefficients represented with K bits; let $\tilde{W}$ and $\tilde{Z}$ be two binary fractions obtained from the corresponding $N+1$ bit state variables W and Z represented as binary fractions shifted K bits right before multiplication and two's complemented if their sign was different from that of the corresponding coefficients; let $\tilde{X}$ and $\tilde{Y}$ be respectively the fractional representations of X and Y. Let W' and Z' be the $(N+K+1)$-bit 2's-complement fractional representations of W and Z. The a.m. input and output are represented as follows:

$$\begin{aligned} |P| &= \sum_{i=0}^{K-1} p_i 2^i \\ |Q| &= \sum_{i=0}^{K-1} q_i 2^i \end{aligned} \tag{5}$$

$$\begin{aligned} \tilde{W} &= W_0 + \sum_{h=1}^{N+K} W_h 2^{-h} \\ \tilde{Z} &= Z_0 + \sum_{h=1}^{N+K} Z_h 2^{-h} \\ \tilde{X} &= X_0 + \sum_{h=1}^{N+K} X_h 2^{-h} \end{aligned} \tag{6}$$

$$\tilde{Y} = \left| |P|\tilde{W} + |Q|\tilde{Z} + \tilde{X} \right|_2 = Y_0 + \sum_{h=1}^{N+K} Y_h 2^{-h}. \tag{7}$$

The cells of the structure of Fig. 5 have the logical diagram of Fig. 6 and are specified by the bits of $|P|$ and $|Q|$. Variable bits of $\tilde{X}$, $\tilde{W}$, and $\tilde{Z}$ are serially sent to the array which gives serially the output bits of $\tilde{Y}$.

Before the first clock interval, the array executes the carry-save addition:

$$\begin{aligned} &\left| |P| W_{N+K} 2^{-(N+K)} + |Q| Z_{N+K} 2^{-(N+K)} + X'_{N+K} 2^{-(N+K)} \right|_2 \\ &\quad = \left| Y_{N+K} \cdot 2^{-(N+K)} + A(N+K-1) + B(N+K-1) \right|_2; \end{aligned}$$

with the first clock pulse $Y_{N+K} 2^{-(N+K)}$ is stored into the sum flip-flop (s.f.f.) which precedes the serial output of the array and $A(N+K-1)$, $B(N+K-1)$ are two K bit fractions having $2^{-(N+K-1)}$ as least weight. They are stored respectively in the s.f.f. and the carry flip-flops (c.f.f.) of the array. During the jth clock interval just before the jth clock pulse the following computation is performed:

$$\begin{aligned} &\left| |P| W_{N+K-(j-1)} 2^{-(N+K)+(j-1)} + \right. \\ &\qquad + |Q| Z_{N+K-(j-1)} 2^{-(N+K)+(j-1)} + \\ &\qquad + X_{N+K-(j-1)} 2^{-(N+K)+(j-1)} \\ &\qquad \left. + A(N+K-j+1) + B(N+K-j+1) \right|_2 \\ &= \left| Y_{N+K-(j-1)} 2^{-(N+K)+(j-1)} + A(N+K-j) + \right. \\ &\qquad \left. + B(N+K-j) \right|_2 \\ &\qquad\qquad (j = 1, \ldots, N+K); \end{aligned} \tag{8}$$

equation (8) describes the recursive operation of the array.

The initial conditions are $A(N+K) = B(N+K) = 0$.

After $N+K$ clock pulses, during the $(N+K+1)$-th clock interval the second term of (8) becomes $Y_0 2^0 + A(1) + B(1)$; at the next clock interval the sign of $\tilde{Y}$ is available at the serial output while inside the array remain bits of weight higher or equal to 2^1 which must be neglected in a modulo-2 addition.

Starting from the left side of the array shown in Fig. 6, the kth cell handles, during the jth clock interval, 5 bits of weight $2^{-(N+K-k+j)}$ giving one bit of weight $2^{-(N+K-k+j)+1}$ which is sent to the cell on the right, another bit of the same weight which is stored in the c.f.f. inside the cell and one bit weighting $2^{-(N+K-k+j)}$ stored in the s.f.f. of the cell. Each cell produces also partial product bits by logical ANDs. Thus an array computes equation (2) in $N+K+1$ clock intervals whose durations are limited by the delay of a two-carry-save adder cascade.

Then, if σ is the clock interval and $2L$ are the poles of the filter, an output sample is computed in $T_s = (N+K+1+L)\sigma$ seconds.

An important result of this solution is that the time required for performing a pair of multiplications gives only an additive contribution to the whole operation time.

This solution requires K cells for each a.m.

Fig. 6. Cell configuration for the sequential a.m.

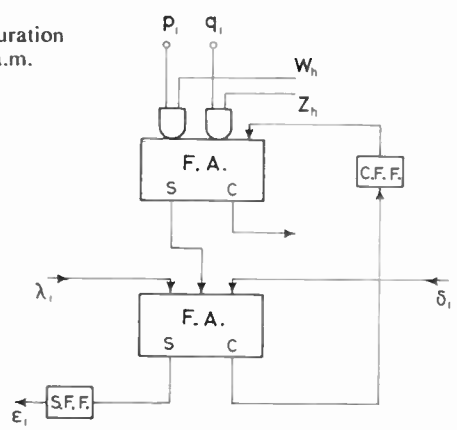

3 Arithmetic Module Parallel Implementation

The algorithm proposed in the last Section can be implemented by the parallel cellular iterative array shown in Fig. 7.

The cell structure is depicted in Fig. 8 (a); it is derived from that of Fig. 6 eliminating c.f.f. and s.f.f. flip-flops

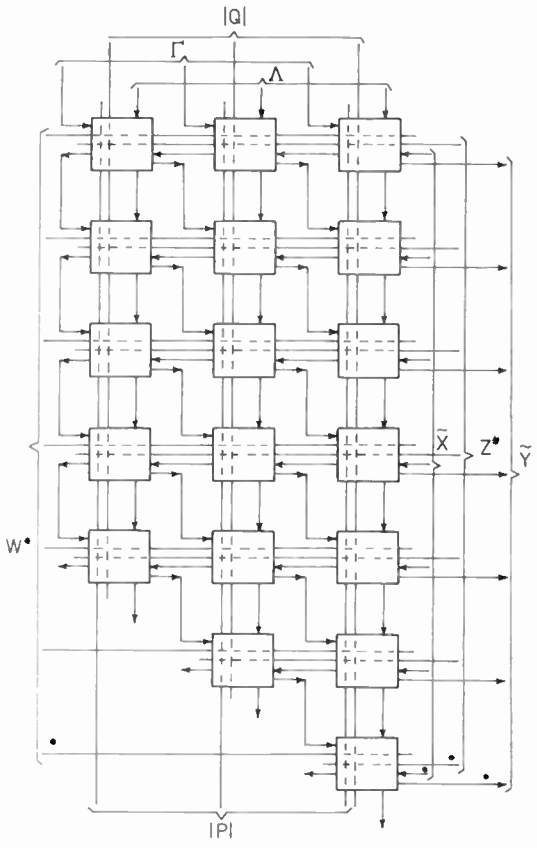

Fig. 7. Iterative array for parallel a.m. implementation.

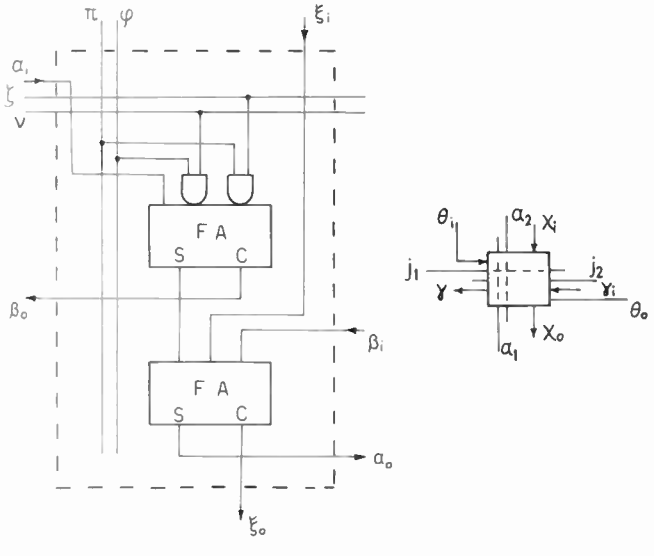

(a)

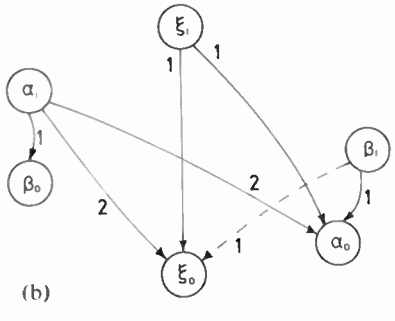

(b)

Fig. 8. Cell configuration for the parallel a.m.

and is described by the following logic functions:

$$\beta_0 = \nu\pi\varphi\zeta + \zeta\pi\alpha_i + \nu\varphi\alpha_i$$
$$\alpha_0 = \zeta\pi \oplus \varphi\nu \oplus \alpha_i \oplus \beta_i \oplus \xi_i$$
$$\xi_0 = (\nu\varphi \oplus \pi\zeta \oplus \alpha_i)(\beta_i + \xi_i) + \beta_i\xi_i.$$

The array is practically a double parallel multiplier where partial product additions are overlapped; variable factors enter in 2's complement notation on the vertical sides of the array; the least significant bit feeds the highest row, the most significant, the sign, feeds the lowest.

The coefficients enter the array from the horizontal sides with the least significant bit in the right-most position; the result is produced at the right side where the bits of $\tilde{X}$ to be added are also introduced. Cells connected diagonally have inputs of the same weight.

A generic row of the array (Fig. 9) performs exactly the recursive relation (8) of the algorithm. Bits having weight $\geqslant 2$ are neglected, according with the fact that multiplications are performed with modulo-2 additions of partial products; for this reason all the cell outputs in Fig. 7 giving bits of weight $\geqslant 2$ are disregarded.

When a variable is to be 2's complemented before multiplication, it is 1's complemented and the corresponding coefficient is added at one of the two additive inputs Γ and Λ available at the top of the array. In fact, if $\overline{W}$ is the 1's complement of W' having $2^{-(N+K)}$ as weight of the least significant bit, and the correct result is to be $\widetilde{PW} = |P|(2-W')$, then:

$$|P|\overline{W} + |P|2^{-(N+K)} = |P|\{2 - W' - 2^{-(N+K)} + 2^{-(N+K)}\}$$
$$= |P|(2-W') = \widetilde{PW}; \qquad (9a)$$

thus the state variables enter the array in the following form:

$$W^* = \begin{cases} W' & \text{if } \operatorname{sgn} P = 0 \\ \overline{W} & \text{if } \operatorname{sgn} P = 1 \end{cases}$$
$$Z^* = \begin{cases} Z' & \text{if } \operatorname{sgn} Q = 0 \\ \overline{Z} & \text{if } \operatorname{sgn} Q = 1. \end{cases} \qquad (9b)$$

The a.m. number of cells is

$$N_c = K(N+1) + \frac{K(K+1)}{2};$$

the total time T_p required for computing an output sample can be obtained from the 'delay diagram' shown in Fig. 8(b). Here each circle represents an input or an output of the cell; if an output is function of an input, an arrow joins these two terminals with a label indicating the number of full-adders through which an input change can cause an output change. It is important to notice that only the α_i input can have two full-adder delays and that a propagation to left has only one full-adder delay and is always limited to one cell.

Thus, if σ_A is the delay introduced by a full adder, then the total array delay is

$$T_a = (2K + N + 1)\sigma_A.$$

If more arrays are connected as in Fig. 2, 3 and 4, multiplications and additions are overlapped: after a delay of $2\sigma_A$ the first row of the array gives its correct result at the cell outputs; in particular the least significant

bit of $\tilde{Y}$ is already available, it can feed an additive or a multiplicative input of another array, and so on. It is easy to verify that, for each configuration of Figs. 2, 3 and 4, a filter having L pole pairs requires, for computing an output sample, a time

$$T_p = (2K+N+1+2L)\sigma_A.$$

All the proposed solutions for recursive filters give the state variables on $N+1+K$ bits; they have to be rounded or truncated to $N+1$ bits before being stored; otherwise their length would increase arbitrarily.

These effects have been thoroughly investigated by Knowles and Edwards.[6]

4 Sequential Cellular Array for Nonrecursive Digital Filters

A nonrecursive digital filter actuates a discrete convolution between a set of coefficients and a set of successive samples of a band-limited waveform $X(t)$.

If $A_0, \ldots, A_l, \ldots, A_L$ are the coefficients and $X(nT-T)$, $\ldots$, $X(nT-lT), \ldots, X(nT-LT)$, are the L samples preceding the nth sample of the input signal $X(nT)$, then the nth sample of the filter output $Y(nT)$ is given by:

$$Y(nT) = \sum_{l=0}^{L} A_l X(nT-lT). \tag{10}$$

Assume that input samples are represented with 2's-complement binary fractions with $N+1$ bits, while coefficients are represented with sign and magnitude binary fractions having $K+1$ bits; for example the constant A_l is represented by $\tilde{A}_l = S_{Al}+|A_l|2^{-K}$, where $S_{Al} = 1$ if A_l is negative, $S_{Al} = 0$ otherwise and

$$|A_l| = \sum_{i=0}^{K-1} a_{i,l}2^i;$$

let $S_{n,l}$ be the sign of the representation $X'_{n,l}$ of $X(nT-lT)$.

The nth output sample $Y(nT)$ is assumed to be obtained as an $(N+K+1)$-bit 2's complement fraction $\tilde{Y}_n$ as follows:

$$\tilde{Y}_n = \left|\tilde{Y}_{n,0}+\tilde{Y}_{n,1}+\ldots+\tilde{Y}_{n,l}+\ldots+\tilde{Y}_{n,L}\right|_2 \tag{11}$$

where

$$\tilde{Y}_{n,l} = |Al|\tilde{X}_{n,l}$$

and

$$\tilde{X}_{n,l} = \begin{cases} X'_{n,l}\,2^{-K} & \text{if } S_{n,l} \oplus S_{Al} = 0 \\ (2-X'_{n,l}\,2^{-K}) & \text{if } S_{n,l} \oplus S_{Al} = 1. \end{cases} \tag{12}$$

The relation (12) shows that a convolution is obtained by a sequence of modulo-2 additions. The addends are products which can also be obtained by modulo-2 additions of the bits of the fractions $\tilde{X}_{n,l}$ shifted and controlled by the bits of $|A_l|$ $(l = 0, 1, \ldots, L)$. The two different types of additions can overlap allowing a large saving in time. This saving can be improved if the additions are performed with carry-save techniques.

A single array whose configuration is shown in Fig. 10(a) is proposed for performing convolutions with an arbitrary number of coefficients. The cell structure is represented in Fig. 10(b).

The array is timed by a clock. During the first clock interval, the inputs to the array are given by the following equations:

$$\text{A1} = |A_L|; \qquad \text{I1} = \tilde{X}_{n,L}$$
$$\text{A2} = |A_{L-1}|; \quad \text{I2} = \tilde{X}_{n,L-1};$$

the array produces a set of partial addends whose sum is:

$$S(1) = \left||A_L|\tilde{X}_{n,L}+|A_{L-1}|\tilde{X}_{n,L-1}\right|_2; \tag{13}$$

the bits of these addends are stored into the flip-flops of each cell and the left-side external flip-flops.

The outputs of the full adders within cells of the same column can be seen as the bits of binary fractions, which starting from the right-most column, can be indicated as:

$$s_0(1), s_1(1), \ldots, s_i(1), \ldots, s_{K-1}(1); \tag{14}$$

analogously the carry outputs γ in the cells of a column can be thought of as bits of the binary fractions:

$$c_0(1), c_1(1), \ldots, c_i(1), \ldots, c_{K-1}(1) \tag{15}$$

where, while the least significant bit of $c_i(1)$ has weight $2^{-(N+K)+i+1}$, the least significant bit of $s_i(1)$ has weight $2^{-(N+K)+i}$ $(i = 0, 1, \ldots, K-1)$.

The sum (13) can also be expressed as:

$$S(1) = \left|\sum_{i=0}^{K-1}\{s_i(1)+c_i(1)\}\right|_2. \tag{16}$$

Similar considerations can be done for the full adders of a column, whose outputs θ represent the set of binary fractions:

$$R_0(1), R_1(1), \ldots, R_i(1), \ldots, R_{K-1}(1) \tag{17}$$

and whose outputs χ represent another set of fractions:

$$G_0(1), G_1(1), \ldots, G_i(1), \ldots, G_{K-1}(1). \tag{18}$$

These numbers are related to those of sets (14) and (15) as follows:

$$\begin{aligned} &R_0(1) = s_0(1); \quad G_0(1) = 0 \\ &|R_1(1)+G_1(1)|_2 = |c_0(1)+s_1(1)|_2 \\ &\cdots\cdots\cdots\cdots\cdots\cdots\cdots \\ &|R_i(1)+G_i(1)|_2 = |c_{i-1}(1)+s_i(1)|_2 \\ &\cdots\cdots\cdots\cdots\cdots\cdots\cdots \\ &|R_{K-1}(1)+G_{K-1}(1)|_2 = |c_{K-2}(1)+s_{K-1}(1)|_2. \end{aligned} \tag{19}$$

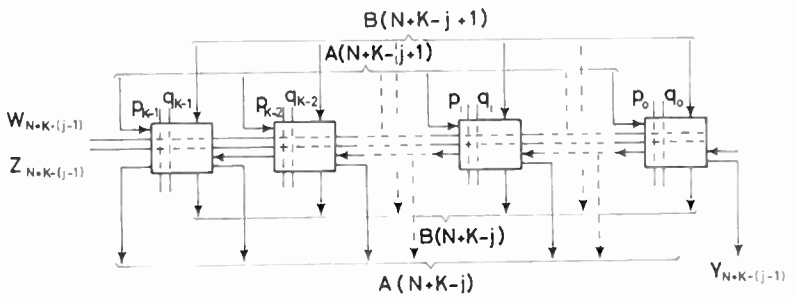

Fig. 9. Generic row of the parallel array.

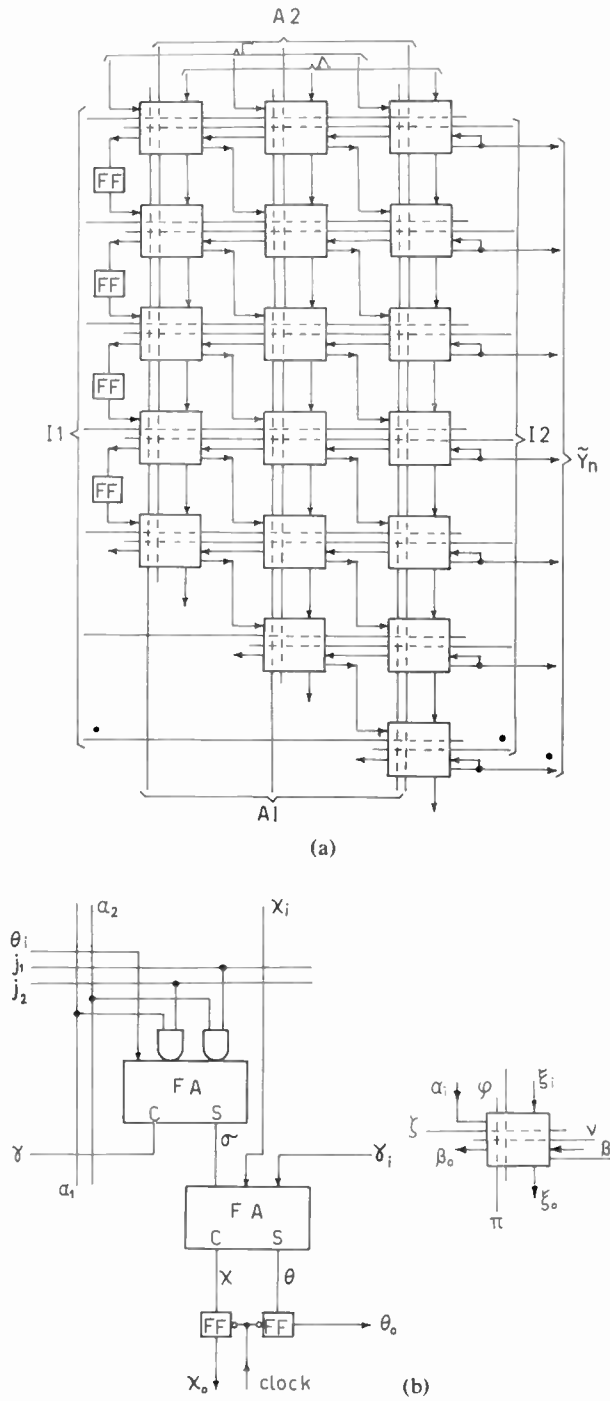

Fig. 10. Iterative array for performing convolutions (a) and the logic of a cell (b).

The numbers $R_0(1),\ldots, R_i(1),\ldots, R_{K-1}(1)$ and $G_0(1), \ldots, G_i(1),\ldots, G_{K-1}(1)$ are stored into the flip-flops inside the cells while into the column of flip-flops at the left-side of the array is stored the number $c_{K-1}(1)$.

Notice that the array performs modulo-2 additions by neglecting the carries having weight 2^1 or higher. Thus $S(1)$ can be obtained from the stored partial addends as follows:

$$S(1) = \left| \sum_{i=0}^{K-1} \{R_i(1)+G_i(1)\} + c_{K-1}(1) \right|_2 . \qquad (20)$$

During the successive clock intervals the array executes similar operations on the stored partial addends, the input samples and the corresponding coefficients up to the F-th interval

$$F = \left[\frac{L+1}{2}\right]^{\dagger}$$

These operations are summarized by the relations:

$$\left|s_i(f)+c_i(f)\right|_2 = \left|a_{i,L-2f}\tilde{X}_{n,L-2f+2} + a_{i,L-2f+1}\tilde{X}_{n,L-2f-1} + R_{i+1}(f-1)\right|_2 \qquad (21)$$

$$c_{K-1}(f) = R_K(f)$$

$$\left|R_i(f)+G_i(f)\right|_2 = \left|c_{i-1}(f)+G_i(f-1)+s_i(f)\right|_2 \qquad (22)$$

$$(f = 1,\ldots, F; \quad i = 0,\ldots, K-1), \quad R_i(0) = G_i(0) = 0.$$

After the Fth clock interval, all the specification inputs (those of the input samples and of the coefficients) are inhibited and during other $N+K$ clock intervals all the stored partial addends are added together to produce an output sample; during these intervals the array operation is described by the following equations:

$$A1 = A2 = A3 = A4 = 0$$

$$\left|R_i(\tau)+G_i(\tau)\right|_2 = \left|G_i(\tau-1)+R_{i+1}(\tau-1)\right|_2 \qquad (23)$$

$$\{\tau = F+1,\ldots, F+N+K; \quad i = 0,\ldots, K-1\}.$$

It is easy to see from Fig. 10(a) that bits of the same weight are carried down from left to right by diagonal paths and the bits of the final result, which are produced sequentially from the least significant, are continuously restored into the cell of the right-most column till all the flip-flops are cleared.

During the last $N+K$ clock intervals, other operations, such serial 2's complementation if required for the next sample computation can be performed outside of the array.

Some details about memory organization and multiplexing are reported in a previous work.[4]

The whole number N_{CL} of clock intervals needed for computing an output sample is:

$$N_{CL} = F+K+N$$

and the clock period must be slightly longer than the delay of two full adders.

The last $N+K$ clock intervals can be substituted by a longer one providing a by-pass command for the flip-flops in the cells.

Two's-complementation of the input variables can be obtained by 1's-complementation and the addition of the corresponding factor through auxiliary inputs Γ and Λ, in accordance with (9).

5 An Alternative Parallel Structure

A large saving in the number of cells can be achieved for the parallel structure using the cellular but not fully iterative array of Fig. 11. The basic cell of the array is that of Fig. 8(a).

The array refers to coefficients of 3 bits plus sign and variables of 3 bits plus sign.

† $[V]$ means V if it is an integer; the higher integer otherwise.

The fourth row of the array adds corrective terms when the variables are negative and the last row performs the final addition to obtain the most significant bits of the output fraction $\tilde{Y}$.

The algorithm follows a suggestion by Deegan[5] for combinational multipliers.

A multiplication, when a variable enters the array as a negative fraction W^*, is performed with the following algorithm.

Let $W^* = 2 - w$.

Let $\widetilde{PW}$ be the fraction representing the product PW.

It is possible to write the fractional part of $\widetilde{PW}$ as follows:

$$\widetilde{PW} - 1 = |P|2^{-K}(1 - w) + 1 - |P|2^{-K}.$$

This fraction is obtained by multiplying $|P|2^{-K}$ by the fractional part of W^* and adding the fractional part of the 2's-complement of $|P|2^{-K}$. The fractional part of the 2's-complement of $|P|2^{-K}$ is obtained complementing all the bits of $|P|2^{-K}$ and adding 2^{-K}.

Analogously the corrective term $1 - |Q|2^{-K}$ is added to the partial product sums if the corresponding variable Z^* is negative.

It is easy to see from Fig. 11 how the corrective terms are conditioned by the signs of the variables.

All the carries having weight 2^0 are added in the two left-most cells of the last row of Fig. 11 with the sign bits of W^*, Z^*, complemented according with (9b), and $\tilde{X}$ for producing the sign bit of $\tilde{Y}$.

The same array with the cell of Fig. 10(b) can be used for performing convolutions.

The proposed alternative solution does not change practically the operation time; the interconnexion path is not fully iterative, but the number of cells is reduced to

$$N_{2c} = K(N+2)+2.$$

6 Performances of the Proposed Techniques

An advantage of the proposed techniques comes from the fact that the most important forms for digital filters can be implemented as iterative arrays of equal modules and each module is an iterative array of equal cells. Hence any sub-array that results and is convenient to be manufactured can be considered as a basic macrocell. Furthermore the cell diagrams of Figs. 6 and 8(a) can be obtained by that of Fig. 10(b) adding respectively an external connexion for c.f.f. or two outputs before the flip-flops. The resulting multi-purpose cell can be obtained as a 16-lead m.s.i. integrated circuit.

All the sequential structures presented in this paper are of the pipe-line type; the overlapping between multiplications and additions leads to a considerable saving in time compared with the solutions that perform multiplications and additions separately.

In the latter case the total time T_0 required for computing an output sample is given by:

$$T_0 = T_a + T_m,$$

where T_a is the time of an addition multiplied by the number of additions and T_m is the time of a multiplication multiplied by the number of multiplications. The designs proposed in Refs. 1, 2 and 3 are of such type.

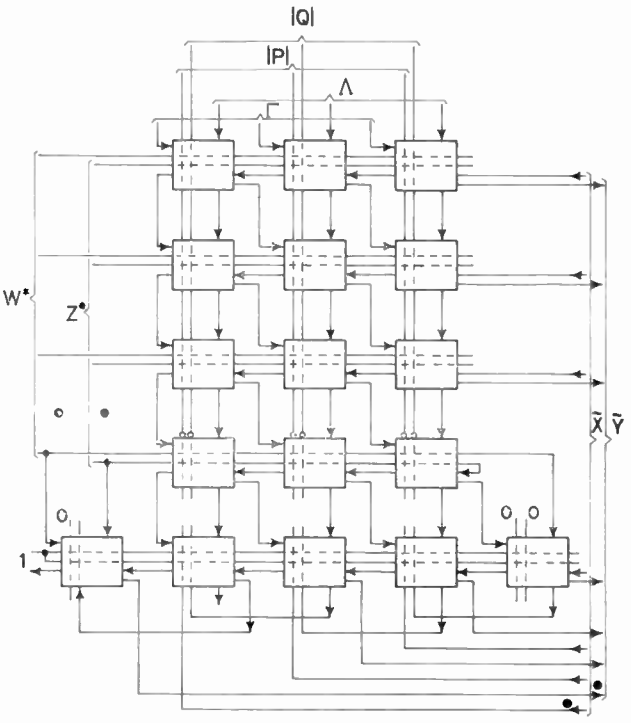

Fig. 11. Alternative cellular array.

The solution proposed here reduces T_m to the time of a single multiplication. Furthermore it requires two flip-flops for each cell as for a sequential carry-save multiplier, but it performs two multiplications and three additions at a time.

The sequential array of Fig. 5 could be realized in a single l.s.i. i.c. The same possibility holds for the convolution array of Fig. 10 or for a more economical version that can be derived from the array of Fig. 11. With such an i.c. and a suitable memory, digital convolutions on video signals could be performed in real-time.

The combinatorial arrays of Fig. 7 or of Fig. 11 could be combined in a three-dimensional structure performing a filter with a very high operating speed to be used for high-frequency signals.

Table 1 summarizes the performances of the proposed solutions. For the recursive filters, solutions (a) refer to implementations according with Figs. 2, 3 and 4, while solutions (b) refer to the case in which only a sub-assembly, corresponding to a second-order filter, is used sequentially to compute an output sample of a higher-order filter. In the latter case, when arrays of Fig. 5 are used, the l.s.b. of a new second-order-block can be obtained immediately after the m.s.b. of the previous second-order-block without requiring any clock interval to be spent only for scaling. Furthermore long shift registers can be used for storing the state variables, while coefficients should be stored into r.o.m.s or r.a.m.s sequentially addressed.

Table 1 can be compared with a valuable solution recently presented by Tewksbury.[10]

Table 1. Performance of the proposed techniques

		Number of modules	Number of cells for a module	Total number of clock intervals	Limit on the duration of a clock interval
Sequential recursive filter	(a)	$2L+1$	K	$N+K+1+L$	$2\sigma_A$
	(b)	2	K	$L(N+K+1)$	$2\sigma_A$
Parallel recursive filter	(a)	$2L+1$	$K\left(N+1+\frac{K+1}{2}\right)$	1	$(2K+N+1+2L)\sigma_A$
	(b)	2	$K\left(N+1+\frac{K+1}{2}\right)$	L	$(2K+N+1)\sigma_A$
Alternative solution	(a)	$2L+1$	$K(N+2)+2$	1	$(2K+N+1+2L)\sigma_A$
	(b)	2	$K(N+2)+2$	L	$(2K+N+1)\sigma_A$
Sequential non-recursive filter		1	$K\left(N+1+\frac{K+1}{2}\right)$	$F+K+N$	$2\sigma_A$
Alternative solution		1	$K(N+2)+2$	$F+K+N$	$2\sigma_A$

Order of the filter: $2L$ — Number of addends in a convolution: $2F$

Number of bits: $\begin{cases}\text{coefficients: } K\\ \text{variables: } N\end{cases}$ — Delay of a gated-full-adder: σ_A

The sequential arithmetic module presented in this paper is comparable with Tewksbury's serial clocked cascade multiplier. The number of delays elements is the same for both the solutions, the elemental cell is more complex in this solution (2 f.a.s instead of 1); the number of cells is identical. Moreover Tewksbury's pipeline multiplier performs a single multiplication in a time equal to $8K\sigma$, while the a.m. proposed here performs two multiplications and three additions in a time equal to $2(N+K+1)\sigma$. Recall that in practice $N \simeq K$. σ is the delay of a carry-save adder.

It is worth noticing that the time of the solution proposed here can be reduced by a half by implementing the two full adders with two logical levels.

Another advantage of the modular assemblage proposed here is that full overlapping is allowed between multiplications and additions, due to the number representation. In this case the results come out as two's-complement fractions; the variable fraction is the only number that needs to be complemented during processing and is sent to the a.m. sequentially. Thus the only possible complementation that is needed is a serial one at the input of the a.m. while Tewksbury's solution requires possible complementations before and after each multiplication.

The sequential non-recursive filter proposed here can be compared with Tewksbury's parallel clocked cascade multiplier for which the time of a single multiplication is

$$\{2[\text{Max}\,(K, N)]+6\}\sigma.$$

In less time, i.e. $2[K+N]\sigma$, the solution presented here performs two multiplications and three additions. The two structures have about the same number of cells; the cells have the same number of delay elements and the solution proposed here has two full-adders per cell instead of one. Again the time of this solution can be reduced by a half by implementing the two full-adders of a cell on two logical levels. Furthermore the algorithm and the structure proposed here allows a large overlapping of multiplications and additions while the pipeline multiplier of positive numbers does not.

In practice, K and N are not very different (typical values are $K = N = 14$); the solutions proposed here have a complexity of about 1·5 with respect to Tewksbury's corresponding solutions but the former are 4 times faster than the latter. Furthermore the complexity of the solutions proposed in this paper is compensated by the fact that the arrays are cellular iterative.

Another interesting comparison can be done with the hardware implementation recently proposed by Peled and Liu.[11] It contains an arithmetic unit that uses read-only memories (r.o.m.); the multiplications are partially performed with table look-up methods. These r.o.m.s substitute the memories used for storing the coefficients but their extension increases exponentially with the number of coefficients. Thus if a second-order section is considered, the solution proposed in this paper requires 5kbits of storage for the coefficients while the Peled and Liu solution requires 2^5kbits of storage. Moreover, the Peled and Liu solution does not appear convenient for programmable filters.

The Peled and Liu solution is compared in Ref. 11 with the solutions of Tewksbury[7] and Jackson *et al.*[1]

A comparison is reported for a multiplexed digital filter where the arithmetic unit of the second-order filter is shared between 128 second-order filters operating at 8 kHz word rate each with words of 12 bits.

The Peled and Liu arithmetic unit requires six 4096-bit r.o.m.s, an adder and some registers for a total of 18 i.c.s consuming about 10 watts.

In Ref. 11 it is shown that the other solutions require many more i.c.s and higher power-consumption.

The sequential a.m. proposed in this paper could be partitioned using 4-bit units. Each such unit would have 16 leads and consume about 0·88W for the carry-save full adders (data from Texas SN74H183) and about 0·5 W for the flip-flops (data from Texas SN74S175). The function to be performed requires two a.m.s clocked at 40 MHz (no carry propagation is involved for the a.m.).

A total of 6 i.c.s is required for implementing the a.m.s proposed in this paper consuming a power of about 9 W. The coefficients can be stored in a memory four times smaller than the one required by Peled and Liu. Furthermore the performances of the logic-in-memory solution proposed here are comparable with those of the Peled and Liu design when considering speed and power consumption of a fixed filter. Peled and Liu have shown that their arithmetic unit is remarkably more convenient than Tewksbury's pipeline multiplier. Thus the same conclusion holds for the array proposed in this paper which has the further advantage that it is easily and quickly programmable while the Peled and Liu arithmetic unit is not.

The advantages of the solutions proposed here open new areas of applications. One of such applications is in speech processing. Assuming $\sigma = 5$ ns for new, fast i.c.s in accordance with Tewksbury, an output sample of a non-recursive digital filter with $F = 30$, $K = 15$ and $N = 10$, can be computed with $N_c = 15+15+10 =$ 40 clock pulses, i.e. in 400 ns.

Using a sampling rate for the speech waveform of 20 kHz a total of 50/0·4 = 125 spectral samples could be obtained in real-time with a single array. Using another array for rectifying and smoothing, a digital spectral analyser with fine frequency resolution could be implemented. The numbers of the above example are of course optimistic but a value of $2\sigma = 20$ ns is certainly acceptable for carry-save adders and the application is still interesting.

Another application of the non-recursive array is for digital adaptive equalizers. These equalizers are required, for example, for a single-side-band modem with class IV-PR-coding, transmitting 128 kbit/s on 32 kHz of the basic group band (60–108 kHz) of a f.d.m. channel.[12] The digital equalizer has to operate at a rate of 32 kHz performing a convolution of about 20 coefficients of 16 bits. A single non-recursive array can be used with a clock rate F_T given by:

$$F_T = (10+16+16) \times 32 \text{ kHz} = 1{\cdot}344 \text{ MHz}.$$

Thus a single array can be used for this purpose and it can be implemented with m.o.s. technology that is particularly suited for low power l.s.i.

Faster arrays can be obtained using bipolar technologies; they can implement fast adaptive equalizers to be used in modems for the supergroup (312–552 kHz) and the pseudo-quaternary group (312–4028 kHz).

The Peled and Liu solutions are not suitable for such applications even if random access memories are used. In fact, an adaptive filter requires a continuous updating of the coefficients that will cause a long time to be spent for loading the r.a.m.s at each sampling interval.

7 Conclusions

Cellular structures for implementing recursive and non-recursive digital filters have been introduced.

They allow very fast filters to be designed where the time required for performing a single multiplication gives only an additive contribution to the total time required for computing an output sample in contrast with the solutions previously proposed[1–3] for which a single multiplication time gives a multiplicative contribution to the total operation time.

Some solutions proposed here are fully iterative representing an attractive possibility for an l.s.i. implementation of high frequency digital filters.

8 Acknowledgments

This work was carried out at the Centro di Elaborazione Numerale dei Segnali of the Consiglio Nazionale delle Ricerche, Italy, as part of a research programme on digital signal processing techniques.

9 References

1. Jackson, L. B., Kaiser, J. F. and McDonald, H. S., 'An approach to the implementation of digital filters'. *IEEE Trans. on Audio and Electroacoustics*, AU-16, No. 3, pp. 413–21, September 1968.
2. Berkley, D. A. and Bateman, T. B., 'General purpose digital filtering for real-time speech processing', Proc. 7th Int. Congr. on Acoustics, Vol. C, pp. 101–5 (Akademiai Kiado, Budapest, 1971).
3. Rabiner, L. R., 'Digital hardware for speech synthesis', *ibid.*, pp. 157–60.
4. De Mori, R., 'Cellular iterative arrays for implementing digital filters', Proc. VIth FCIP Symp. on Information Processing, Mem. D1-5, Bled, Yugoslavia, September 1970.
5. Deegan, I. D., 'Cellular multiplier for signed binary numbers', *Electronics Letters*, 7, pp. 436–7, 1971.
6. Knowles, J. B. and Edwards, R., 'Effect of a finite-word-length computer in a sampled-data feedback system', *Proc. Instn Elect. Engrs.*, 112, pp. 1197–1207, June 1965.
7. Kaiser, J. F., 'Consideration in the hardware implementation of digital filters', Proc. IEEE Conference on Decision and Control, Phoenix, Arizona, November 1974, Paper No. WA 5.1.
8. De Mori, R., 'Design for a syntax-controlled acoustic classifier'. Proc. IFIP Congress, pp. 753–7, 1974 (North Holland Publishing Co., Amsterdam, 1974).
9. Bass, S. C., Leon, B. J. and Jenkins, W. K., 'Multiplier architecture for digital filters', Proc. IEEE Conference on Decision and Control, Phoenix, Arizona, November 1974, Paper No. WA 5.5.
10. Tewksbury, S. K., 'Special purpose hardware implementation of digital filters', Proc. IEEE International Symposium on Circuit Theory, Toronto, Canada, April 1973, pp. 418–21.
11. Peled, A. and Liu, B., 'A new hardware realization of digital filters', *IEEE Trans. on Acoustics, Speech and Signal Processing*, ASSP-22, No. 6, pp. 456–62, December 1974.
12. Gerrish, A. M. and Lawless, W. J., 'A new wideband partial-response data set', Conference Record, 1970 IEEE International Conference on Communications, Mem 70-CP-217-COM, pp. 4–1–4–7.

Manuscript first received by the Institution on 23rd April 1974, in revised form on 3rd July 1974 and in final form on 6th May 1975. (Paper No. 1712/CC 248).

Helicopter Rotor Blade Radar

An interesting new radar that uses the rotor blade of a helicopter as the aerial has been designed and built by the Ferranti Electronic Systems Department, Edinburgh. The first experimental equipment was delivered to the Royal Signals and Radar Establishment at Malvern for installation in a Westland *Wessex* helicopter earlier this year and the development flight trials have now started.

The greatest operational merit derived from incorporating a radar transmitting and receiving aerial in a helicopter's rotor blade is that because of the large span of the rotor blade a very narrow beam in azimuth is produced (approximately $\frac{1}{2}°$). This, in conjunction with the radar's shortest selectable pulse transmission of 50 ns and an aerial rotational speed of 240 rev/min results in a radar picture of exceptionally high resolution being obtained. Thus, with the radar functioning on its shortest range scale of 0·5 km, small features on land can be detected and differentiated one from another at a minimum distance of about 30 m.

These characteristics can significantly extend the operational capabilities of helicopters in which the radar is fitted. For example, in conditions of bad visibility, helicopters will still be able to navigate with precision over land, and safely operate at low altitudes, or keep station with one another. They will also be able to return to their base in bad weather without the need for external assistance, such as GCA. In search-and-rescue operations the high definition of the short-range radar picture should enable small objects, such as survivors at sea, to be detected with certainty.

The radar aerial is built into one blade of the rotor assembly and wholly contained within the existing aerofoil section. The radar picture is projected on two direct-view storage tubes which provide bright displays suitable for viewing under normal lighting conditions. A new in-flight c.r.t. photographic recorder designed by Ferranti is included in the RSRE's trial installation for continuously recording the display together with eight radar operational parameters for subsequent analysis.

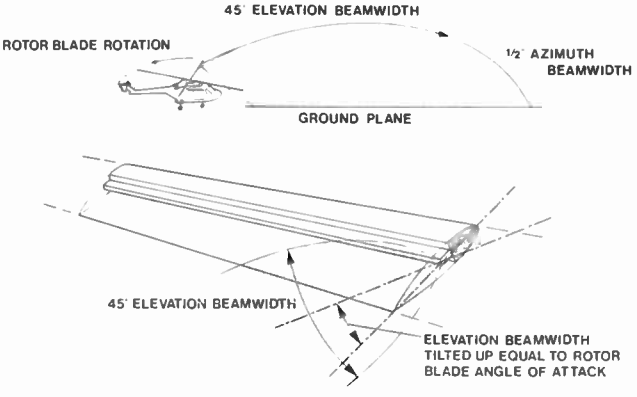

Ferranti rotor blade radar (RODAR).

Operationally the radar display can be selected to be fully ground stabilized in bearing, heading or track. Line-to-line scan conversion is used and the electronic equipment modules incorporate comprehensive built-in test facilities.

Digital Television Trials with Compact Transmission Equipment

Engineers of the Independent Broadcasting Authority's Experimental and Development Department at Crawley, near Winchester, have completed preliminary field trials of very compact digital terminal equipment which occupies only 7 in of a standard 19-in rack. This experimental equipment has been developed as part of the current research into the transmission of high-speed digital video information over broadband channels.

The equipment has been evaluated by sending digitally-encoded 120 Mbits/s colour television signals over a high-capacity coaxial cable system recently installed by the Post Office. Digital waveforms were sent from Southampton to Guildford, via Portsmouth and back again, a route length of approximately 200 200 km. The trials showed that broadcast-standard pictures can be transmitted via the compact terminals without detectable impairment. The inclusion with the picture of ORACLE teletext data requires no special treatment.

The IBA's terminal equipment samples the analogue television waveform at three times the colour sub-carrier frequency, a sampling rate of just over 13·3 MHz. With this sampling rate, linear pulse code modulation at eight bits per sample plus an error-protecting parity bit results in an encoded waveform at 119·8 Mbits/s. This would be outside the tolerances of the Post Office's 120 Mbits/s experimental system so small amounts of extra data are added to the encoded video to increase the bit-rate to 120 Mbits/s $\pm$ 15 parts in 10^6: these extra data are subsequently removed at the receiving terminal.

Though not forming part of these trials, a sound channel can be transmitted without increasing the bit-rate by omitting only three digital words from the video signal during the line synchronizing pulse periods, or by other techniques.

The field trials have confirmed the design features of the IBA's compact terminal equipment and have provided further experience in digital-video transmission. The equipment is to be modified for operation at 150 Mbits/s which may become established, in place of the 120 Mbits/s originally envisaged, as an international digital transmission standard. Two sets of video and sound signals could be transmitted over a 140 Mbits/s channel by digitally-multiplexing the signals and by using any of a number of bit-rate reduction techniques.

The IBA plans to carry out further tests, in co-operation with the Post Office, to investigate the technical and economic potential of long-distance digital transmission systems.

UDC 621.372.543.2:621.372.412

Crystal band-pass lattice filters with equal ripple pass bands and arbitrary stop bands

J. K. STEVENSON, B.Sc., Ph.D.,
M.Inst.P., A.F.I.M.A., C.Eng., M.I.E.E., M.I.E.R.E.*

SUMMARY

A design procedure is given for crystal lattice filters with the attenuation poles (frequencies of infinite attenuation) set to any value. Simple formulae are then provided in terms of the specification data.

The designer selects the number of lattices and the distribution of attenuation poles in each lattice. This flexibility, which is not possible for designs resulting from modern insertion loss theory, is achieved here by returning to image parameter techniques. Different expressions for the image impedance function are given, including equal ripple solutions, to enable the pass-band characteristics to be altered as required with minimal effect on the stop-band response.

* *The General Electric Company Limited, Telecommunications Research Laboratories, Hirst Research Centre, Wembley, Middlesex; now at the Department of Electrical and Electronic Engineering, Polytechnic of the South Bank, London SE1 0AA.*

Principal Symbols

$m = \left(\frac{x_\infty - 1}{x_\infty + 1}\right)^{\frac{1}{2}}$	
P	polynomial in m
R_L	load resistance
T	$\tanh \frac{1}{2}\gamma$
$t = \left(\frac{x+1}{x-1}\right)^{\frac{1}{2}}$	
x, x_∞	normalized real frequency variable, value at attenuation pole
Y_a, Y_b	admittance of series, shunt lattice arms
$y = 10 \log_{10}\left(\frac{x-1}{x+1}\right)$	
Z_i	image impedance
Z_a, Z_b	impedance of series, shunt lattice arms
z	scaling constant for Kosowsky IIm image impedance function
α	insertion loss in dB
$\alpha', \alpha'_r, \alpha'_T$	image attenuation, value for single pole, total value in dB
α'_N	image attenuation in nepers
β	phase shift in radians (source voltage/load voltage)
β'	image phase shift
γ	image transfer function
ω	angular frequency
ω_L	low-pass cut-off frequency
$\omega_0, \omega_{-c}, \omega_c$	band-pass centre, lower cut-off, upper cut-off frequencies
$\Delta\omega$	bandwidth of a band-pass network

1 Introduction

In filter design, image parameter techniques are generally avoided, where possible, owing to the non-optimum solutions obtained, often with unsatisfactory pass bands. The theoretically preferable insertion loss method provides filters with pre-determined characteristics, but affords less control over the grouping of network elements and their relative magnitudes, which is particularly important when crystal resonators are involved.

Image parameter methods are advantageous for realizing a filter with unusual stop-band requirements, since a simple frequency transformation enables a template to be used[1] to rapidly assess the insertion loss resulting from attenuation poles at arbitrary frequencies, which may then be modified to optimize the characteristics. Although this property has subsequently been used in general parameter filters,[2] an excessive amount of computation is involved; also, the final structure is in ladder form and conversion to lattices is rarely possible owing to the lack of network symmetry. For highly selective filters, a single lattice is unsuitable and the subsequent conversion to a multi-lattice structure is only possible if image parameter methods are used, since

surplus factors need to be introduced to maintain the precise image matching of lattice networks of different orders.† The main advantage of the lattice representation is that resistive elements introduce an almost constant insertion loss and result in a reduction of the pass-band ripple, whereas losses in ladder networks distort the pass band.

The image parameter filters considered here are directly realizable in lattice form and involve simple calculations. The synthesis procedure, developed independently of the image impedance function, is a modification and extension of a method by Bown.[3] The most efficient image impedance functions are briefly reviewed, and direct solutions are given for networks up to sixth order with all attenuation poles at infinite frequency, and also general solutions up to third order (all verified by independent analyses). The paper includes results obtained in reference 5. The Kosowsky II image impedance function is recommended for general use, with mismatch at the centre frequency as specified here; this function requires a redundant crystal in each lattice, but in return provides rapid solutions with good pass bands and is less sensitive to component variations than minimum-crystal designs.

2 Analysis of Lattice Networks

For a general two-port network as shown in Fig. 1, the input and output voltages and currents are related as follows,

$$\begin{pmatrix} V_1 \\ I_1 \end{pmatrix} = (T_0)\begin{pmatrix} V_2 \\ I_2 \end{pmatrix} = \begin{pmatrix} A & B \\ C & D \end{pmatrix}\begin{pmatrix} V_2 \\ I_2 \end{pmatrix}, \quad e^{-2\gamma} = \frac{V_2 I_2}{V_1 I_1}.$$

If the network is symmetrical, the transmission matrix is given by

$$(T_0) = \begin{pmatrix} \cosh\gamma & Z_i \sinh\gamma \\ \sinh\gamma / Z_i & \cosh\gamma \end{pmatrix}. \tag{1}$$

† Two lattices, which are composed of series, shunt impedances Z_{a1}, Z_{b1} and Z_{a2}, Z_{b2}, can be combined to form a single lattice, provided that the image impedances are equal, i.e.

$$(Z_{a1}Z_{b1})^{\frac{1}{2}} = (Z_{a2}Z_{b2})^{\frac{1}{2}} = Z_i.$$

Then,

$$(Z_aZ_b)^{\frac{1}{2}} = Z_i$$

where Z_a and Z_b, the impedances of the equivalent single lattice, are given as follows,[3,4]

$$Z_a = \frac{(Z_{a1}+Z_{a2})(Z_{b1}+Z_{b2})}{Z_{a1}+Z_{b1}+Z_{a2}+Z_{b2}}, \quad Z_b = \frac{(Z_{a1}+Z_{b2})(Z_{a2}+Z_{b1})}{Z_{a1}+Z_{b1}+Z_{a2}+Z_{b2}}.$$

We are concerned with the reverse problem, namely the breaking down of a single lattice into two or more lattices whose tandem combination is equivalent to the original. Since Z_a and Z_b are of a higher order than Z_{a1}, Z_{b1}, Z_{a2} and Z_{b2}, they need to contain factors which cancel on multiplication. In the design method described here, a low-order function is chosen for Z_i and the lattice arm impedances are obtained by multiplying this function by factors of the form Z_1/Z_2 and its inverse, i.e.

$$Z_a = Z_i\frac{Z_1}{Z_2}, \quad Z_b = Z_i\frac{Z_2}{Z_1}.$$

Note that Z_i defines the upper limit of insertion loss in the pass band, and γ or Z_1/Z_2 define the lower limit of insertion loss in the stop band.

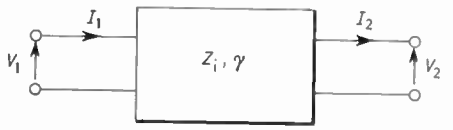

Fig. 1. General representation of a two-port network.

In image parameter theory, Z_i and γ, the characteristic impedance and propagation coefficient, respectively, are generally referred to as the image impedance and image transfer function. We will restrict ourselves to a symmetrical lattice network as given in Fig. 2. Then,[6]

$$(T_0) = \begin{pmatrix} \frac{Z_b+Z_a}{Z_b-Z_a} & \frac{2Z_aZ_b}{Z_b-Z_a} \\ \frac{2}{Z_b-Z_a} & \frac{Z_b+Z_a}{Z_b-Z_a} \end{pmatrix}. \tag{2}$$

Hence,

$$Z_a = \frac{A-1}{C}, \quad Z_b = \frac{A+1}{C}.$$

Using equation (1),

$$\left.\begin{aligned} Z_a &= Z_i\frac{\cosh\gamma-1}{\sinh\gamma} = Z_i\tanh\tfrac{1}{2}\gamma \\ Z_b &= Z_i\frac{\cosh\gamma+1}{\sinh\gamma} = Z_i\coth\tfrac{1}{2}\gamma \end{aligned}\right\} \tag{3}$$

Therefore,

$$Z_i = (Z_aZ_b)^{\frac{1}{2}} \tag{4}$$

$$\tanh\tfrac{1}{2}\gamma = \left(\frac{Z_a}{Z_b}\right)^{\frac{1}{2}}. \tag{5}$$

Let Z_a and Z_b be lossless, i.e. reactive. Z_i is resistive when these reactances are of opposite sign and reactive when of the same sign, as seen from equation (4). This defines the pass and stop bands, respectively. The insertion loss α for the circuit in Fig. 2 is given as follows,

$$\alpha = 20\log_{10}\left|\frac{\frac{1}{2}V_0}{V_2}\right| = 20\log_{10}\left|\frac{AR_L+B+CR_L^2+DR_L}{2R_L}\right|$$

From equation (2),

$$\alpha = 10\log_{10}\left[1+\left|\frac{R_L^2-Z_aZ_b}{R_L(Z_a-Z_b)}\right|^2\right] \tag{6}$$

$\frac{1}{2}V_0/V_2$ is the ratio of the maximum output voltage (for given source and load terminations) to the actual output voltage. Let T_1 represent the transmission matrix for the

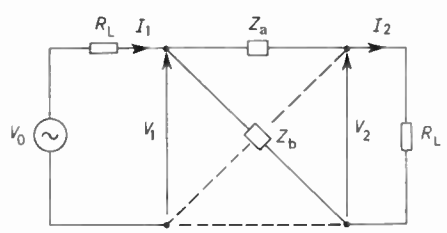

Fig. 2. Terminated single lattice network.

given network plus source resistance R_L. Then

$$(T_1) = \begin{pmatrix} A' & B' \\ C' & D' \end{pmatrix} = \begin{pmatrix} 1 & R_L \\ 0 & 1 \end{pmatrix} (T_0)$$

$$= \begin{pmatrix} \cosh\gamma + \dfrac{R_L}{Z_i}\sinh\gamma & R_L\cosh\gamma + Z_i\sinh\gamma \\ \dfrac{1}{Z_i}\sinh\gamma & \cosh\gamma \end{pmatrix}$$

From Fig. 2,

$$\begin{pmatrix} V_0 \\ I_1 \end{pmatrix} = (T_1)\begin{pmatrix} V_2 \\ V_2/R_L \end{pmatrix}.$$

Hence

$$\alpha = 20\log_{10}\left|\frac{1}{2}\left(A' + \frac{B'}{R_L}\right)\right|$$

$$= 20\log_{10}\left|\cosh\gamma + \frac{1}{2}\left(\frac{Z_i}{R_L} + \frac{R_L}{Z_i}\right)\sinh\gamma\right| \qquad (7)$$

Let

$$\gamma = \alpha'_N + j\beta'$$

where α'_N is the image attenuation in nepers and β' the image phase shift.

2.1 Insertion Loss in Pass band

In the pass band, Z_i is real and γ imaginary. Equation (7) becomes

$$\alpha = 20\log_{10}\left|\cos\beta' + j\frac{1}{2}\left(\frac{Z_i}{R_L} + \frac{R_L}{Z_i}\right)\sin\beta'\right|$$

$$= 10\log_{10}\left[\cos^2\beta' + \frac{1}{4}\left(\frac{Z_i}{R_L} + \frac{R_L}{Z_i}\right)^2\sin^2\beta'\right]. \qquad (8)$$

The phase shift β is given by

$$\beta = \tan^{-1}\left[\frac{1}{2}\left(\frac{Z_i}{R_L} + \frac{R_L}{Z_i}\right)\tan\beta'\right].$$

Note that $\beta = \beta'$ when $\beta' = \frac{1}{2}r\pi$; r is an integer or zero. The insertion loss varies between zero when $\beta = \beta' = r\pi$ and a maximum value when $\beta = \beta' = (r+\frac{1}{2})\pi$, as follows

$$\alpha_{max} = 20\log_{10}\frac{1}{2}\left(\frac{Z_i}{R_L} + \frac{R_L}{Z_i}\right) \qquad (9)$$

..maximum insertion loss in pass band.

Putting $Z_i = R_i$, equation (3) becomes

$$Z_a = jR_i\tan\tfrac{1}{2}\beta', \quad Z_b = -jR_i\cot\tfrac{1}{2}\beta'.$$

The insertion loss is therefore zero when $Z_i = R_i = R_L$ as suggested by equation (9). It is also zero when either of the following is satisfied.

$$Z_a = 0, \quad Z_b = \infty; \qquad Z_a = \infty, \quad Z_b = 0.$$

These last two conditions correspond to $\beta\ (=\beta') = 0, \pm 2\pi, \pm 4\pi, \ldots$, and $\beta\ (=\beta') \pm\pi, \pm 3\pi, \pm 5\pi, \ldots$, respectively. The insertion loss is the maximum value, as given by equation (9), when $\beta\ (=\beta') = \pm\pi/2, \pm 3\pi/2, \pm 5\pi/2, \ldots$. The network then behaves as an impedance inverter and produces the maximum mismatch between source and load for given values of R_L and R_i. The load termination R_L appears to the source as a resistance of value R_i^2/R_L, and the network arms at these frequencies may be represented as follows,†

$$Z_a = \pm jR_i, \quad Z_b = \mp jR_i.$$

2.2 Insertion Loss in Stop Band

In the stop band, Z_i is imaginary and γ real ($\pm j\pi$ if $Z_a > Z_b$, as shown in Section 3.2). Equation (7) becomes

$$\alpha = 10\log_{10}\left[1 - \frac{1}{4}\left(\frac{Z_i}{R_L} - \frac{R_L}{Z_i}\right)^2\sinh^2\gamma\right]$$

$$= 10\log_{10}\left[1 + \left|\frac{1}{2}\left(\frac{Z_i}{R_L} - \frac{R_L}{Z_i}\right)\sinh\gamma\right|^2\right].$$

α varies between infinity when $Z_i = 0, \infty$ and a minimum value when $Z_i = \pm jR_L$ given as follows,

$$\alpha_{min} = 20\log_{10}|\cosh\gamma| \simeq 20\log_{10}\left|\frac{e^{\gamma}}{2}\right|$$

$$= 20\alpha'_N\log_{10}e - 6{\cdot}021 = 8{\cdot}686\alpha'_N - 6{\cdot}021.$$

α'_N is the image attenuation in nepers; it is more convenient to consider attenuation in decibels so we will introduce $\alpha' = 8{\cdot}686\alpha'_N$ as the equivalent image attenuathen in dB. Then

$\alpha_{min} = \alpha' - 6$..minimum insertion loss in stop band (10)

3 General Design Procedure

3.1 Frequency Transformation

The design algebra is simplified by introducing a normalized real frequency variable, x. With ω_0, ω_c, ω_{-c} denoting the band-pass centre, upper cut-off, and lower cut-off frequencies, respectively, the frequency variable is given as follows,

$$x \equiv \left(\frac{\omega}{\omega_L}\right)_{\text{low-pass}} \equiv \left(\frac{\omega/\omega_0 - \omega_0/\omega}{\omega_c/\omega_0 - \omega_0/\omega_c}\right)_{\text{band-pass}}.$$

With $x = -1, 0, 1$ at $\omega = \omega_{-c}, \omega_0, \omega_c$, respectively, we obtain

$$\omega_{-c}\omega_c = \omega_0^2.$$

The pass-band of the majority of filters is sufficiently narrow for the following approximation to be used,

$$x \simeq \frac{\omega - \omega_0}{\omega_c - \omega_0} \simeq \frac{2}{\Delta\omega}(\omega - \omega_0)$$

$$\omega_{-c} + \omega_c \simeq 2\omega_0$$

where $\Delta\omega = \omega_c - \omega_{-c}$. For filters with attenuation poles realized by crystal motional reactances, these 'approximate' expressions are in fact more accurate,[7]

† Note that for given values of R_L and R_i, the variation of insertion loss with phase shift at any frequency in the pass band can be found by treating the lattice (or image-matched multi-lattice structure) as a transmission line. The equivalence is suggested by equation (1) which applies to a line when γ is replaced by γl, where l is the length of line; the difference arises from the definition of γ, which for a line is no longer the propagation coefficient for the whole filter but the value per unit length. For a transmission line, the insertion loss is zero when its length is an integral number of half wavelengths, and maximum when its length is an odd number of quarter wavelengths; the insertion loss is always zero when $R_i = R_L$. Similar results are given by the lattice analysis in Section 2.1.

the original band-pass expression for x being based on a circuit composed of lumped elements.

3.2 Single Attenuation Pole

Using equation (5) we will define

$$T = \tanh \tfrac{1}{2}\gamma = \left(\frac{Z_a}{Z_b}\right)^{\frac{1}{2}}.$$

Then, from equation (3),

$$Z_a = Z_i T, \quad Z_b = \frac{Z_i}{T}. \tag{11}$$

Also,

$$\gamma = \log \frac{1+T}{1-T}$$

i.e.

$$\gamma = \log \left|\frac{1+T}{1-T}\right| \qquad \text{for } Z_a < Z_b$$

$$\gamma = \log \left(-\left|\frac{1+T}{1-T}\right|\right)$$

$$= \log \left|\frac{1+T}{1-T}\right| \pm j\pi \qquad \text{for } Z_a > Z_b.$$

Hence,

$$\alpha' = 20 \log_{10} \left|\frac{1+T}{1-T}\right|. \tag{12}$$

A phase shift of π occurs when $Z_a > Z_b$.

We next define

$$t = \left(\frac{x+1}{x-1}\right)^{\frac{1}{2}} \simeq \left(\frac{\omega-\omega_c}{\omega-\omega_c}\right)^{\frac{1}{2}} \tag{13}$$

and for a lattice network with one attenuation pole at $\omega = \omega_\infty$ (which corresponds to $x = x_\infty$) let

$$T = mt. \tag{14}$$

At an attenuation pole, $T = \tanh \frac{1}{2}\gamma = 1$, and therefore the value of m corresponding to a pole at $x = x_\infty$ is given by

$$m = \left(\frac{x_\infty - 1}{x_\infty + 1}\right)^{\frac{1}{2}}. \tag{15}$$

From equations (12) and (14), the image attenuation in decibels at any value of x in the stop band, resulting from a network with a single attenuation pole at $x = x_\infty$, is given as follows,

$$\alpha' = 20 \log_{10} \left|\frac{1+mt}{1-mt}\right|$$

$$= 20 \log_{10} \left|\frac{1 + \left(\frac{x_\infty - 1}{x_\infty + 1}\right)^{\frac{1}{2}} \left(\frac{x+1}{x-1}\right)^{\frac{1}{2}}}{1 - \left(\frac{x_\infty - 1}{x_\infty + 1}\right)^{\frac{1}{2}} \left(\frac{x+1}{x-1}\right)^{\frac{1}{2}}}\right|. \tag{16}$$

The admittances of the arms a and b are given by equations (11), (13) and (14) as follows,

$$\left.\begin{aligned} Y_a &= \frac{1}{Z_a} = \frac{1}{mR_L}\left(\frac{R_L}{Z_i}\right)\left(\frac{x-1}{x+1}\right)^{\frac{1}{2}} \\ Y_b &= \frac{1}{Z_b} = \frac{m}{R_L}\left(\frac{R_L}{Z_i}\right)\left(\frac{x+1}{x-1}\right)^{\frac{1}{2}} \end{aligned}\right\} \begin{array}{l}\text{Lattice arm} \\ \text{admittances for} \\ \text{one attenuation} \\ \text{pole}\end{array} \tag{17}$$

The ratio Z_i/R_L, which is dealt with in Section 4, is termed the image impedance function; it is chosen by the designer as a function of x.

3.3 Multiple Attenuation Poles

Equation (16) gives the contribution to the total image attenuation resulting from an individual pole in a multi-pole network, i.e.

$$\alpha'_r = 20 \log_{10} \left|\frac{1 + \left(\frac{x_{\infty r} - 1}{x_{\infty r} + 1}\right)^{\frac{1}{2}} \left(\frac{x+1}{x-1}\right)^{\frac{1}{2}}}{1 - \left(\frac{x_{\infty r} - 1}{x_{\infty r} + 1}\right)^{\frac{1}{2}} \left(\frac{x+1}{x-1}\right)^{\frac{1}{2}}}\right| \tag{18}$$

where α'_r is the image attenuation resulting from a single pole at $x = x_{\infty r}$. For a network containing n poles, the total image attenuation is given by

$$\alpha'_T = \sum_{r=1}^{n} \alpha'_r = \sum_{r=1}^{n} 20 \log_{10} \left|\frac{1+m_r t}{1-m_r t}\right|$$

$$= 20 \log_{10} \left|\prod_{r=1}^{n} \frac{1+m_r t}{1-m_r t}\right|$$

$$= 20 \log_{10} \left|\frac{(1+m_1 t)(1+m_2 t)\ldots(1+m_n t)}{(1-m_1 t)(1-m_2 t)\ldots(1-m_n t)}\right|.$$

Using equation (12),

$$\alpha'_T = 20 \log_{10} \left|\frac{1 + a_1 t + a_2 t^2 + \ldots + a_n t^n}{1 - a_1 t + a_2 t^2 - \ldots + (-1)^n a_n t^n}\right|$$

$$= 20 \log_{10} \left|\frac{1+T}{1-T}\right|. \tag{19}$$

The n values of m are denoted m_1 to m_n, T corresponds to the composite network, and a_1 to a_n are constants. Let

$$P = (1+m_1 t)(1+m_2 t)\ldots(1+m_n t)$$

$$= 1 + a_1 t + a_2 t^2 + \ldots + a_n t^n. \tag{20}$$

From equation (19),

$$\alpha'_T = 20 \log_{10} \left|\frac{1 + \dfrac{a_1 t + a_3 t^3 + \ldots + a_n t^n}{1 + a_2 t^2 + \ldots + a_{n-1} t^{n-1}}}{1 - \dfrac{a_1 t + a_3 t^2 + \ldots + a_n t^n}{1 + a_2 t^2 + \ldots + a_{n-1} t^{n-1}}}\right| \quad \text{for } n \text{ odd}$$

$$= 20 \log_{10} \left|\frac{1 + \dfrac{a_1 t + a_3 t^3 + \ldots + a_{n-1} t^{n-1}}{1 + a_2 t^2 + \ldots + a_n t^n}}{1 - \dfrac{a_1 t + a_3 t^3 + \ldots + a_{n-1} t^{n-1}}{1 + a_2 t^2 + \ldots + a_n t^n}}\right| \quad \text{for } n \text{ even}$$

$$= 20 \log_{10} \left|\frac{1 + \dfrac{P_o}{P_e}}{1 - \dfrac{P_o}{P_e}}\right|.$$

Hence,

$$T = \frac{P_o}{P_e} \tag{21}$$

where P_e and P_o denote the even and odd parts of the polynomial P in t.

Using equations (11), (13) and (21), the general form

of equation (17) is seen to be

$$\left.\begin{aligned} Y_a &= \frac{1}{R_L}\left(\frac{R_L}{Z_i}\right)\left(\frac{x-1}{x+1}\right)^{\frac{1}{2}}\frac{P_e}{P_o/t} \\ Y_b &= \frac{1}{R_L}\left(\frac{R_L}{Z_i}\right)\left(\frac{x+1}{x-1}\right)^{\frac{1}{2}}\frac{P_o/t}{P_e} \end{aligned}\right\} \qquad (22)$$

$P_o/(tP_e)$, which is a rational function in t^2, is converted to a rational function in x using equation (13), i.e.

$$f(x) = \frac{P_o/t}{P_e} = \frac{a_1 + a_3t^2 + a_5t^4 + \ldots}{1 + a_2t^2 + a_4t^4 + \ldots}$$

$$= \frac{a_1 + a_3\left(\frac{x+1}{x-1}\right) + a_5\left(\frac{x+1}{x-1}\right)^2 + \ldots}{1 + a_2\left(\frac{x+1}{x-1}\right) + a_4\left(\frac{x+1}{x-1}\right)^2 + \ldots}$$

where

$$a_1 = \sum_{u=1}^{n} m_u$$

$$a_2 = \sum_{u=1}^{n-1}\sum_{v=u+1}^{n} m_u m_v$$

$$a_3 = \sum_{u=1}^{n-2}\sum_{v=u+1}^{n-1}\sum_{w=v+1}^{n} m_u m_v m_w, \text{ etc.}$$

The summation limits indicate that $u < v < w$.

3.4 Determination of Network Order and Values for m

To determine the number and location of attenuation poles to meet a particular specification, tables of α' against x for different values of x_∞ are easily prepared based on equation (18).[3] The image attenuation resulting from each of the poles is then added and 6 dB subtracted from the total to give the minimum stop-band insertion loss, as given by equation (10).

Instead of tables, templates may be used. Laurent's transformation[1] is more conveniently replaced by the following,

$$y = 10\log_{10}\left(\frac{x-1}{x+1}\right)$$

with logarithms to base 10 for numerical simplicity. Putting

$$y_\infty = 10\log_{10}\left(\frac{x_\infty - 1}{x_\infty + 1}\right) \qquad (23)$$

equation (16) becomes

$$\alpha' = 20\log_{10}\left|\frac{1 + 10^{y_\infty/20}10^{-y/20}}{1 - 10^{y_\infty/20}10^{-y/20}}\right|$$

$$= 20\log_{10}\left|\frac{10^{(y-y_\infty)/20} + 1}{10^{(y-y_\infty)/20} - 1}\right|$$

$$= 20\log_{10}\coth\left|\frac{y - y_\infty}{40}\log 10\right|$$

$$= 20\log_{10}\coth\left|\frac{y - y_\infty}{17{\cdot}37}\right| \qquad (24)$$

The image attenuation depends only on the difference between y and y_∞, so a template is easily constructed of γ against $(y - y_\infty)$ using equation (24). A curve is drawn for each pole and the γ values added. Having determined the most suitable values of y_∞, we obtain x_∞ and m from equations (15) and (23) as follows,

$$x_\infty = \frac{1 + 10^{y_\infty/10}}{1 - 10^{y_\infty/10}}, \quad m = 10^{y_\infty/20}. \qquad (25)$$

4 Criteria for Choosing Image Impedance Functions

We require the image impedance function Z_i/R_L to be chosen so that Y_a and Y_b in equation (22) are rational functions of x. Also

$$Z_i/R_L \text{ real for } -1 < x < 1$$

$$Z_i/R_L \text{ imaginary for } |x| > 1.$$

These are basic requirements fundamental to image parameter theory. In addition, maximum transmission occurs when $Z_i/R_L = 1$ (usually required at the centre frequency, $x = 0$). The order of the numerator of Y_a and Y_b should in general not exceed that of the denominator, otherwise the realization will include parallel resonant circuits. An exception is the introduction of a single parallel resonant circuit to provide an inductor of suitable value to resonate with circuit capacitance. The order of the denominator gives the number of resonant circuits to be realized with crystals, so this value should be as small as possible.

When the network order, n, is even, the numerator of $P_o/(tP_e)$ is one order in t^2 less than the denominator, resulting in a term $(x-1)$ in the numerator of the equivalent rational function in x. Equation (22) may be rewritten

$$\left.\begin{aligned} Y_a &= \frac{1}{R_L}\left(\frac{R_L}{Z_i}\right)\left(\frac{x-1}{x+1}\right)^{\frac{1}{2}}\frac{1}{f(x)} \\ Y_b &= \frac{1}{R_L}\left(\frac{R_L}{Z_i}\right)\left(\frac{x+1}{x-1}\right)^{\frac{1}{2}} f(x) \end{aligned}\right\} \text{for general usage}$$

$$\left.\begin{aligned} Y_a &= \frac{1}{R_L}\left(\frac{R_L}{Z_i}\right)\left(\frac{1}{x^2-1}\right)^{\frac{1}{2}}\frac{1}{f_1(x)} \\ Y_b &= \frac{1}{R_L}\left(\frac{R_L}{Z_i}\right)(x^2-1)^{\frac{1}{2}} f_1(x) \end{aligned}\right\} \text{for } n \text{ even}$$

where

$$f(x) = (x-1)f_1(x) = \frac{P_o/t}{P_e}$$

$f(x)$ is a rational function in x with numerator and denominator of the same degree; values for sections up to third order (corresponding to three-pole single lattices) are given in Table 1. When n is even, $f(x)$ always contains a zero at $x = 1$.

It is desirable for the image impedance function to cancel or partly cancel the 'square root' expressions in x to reduce the order. The most obvious choices for Z_i/R_L are therefore as follows,

$$\frac{Z_i}{R_L} = \left(\frac{1+x}{1-x}\right)^{\frac{1}{2}} \qquad \text{Kosowsky I} \qquad (26)$$

$$\left.\begin{aligned} \frac{Z_i}{R_L} &= (1-x^2)^{\frac{1}{2}} && \text{Kosowsky II} \\ \frac{Z_i}{R_L} &= z(1-x^2)^{\frac{1}{2}}, \quad z > 1 && \text{Kosowsky IIm} \end{aligned}\right\} \qquad (27)$$

Table 1. Value of response function, $f(x)$

Order of section	$f(x)$
1	m
2	$\dfrac{m_1+m_2}{1+m_1m_2}\cdot\dfrac{x-1}{x+\dfrac{m_1m_2-1}{m_1m_2+1}}$
3	$\dfrac{m_1+m_2+m_3+m_1m_2m_3}{1+m_1m_2+m_2m_3+m_3m_1}\cdot\dfrac{x-\dfrac{m_1+m_2+m_3-m_1m_2m_3}{m_1+m_2+m_3+m_1m_2m_3}}{x+\dfrac{m_1m_2+m_2m_3+m_3m_1-1}{m_1m_2+m_2m_3+m_3m_1+1}}$

Since

$$\left(\frac{\omega-\omega_{-c}}{\omega_c-\omega}\right)\simeq\left(\frac{1+x}{1-x}\right)^{\frac{1}{2}}$$

$$\left[\frac{(\omega-\omega_{-c})(\omega_c-\omega)}{(\omega_c-\omega_0)^2}\right]^{\frac{1}{2}}\simeq(1-x^2)^{\frac{1}{2}}$$

equations (26) and (27) are the Kosowsky characteristics type I and II,† respectively.[8] The inverse of equation (26) results in a parallel negative capacitor in each arm; the corresponding realization with an inductor is possible but undesirable. The Kosowsky admittances are as follows:

	n odd	n even
Kosowsky I		
$Y_a=-\dfrac{1}{jR_L}\dfrac{x-1}{x+1}\dfrac{1}{f(x)}$	$\frac{1}{2}(n+1)$,	$\frac{1}{2}n$ crystals
$Y_b=-\dfrac{1}{jR_L}f(x)$	$\frac{1}{2}(n-1)$,	$\frac{1}{2}n$ crystals
Kosowsky II		
$Y_a=\dfrac{1}{jzR_L}\dfrac{1}{x+1}\dfrac{1}{f(x)}$	$\frac{1}{2}(n+1)$,	$\frac{1}{2}n+1$ crystals
$Y_b=\dfrac{1}{jzR_L}\dfrac{1}{x-1}f(x)$	$\frac{1}{2}(n+1)$,	$\frac{1}{2}n$ crystals

Note that the sign of j (resulting from a square root) is chosen for realization with positive elements. The addition of the multiplying factor, z, to the Kosowsky II response (to produce IIm) results in two matching frequencies in place of one, and a reduction in overall ripple. Type II, unlike type I, requires an extra crystal per lattice, i.e. $(n+1)$ for a single-lattice filter.

Stop-band insertion loss minima are associated with image impedance functions; at these frequencies, x_{min}, the insertion loss in decibels is given by equation (10), i.e. $\alpha_{min}=\alpha'-6$. Provided that no attenuation poles are below the first 'minimum', the response will be monotonic between the final 'maximum' in the pass band and first 'minimum' in the stop band. Values for the minima of Kosowsky characteristics are given in Table 2. They are obtained by setting the second expression in equation (7) to zero, i.e. $Z_i/R_L=\pm j$.

† Kosowsky IIm denotes a Kosowsky II image impedance function which is mismatched by a factor z at the centre frequency (but matched at a frequency on either side).

For Kosowsky IIm, values of x_{min} for different values of z are given by

$$\frac{Z_i}{R_L}=j=z(1-x_{min}^2)^{\frac{1}{2}}.$$

Hence,

$$x_{min}=\left(1+\frac{1}{z^2}\right)^{\frac{1}{2}}.$$

for the frequency at which the stop-band insertion loss is given by $\alpha'-6$.

5 Design of a Kosowsky IIm Lattice Filter

5.1 Determination of Lattice Arm Admittances

We will demonstrate the synthesis procedure by designing a filter with a Kosowsky IIm image impedance function, and with attenuation poles at any frequency. Having decided the number and location of these poles, we determine the values of m from equations (15) or (25). The filter may then be realized as a single lattice, or alternatively the m-values may be divided between several lattices which are realized individually. We consider here the realization of a third-order lattice with m-values m_1, m_2 and m_3.

We firstly derive P using equation (20):

$$\begin{aligned}P&=(1+m_1t)(1+m_2t)(1+m_3t)\\&=1+(m_1+m_2+m_3)t+\\&\quad+(m_1m_2+m_2m_3+m_3m_1)t^2+m_1m_2m_3t^3.\end{aligned}$$

To simplify the algebra we set

$$\begin{aligned}a_1&=m_1+m_2+m_3,\\a_2&=m_1m_2+m_2m_3+m_3m_1,\\a_3&=m_1m_2m_3.\end{aligned}$$

Hence,

$$f(x)=\frac{P_o/t}{P_e}=\frac{a_1+a_3t^2}{1+a_2t^2}=\frac{a_1+a_3\left(\dfrac{x+1}{x-1}\right)}{1+a_2\left(\dfrac{x+1}{x-1}\right)}$$

$$=\frac{a_1+a_3}{1+a_2}\cdot\frac{x+\dfrac{a_3-a_1}{a_3+a_1}}{x+\dfrac{a_2-1}{a_2+1}}.$$

Table 2. General properties of image impedance functions†

	Insertion loss	Values of x						
		Kosowsky I	Kosowsky II	Kosowsky IIm (defined by z below)				
				1·05	1·10	1·15	1·20	1·25	1·30
x_0	Zero	0	0	0·30	0·42	0·49	0·55	0·60	0·64
x_p	Equals value at $x = 0$	—	—	0·42	0·56	0·65	0·72	0·77	0·81
x_{min}	Stop-band minimum	∞	1·41	1·38	1·35	1·33	1·30	1·28	1·26

† This Table gives the normalized frequencies at which (a) the insertion loss is zero: $x = x_0$; (b) the upper limit of insertion loss in the pass band equals the value at zero frequency: $x = x_p$; (c) the insertion loss in the stop band equals the lower limit, as defined by γ: $x = x_{min}$.

Therefore,

$$Y_a = \frac{1}{jzR_L}\frac{1}{x+1}\frac{1}{f(x)}$$

$$= \frac{1}{jzR_L}\frac{1+a_2}{a_1+a_3}\left[\frac{x+\dfrac{a_2-1}{a_2+1}}{(x+1)\left(x+\dfrac{a_3-a_1}{a_3+a_1}\right)}\right]$$

$$Y_b = \frac{1}{jzR_L}\frac{1}{x-1}f(x)$$

$$= \frac{1}{jzR_L}\frac{a_1+a_3}{1+a_2}\left[\frac{x+\dfrac{a_3-a_1}{a_3+a_1}}{(x-1)\left(x+\dfrac{a_2-1}{a_2+1}\right)}\right]$$

Expanding,

$$Y_a = \frac{1}{jzR_L}\left[\frac{\dfrac{1}{a_1}}{x+1}+\frac{\dfrac{a_1a_2-a_3}{a_1(a_1+a_3)}}{x+\dfrac{a_3-a_1}{a_3+a_1}}\right]$$

$$Y_b = \frac{1}{jzR_L}\left[\frac{\dfrac{a_3}{a_2}}{x-1}+\frac{\dfrac{a_1a_2-a_3}{a_2(1+a_2)}}{x+\dfrac{a_2-1}{a_2+1}}\right]$$

5.2 Determination of Element Values from Lattice Arm Admittances

The lattice admittances Y_a and Y_b are realized as a parallel combination of series resonant circuits. If we express Y_a and Y_b as follows:

$$Y = \frac{1}{j}\left(\frac{b_1}{x+c_1}+\frac{b_2}{x+c_2}+\ldots\right)$$

then the inductance and resonant frequency corresponding to the rth term are given by

$$L_r = \frac{1}{\Delta\omega . b_r}, \quad x_r = -c_r, \quad \omega_r = \omega_0 - \tfrac{1}{2}\Delta\omega . c_r. \quad (28)$$

Equation (28) is obtained by considering the reactance of a series resonant circuit (in this case the motional reactance of a crystal) in the neighbourhood of the resonant frequency. Then,

$$\frac{1}{Y} = j2L_r(\omega-\omega_r).$$

Using

$$x = \frac{\omega-\omega_0}{\omega_c-\omega_0} = \frac{\omega-\omega_0}{\frac{1}{2}\Delta\omega}$$

we obtain

$$Y = \frac{1}{j2L_r(\omega-\omega_r)} = \frac{1}{j\Delta\omega . L_r(x-x_r)}$$

$$\omega = \omega_0 + \tfrac{1}{2}\Delta\omega . x.$$

The inductances and resonant frequencies are therefore as follows,

$$L_{a1} = \frac{zR_L}{\Delta\omega}a_1 \qquad \omega_{a1} = \omega_0 - \tfrac{1}{2}\Delta\omega$$

$$L_{a2} = \frac{zR_L}{\Delta\omega}\frac{a_1(a_1+a_3)}{a_1a_2-a_3} \qquad \omega_{a2} = \omega_0 + \tfrac{1}{2}\Delta\omega\frac{a_1-a_3}{a_1+a_3}$$

$$L_{b1} = \frac{zR_L}{\Delta\omega}\frac{a_2}{a_3} \qquad \omega_{b1} = \omega_0 + \tfrac{1}{2}\Delta\omega$$

$$L_{b2} = \frac{zR_L}{\Delta\omega}\frac{a_2(1+a_2)}{a_1a_2-a_3} \qquad \omega_{b2} = \omega_0 + \tfrac{1}{2}\Delta\omega\frac{1-a_2}{1+a_2}$$

Further results, including formulae for Kosowsky I lattice sections, are given in Tables 3 and 4.†

5.3 Practical Considerations

Figure 2 shows the basic lattice network and Fig. 3 the realization of Z_a and Z_b as a parallel combination of series resonant circuits. Figure 4 gives the circuit in equivalent Jaumann form, with inductances included to resonate with the crystal parallel capacitances and circuit strays. C_s represents the sum of the crystal parallel capacitances in each arm plus an additional capacitor, if required, to ensure that the arm capacitances are equal.

C_c and C_t should be as small as possible to maximize L_c and L_t. This has two advantages. Firstly, the admittances of the parallel resonant circuits, which are ideally zero (and are set to zero at the centre frequency)

† Note that in realizing a Kosowsky I image impedance function we obtain a constant term in the partial fraction expansions of Y; this corresponds to a capacitor.

are a minimum; using the symbols in Fig. 4,

$$Y_c \simeq j2(\omega-\omega_0)(C_c+2C_s) = j\,\frac{2(\omega-\omega_0)}{\omega_0^2}\,\frac{1}{L_c}$$

$$Y_t \simeq j2(\omega-\omega_0)(C_t+2C_s) = j\,\frac{8(\omega-\omega_0)}{\omega_0^2}\,\frac{1}{L_t}$$

where Y_c and Y_t denote the admittances, as seen at the filter terminations, of the single coil and transformer parallel resonant circuits at a frequency ω. The second advantage is that for inductors of given Q-factor, the equivalent parallel resistance of each inductor, R_p, is proportional to L (since $R_p = \omega LQ$); maximizing L therefore reduces inductor losses.

If the design termination R_T ($= \frac{1}{2}R_L$) is greater than required, a resistor-capacitor parallel-series transformation may be performed. The parallel capacitance needed will reduce L_c and L_t, and should this be excessive, the coils may be used as terminating transformers and either tapped or further windings added.

Table 3. Design formulae for Kosowsky I lattice sections

$$L = \frac{R_L}{\Delta\omega}L_D\dagger, \quad \omega = \omega_0 + 2\Delta\omega.x_D, \quad C = \frac{1}{\omega_0 R_L}\,.\,C_D$$

(a) General solutions

Order of section	Unit	L_D	x_D	C_D
1 (m)	a1	$\frac{m}{2}$	-1	$\frac{1}{m}$
	b1	—	—	m
2 (m_1, m_2)	a1	$\frac{m_1+m_2}{2}$	-1	$\frac{1+m_1m_2}{m_1+m_2}$
	b1	$\frac{(1+m_1m_2)^2}{2(m_1+m_2)m_1m_2}$	$\frac{1-m_1m_2}{1+m_1m_2}$	$\frac{m_1+m_2}{1+m_1m_2}$
2† $(m, 1/m)$	a1	$\frac{m^2+1}{2m}$	-1	$\frac{2m}{m^2+1}$
	b1	$\frac{2m}{m^2+1}$	0	$\frac{m^2+1}{2m}$
3 (m_1, m_2, m_3)	a1	$\frac{m_1+m_2+m_3}{2}$	-1	$\frac{1+m_1m_2+m_2m_3+m_3m_1}{m_1+m_2+m_3+m_1m_2m_3}$
	a2	$\frac{(m_1+m_2+m_3)(m_1+m_2+m_3+m_1m_2m_3)^2}{2m_1m_2m_3[(m_1+m_2+m_3)\times(m_1m_2+m_2m_3+m_3m_1)-m_1m_2m_3]}$	$\frac{m_1+m_2+m_3-m_1m_2m_3}{m_1+m_2+m_3+m_1m_2m_3}$	
	b1	$\frac{(1+m_1m_2+m_2m_3+m_3m_1)^2}{2[(m_1+m_2+m_3)\times(m_1m_2+m_2m_3+m_3m_1)-m_1m_2m_3]}$	$\frac{1-m_1m_2-m_2m_3-m_3m_1}{1+m_1m_2+m_2m_3+m_3m_1}$	$\frac{m_1+m_2+m_3+m_1m_2m_3}{1+m_1m_2+m_2m_3+m_3m_1}$
3 $(m_1, m_2, 1)$	a1	$\frac{1+m_1+m_2}{2}$	-1	1
	a2	$\frac{(1+m_1+m_2)(1+m_1+m_2+m_1m_2)}{2m_1m_2(m_1+m_2)}$	$\frac{1+m_1+m_2-m_1m_2}{1+m_1+m_2+m_1m_2}$	
	b1	$\frac{1+m_1+m_2+m_1m_2}{2(m_1+m_2)}$	$\frac{1-m_1-m_2-m_1m_2}{1+m_1+m_2+m_1m_2}$	1
3‡ $(m, 1/m, 1)$	a1	$\frac{m^2+m+1}{2m}$	-1	1
	a2	$\frac{(m^2+m+1)(m+1)^2}{2m(m^2+1)}$	$\frac{m^2+1}{(m+1)^2}$	
	b1	$\frac{(m+1)^2}{2(m^2+1)}$	$-\frac{m^2+1}{(m+1)^2}$	1

† For a Jaumann lattice section, the termination $R_T = \frac{1}{2}R_L$.

‡ The attenuation characteristics are symmetrical about the centre frequency; if m corresponds to x_∞, $1/m$ corresponds to $-x_\infty$.

(b) Solutions with all attenuation poles at infinite frequency ($m = 1$)§

Order of section	Unit	a		b	
		L_D	x_D	L_D	x_D
1	1	0·5	−1	—	—
2	1	1	−1	1	0
3	1	1·5	−1	1	−0·5
	2	3	0·5	—	—
4	1	2	−1	1·172	−0·7071
	2	2	0	6·828	0·7071
5	1	1·910	−0·3090	1·382	−0·8090
	2	2·5	−1	3·618	0·3090
	3	13·09	0·8090	—	—
6	1	2	−0·5	1·608	−0·8660
	2	3	−1	3	0
	3	6	0·5	22·39	0·8660

§ For all designs with an attenuation pole at infinite frequency, $C_D = 1$.

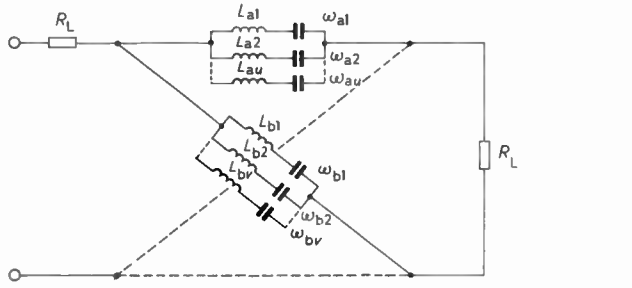

(a) Lattice form.

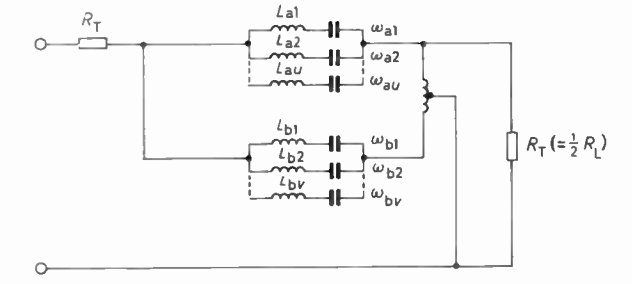

(b) Jaumann form.

Fig. 3. Filter with image impedance function $Z_I/R_L = z(1 - x^2)^{\frac{1}{2}}$.

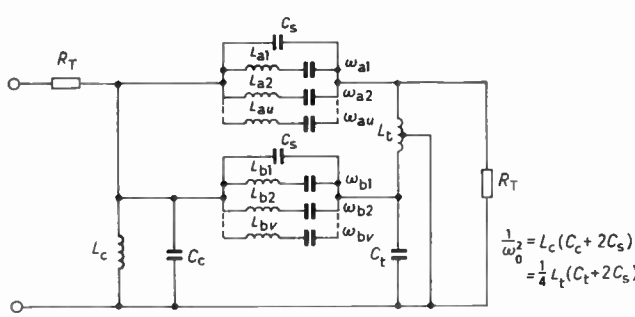

Fig. 4. Practical realization using quartz crystals.

The motional inductance values are given by

$$L = \frac{2zR_T}{\Delta\omega} L_D.$$

Let L_{min} denote the minimum practical value and $(L_D)_{min}$ the minimum of the L_D values. Then,

$$L = \frac{L_D}{(L_D)_{min}} L_{min}, \qquad R_T = \tfrac{1}{2}R_L = \frac{\Delta\omega}{2z} \frac{L_{min}}{(L_D)_{min}}.$$

6 Pass-band Behaviour of Kosowsky Lattice Filters

We consider here the insertion loss in the pass band. The relationships of interest are equations (4), (5) and (8). γ in equation (5) is replaced by $j\beta$, since Z_a and Z_b are imaginary and of opposite sign.

Zero pass-band insertion loss occurs when $Z_a = 0$, $Z_b = \infty$, or vice versa, and the corresponding frequencies are given by the roots of $f(x)$ in Table 5(a). The pass-band insertion loss equals the upper limit, as given by equation (9), when $Z_a = -Z_b$.

Values for the admittances and frequency turning points with all attenuation poles at infinite frequency are given in Table 5. The turning points approach attenuation poles, if finite, but remain symmetrically distributed about $x = 0$ if these poles are similarly distributed; poles at $x = \pm\infty$ are synonymous since the attenuation values at $x = \pm\infty$ are always equal.

6.1 Kosowsky I Response

The image impedance function is given by equation (26). Using equation (9), we obtain the upper limit of insertion loss,

$$\alpha_{max} = 20 \log_{10} \frac{1}{(1 - x^2)^{\frac{1}{2}}} \qquad (29)$$

Table 4. Design formulae for Kosowsky II (and IIm) lattice sections

$$L = \frac{zR_L}{\Delta\omega} \cdot L_D, \dagger \quad \omega = \omega_0 + \tfrac{1}{2}\Delta\omega . x_D$$

(a) General solutions

Order of section	Unit	L_D	x_D
1 (m)	a1	m	-1
	b1	$\frac{1}{m}$	1
2 (m_1, m_2)	a1	$m_1 + m_2$	-1
	a2	$\frac{m_1 + m_2}{m_1 m_2}$	1
	b1	$\frac{1 + m_1 m_2}{m_1 + m_2}$	$\frac{1 - m_1 m_2}{1 + m_1 m_2}$
2 (m, $1/m$)‡	a1	$\frac{m^2 + 1}{m}$	-1
	a2	$\frac{m^2 + 1}{m}$	1
	b1	$\frac{2m}{m^2 + 1}$	0
3 (m_1, m_2, m_3)	a1	$m_1 + m_2 + m_3$	-1
	a2	$\frac{(m_1 + m_2 + m_3)(m_1 + m_2 + m_3 + m_1 m_2 m_3)}{(m_1 + m_2 + m_3)(m_1 m_2 + m_2 m_3 + m_3 m_1) - m_1 m_2 m_3}$	$\frac{m_1 + m_2 + m_3 - m_1 m_2 m_3}{m_1 + m_2 + m_3 + m_1 m_2 m_3}$
	b1	$\frac{m_1 m_2 + m_2 m_3 + m_3 m_1}{m_1 m_2 m_3}$	1
	b2	$\frac{(m_1 m_2 + m_2 m_3 + m_3 m_1)(m_1 m_2 + m_2 m_3 + m_3 m_1 + 1)}{(m_1 + m_2 + m_3)(m_1 m_2 + m_2 m_3 + m_3 m_1) - m_1 m_2 m_3}$	$\frac{1 - m_1 m_2 - m_2 m_3 - m_3 m_1}{1 + m_1 m_2 + m_2 m_3 + m_3 m_1}$
3 (m_1, m_2, 1)	a1	$1 + m_1 + m_2$	-1
	a2	$\frac{1 + m_1 + m_2}{m_1 + m_2}$	$\frac{1 + m_1 + m_2 - m_1 m_2}{1 + m_1 + m_2 + m_1 m_2}$
	b1	$\frac{m_1 + m_2 + m_1 m_2}{m_1 m_2}$	1
	b2	$\frac{m_1 + m_2 + m_1 m_2}{m_1 + m_2}$	$\frac{1 - m_1 - m_2 - m_1 m_2}{1 + m_1 + m_2 + m_1 m_2}$
3 (m, $1/m$, 1)‡	a1	$\frac{m^2 + m + 1}{m}$	-1
	a2	$\frac{m^2 + m + 1}{m^2 + 1}$	$\frac{m^2 + 1}{(m + 1)^2}$
	b1	$\frac{m^2 + m + 1}{m}$	1
	b2	$\frac{m^2 + m + 1}{m^2 + 1}$	$-\frac{m^2 + 1}{(m + 1)^2}$

† ‡ See Table 3 footnotes.

(b) Solutions with all attenuation poles at infinite frequency ($m = 1$)

Order of section	Unit	a		b	
		L_D	x_D	L_D	x_D
1	1	1	−1	1	1
2	1	2	−1	1	0
	2	2	1	—	—
3	1	3	−1	3	1
	2	1·5	0·5	1·5	−0·5
4	1	4	−1	2	−0·7071
	2	4	1	2	0·7071
	3	2	0	—	—
5	1	5	−1	5	1
	2	2·5	−0·3090	2·5	0·3090
	3	2·5	0·8090	2·5	−0·8090
6	1	6	−1	3	−0·8660
	2	6	1	3	0
	3	3	−0·5	3	0·8660
	4	3	0·5	—	—

as shown in Fig. 5. The approximate maximum pass-band insertion loss is found in the following manner; we note the largest value of x at which a minimum occurs (as given in Table 5(c)) and apply equation (29) to the nearest maximum of smaller x. The normalized lattice admittances are given by Section 4 and Table 5(b) as follows,

$$Y'_a = -jR_L Y_a = \left(\frac{x-1}{x+1}\right)\frac{1}{f(x)}$$

$$Y'_b = -jR_L Y_b = f(x).$$

6.2 Kosowsky II Response

The upper limit of insertion loss is given by equations (9) and (27) as follows,

$$\alpha_{max} = 20 \log_{10} \frac{1-\frac{1}{2}x^2}{(1-x^2)^{\frac{1}{2}}}. \qquad (30)$$

We note the largest value of x at which a minimum occurs; applying equation (30) to the nearest maximum of smaller x then gives the approximate pass-band ripple.

The normalized lattice admittances are as follows:

$$Y'_a = jR_L Y_a = \frac{1}{(x+1)f(x)}$$

$$Y'_b = jR_L Y_b = \frac{f(x)}{x-1}.$$

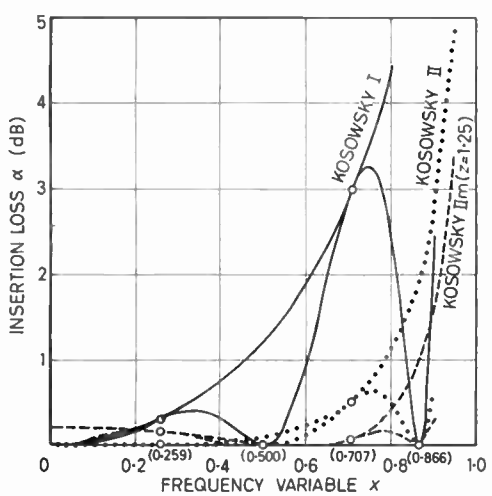

Fig. 5. Characteristics of sixth-order filters with all attenuation poles at infinite frequency. (The upper limit of insertion loss defined by the image impedance function is included with each filter characteristic.)

6.3 Kosowsky IIm Response

The upper limit of insertion loss is given by equations (9) and (27).

$$\alpha_{max} = 20 \log_{10} \frac{(z^2+1)-z^2x^2}{2z(1-x^2)^{\frac{1}{2}}} \qquad (31)$$

as shown in Fig. 5 (with $z = 1{\cdot}25$). The Kosowsky IIm function produces zero insertion loss at a frequency given by equation (27) as follows,

$$\frac{Z_i}{R_L} = z(1-x_0^2)^{\frac{1}{2}} = 1.$$

Hence

$$x_0 = \left(1 - \frac{1}{z^2}\right)^{\frac{1}{2}} \ldots \text{frequency of zero insertion loss.}$$

The non-zero frequency, x_p, at which the upper limit of insertion loss (resulting from the image impedance function) equals the value at zero frequency is given from

equation (31).

$$\frac{z^2+1}{2z} = \frac{(z^2+1)-z^2x_p^2}{2z(1-x_p^2)^{\frac{1}{2}}}.$$

Hence,

$$x_p = \left(1 - \frac{1}{z^4}\right)^{\frac{1}{2}}$$

for the frequency at which the upper limit of insertion loss equals the value at zero frequency.

Results are given in Table 2.† α_p, the value of α_{max} when $x = 0$ and $x = x_p$, is related to z as follows,

$$\alpha_p = 20 \log_{10} \frac{z^2+1}{2z}, \quad z = 10^{\alpha p/20} + (10^{\alpha p/10} - 1)^{\frac{1}{2}}.$$

For a Kosowsky IIm image impedance function, the insertion loss maxima are largest at each end of the range $0 \leq x \leq 1$, and to reduce the pass-band ripple it is convenient to equate the values of α_{max} at the lowest and second highest frequencies at which maxima occur, as given in Table 5(c); the highest frequency is ignored since it is above the highest frequency at which a minimum occurs and does not correspond to an insertion loss maximum. Let x_1 and x_2 denote these values of x. Equation (31) gives

$$10^{\alpha_{max}/20} = \frac{(z^2+1)-z^2x_1^2}{2z(1-x_1^2)^{\frac{1}{2}}} = \frac{(z^2+1)-z^2x_2^2}{2z(1-x_2^2)^{\frac{1}{2}}}.$$

Hence,

$$z = \left(\frac{1}{(1-x_1^2)(1-x_2^2)}\right)^{\frac{1}{2}}$$

is the condition for equal insertion loss at the maxima $x = x_1$ and $x = x_2$. For odd order characteristics with all poles at infinite frequency, $x_1 = 0$. Results are given in Table 5(c).

The normalized lattice admittances are as follows,

$$Y'_a = jR_L Y_a = \frac{1}{z} \cdot \frac{1}{(x+1)f(x)}$$

$$Y'_b = jR_L Y_b = \frac{1}{z} \cdot \frac{f(x)}{x-1}$$

6.4 Insertion Loss in Terms of Normalized Lattice Arm Impedances

In determining the positions of the maxima, we did not consider the variation of the image impedance function with frequency. The true maxima are in the direction of greater insertion loss, as seen from Fig. 5. These maxima, with more detailed pass-band characteristics, are obtainable from equation (6). In normalized notation,

$$Z'^2_a = -\frac{Z_a^2}{R_L^2}, \qquad Z'^2_b = -\frac{Z_b^2}{R_L^2}.$$

† Note that for Kosowsky I and II, x_p does not exist since α_{max}, which is zero when $x = 0$, increases monotonically with frequency; for Kosowsky IIm, α_{max} equals α_p when $x = 0$, decreases to zero when $x = x_0$, and increases monotonically with frequency outside this region, equalling α_p again when $x = x_p$. Since Z_i/R_L reduces from z when $x = 0$ to $1/z$ when $x = x_p$, x_p is given very simply from $1/z = z(1 - x_p^2)^{\frac{1}{2}}$.

Hence,

$$\alpha = 10 \log_{10} \frac{Z'^2_a + Z'^2_b + Z'^2_a Z'^2_b + 1}{(Z'_b - Z'_a)^2}.$$

Results are given in Table 5(d).

6.5 Application to Other Image Impedance Functions

On investigating a new image impedance function, it is a simple matter to determine the pass-band insertion loss at the points where the characteristic meets the boundary (Table 5(c)), and these values give a reasonable assessment of the true maxima. The insertion loss-frequency characteristics for sixth-order filters are given in Fig. 5. The network behaviour is independent of the number of lattices used for realization; cascaded lattices of the same image impedance can always be replaced by a single lattice.

7 Example

To demonstrate the procedure, we will design a 6th-order all-pole band-pass filter with a centre frequency of 50 MHz and a bandwidth of 50 kHz. The design will use crystals whose minimum motional inductance is 1 mH (corresponding to a motional capacitance $\simeq 0{\cdot}01$ pF).

Figure 5 and Table 5(d) show that the pass-band ripple is minimum when a Kosowsky IIm image impedance function is used; the 0·16 dB ripple results from setting $z = 1{\cdot}25$, i.e.

$$\frac{Z_i}{R_L} = 1{\cdot}25(1-x^2)^{\frac{1}{2}}.$$

Using

$$L = \frac{zR_L}{\Delta\omega} \cdot L_D, \quad \omega = \omega_0 + \tfrac{1}{2}\Delta\omega . x_D, \quad R_L = 2R_T,$$

practical values for L, ω and R_T are evaluated by applying the formula in Table 4(b).

Table 5. Investigation of pass-band behaviour with all attenuation poles at infinite frequency

(a) Value of response function, $f(x)$

Order of section	$f(x)$
1	1
2	$\frac{x-1}{x}$
3	$\frac{x-0{\cdot}5}{x+0{\cdot}5}$
4	$\frac{x(x-1)}{(x+0{\cdot}7071)(x-0{\cdot}7071)}$
5	$\frac{(x-0{\cdot}809)(x+0{\cdot}309)}{(x+0{\cdot}809)(x-0{\cdot}309)}$
6	$\frac{(x-1)(x+0{\cdot}5)(x-0{\cdot}5)}{x(x+0{\cdot}866)(x-0{\cdot}866)}$

(b) Normalized lattice admittances

Order of section	Kosowsky I		Kosowsky II†	
	$Y_a' (= -jR_L Y_a)$	$Y_b' (= -jR_L Y_b)$	$Y_a' (= jR_L Y_a)$	$Y_b' (= jR_L Y_b)$
1	$\frac{x-1}{x+1}$	1	$\frac{1}{x+1}$	$\frac{1}{x-1}$
2	$\frac{x}{x+1}$	$\frac{x-1}{x}$	$\frac{x}{(x+1)(x-1)}$	$\frac{1}{x}$
3	$\frac{(x-1)(x+0{\cdot}5)}{(x+1)(x-0{\cdot}5)}$	$\frac{x-0{\cdot}5}{x+0{\cdot}5}$	$\frac{x+0{\cdot}5}{(x+1)(x-0{\cdot}5)}$	$\frac{x-0{\cdot}5}{(x-1)(x+0{\cdot}5)}$
4	$\frac{(x+0{\cdot}7071)(x-0{\cdot}7071)}{x(x+1)}$	$\frac{x(x-1)}{(x+0{\cdot}7071)(x-0{\cdot}7071)}$	$\frac{(x+0{\cdot}7071)(x-0{\cdot}7071)}{x(x+1)(x-1)}$	$\frac{x}{(x+0{\cdot}7071)(x-0{\cdot}7071)}$
5	$\frac{(x-1)(x+0{\cdot}809)(x-0{\cdot}309)}{(x+1)(x-0{\cdot}809)(x+0{\cdot}309)}$	$\frac{(x-0{\cdot}809)(x+0{\cdot}309)}{(x+0{\cdot}809)(x-0{\cdot}309)}$	$\frac{(x+0{\cdot}809)(x-0{\cdot}309)}{(x+1)(x-0{\cdot}809)(x+0{\cdot}309)}$	$\frac{(x-0{\cdot}809)(x+0{\cdot}309)}{(x-1)(x+0{\cdot}809)(x-0{\cdot}309)}$
6	$\frac{x(x+0{\cdot}866)(x-0{\cdot}866)}{(x+1)(x+0{\cdot}5)(x-0{\cdot}5)}$	$\frac{(x-1)(x+0{\cdot}5)(x-0{\cdot}5)}{x(x+0{\cdot}866)(x-0{\cdot}866)}$	$\frac{x(x+0{\cdot}866)(x-0{\cdot}866)}{(x+1)(x-1)(x-0{\cdot}5)(x-0{\cdot}5)}$	$\frac{(x+0{\cdot}5)(x-0{\cdot}5)}{x(x+0{\cdot}866)(x-0{\cdot}866)}$

† For Kosowsky IIm, the tabulated values are divided by z.

(c) Location of turning points relative to image impedance function

Order of network	Values of x		Attenuation (dB)		
	Minima ($\alpha = 0$)	Maxima†	I	II	IIm [z]
1	—	0	—	—	—
2	0	±0·7071	—	—	—
3	±0·5	0, ±0·8660	—	—	—
4	0, ±0·7071	±0·3827, ±0·9239	0·69	0·03	—
5	±0·3090, ±0·8090	0, ±0·5878, ±0·9511	1·84	0·19	0·05 [1·11]
6	0, ±0·5, ±0·8660	±0·2588, ±0·7071, ±0·9659	3·01	0·51	0·11 [1·21]

† These maxima denote points where the insertion loss in the pass band equals the upper limit defined by the image impedance function; $x = x_{max}$.

(d) Location of insertion loss maxima (pass band)

Order of network	Values of x				Attenuation (dB)		
	I	II	IIm†		I	II	IIm [z]
1	—	—	—		—	—	— [1]
2	—	—	—		—	—	— [1]
3	±0·29	±0·35	0	±0·38	0·16	0·004	0·002 [1·02]
4	±0·50	±0·55	±0·23	±0·60	0·97	0·07	0·02 [1·11]
5	±0·65	±0·67	0	±0·71	2·10	0·29	0·09 [1·15]
6	±0·74	±0·76	±0·23	±0·78	3·25	0·63	0·16 [1·25]

† For fifth- and sixth-order filters, an additional maximum of 0·003, 0·001 dB occurs at $x = 0{\cdot}41$, 0·55, respectively; minor maxima also occur for I and II.

7.1 Single Jaumann Network (6th-order)

For a 6th-order Jaumann network we obtain the following:

$$L = \frac{L_D}{(L_D)_{min}} \cdot L_{min} = \tfrac{1}{3} L_D \text{ mH}$$

$$f = f_0 + \tfrac{1}{2}\Delta f . x_D = (50\,000 + 25 x_D) \text{ kHz}.$$

These formulae enable the crystal inductance and frequency values to be determined from L_D and x_D.

Table 6

Unit	Design formulae L_D	x_D	Physical values L (mH)	f (kHz)
a1	6	−1	2	49 975
a2	6	1	2	50 025
a3	3	−0·5	1	49 987·5
a4	3	0·5	1	50 012·5
b1	3	−0·8660	1	49 978·35
b2	3	0	1	50 000
b3	3	0·8660	1	50 021·65

The Jaumann lattice termination for the circuit in Fig. 4 is given by

$$R_T = \frac{\Delta\omega}{2z} \cdot \frac{L_{min}}{(L_D)_{min}} = 41{\cdot}89\ \Omega.$$

If we assume a static capacitance of 2·5 pF for a 1 mH crystal (corresponding to a static to motional capacitance ratio $\simeq 250$) and ignore C_c and C_t in Fig. 4, the total static capacitance and the inductance which resonates with this capacitance are given as follows,†

$$C_S = (1{\cdot}25 + 1{\cdot}25 + 2{\cdot}5 + 2{\cdot}5)\text{ pF} = 7{\cdot}5\text{ pF}$$

$$L_C = \tfrac{1}{4} L_t = \frac{1}{2\omega_0^2 C_S} = 0{\cdot}675\ \mu\text{H}.$$

7.2 Double Jaumann network (2 × 3rd-order)

For a 3rd-order Jaumann network we obtain the following,

$$L = \frac{L_D}{(L_D)_{min}} \cdot L_{min} = \frac{L_D}{1{\cdot}5} \text{ mH}$$

$$f = f_0 + \tfrac{1}{2}\Delta f . x_D = (50\,000 + 25 x_D) \text{ kHz}.$$

Table 7

Unit	Design formulae L_D	x_D	Physical values L (mH)	f (kHz)
a1	3	−1	2	49 975
a2	1·5	0·5	1	50 012·5
b1	3	1	2	50 025
b2	1·5	−0·5	1	49 987·5

† The static capacitance is proportional to the motional capacitance, which is inversely proportional to the specified motional inductance.

$$R_T = \frac{\Delta\omega}{2z} \cdot \frac{L_{min}}{(L_D)_{min}} = 83{\cdot}78\ \Omega$$

$$C_S = (1{\cdot}25 + 2.5)\text{ pF} = 3{\cdot}75\text{ pF}$$

$$L_C = \tfrac{1}{4} L_t = \frac{1}{2\omega_0^2 C_S} = 1{\cdot}351\ \mu\text{H}.$$

7.3 Analysis

The analysis of the filters in Table 8 shows good agreement between the two characteristics: the values of insertion loss differ by less than 0·1 dB over the given frequency range. The pass-band behaviour varies as predicted in Fig. 5 and Table 5(d).

Note that the insertion loss is undefined at the cut-off frequencies of image parameter filters. Our analysis gives a value of 8·3 dB for a design bandwidth of 50 kHz. A more detailed analysis shows that the 1 dB bandwidth is 46 kHz, which is 92% of our design bandwidth; therefore, if we wish to obtain a filter with a 1 dB bandwidth of 50 kHz, the design bandwidth must be increased to 54·3 ($= 50^2/46$) kHz.

8 Discussion of Results

The improvement in pass-band behaviour from using a modified Kosowsky II image impedance function in place of Kosowsky I or II for higher-order filters, is seen from Table 5 and Fig. 5. Tables 3 and 4 show the improved element values for Kosowsky II and IIm at higher orders; for sixth-order networks with attenuation poles at infinite frequency, the motional reactances vary by a factor of 14 for Kosowsky I, and 2 for Kosowsky II (and IIm), and with finite poles these variations are usually greater.

Suitable values of z for Kosowsky IIm solutions of order 1 to 6 with attenuation poles at infinite frequency are given in Table 5(d). For first- and second-order networks, a monotonic characteristic is obtained; for third- to sixth-order networks, the equal ripple pass-band attenuation is 0·002, 0·02, 0·09, 0·16 dB, respectively.

9 Acknowledgments

The author would like to acknowledge helpful discussions with Mr. G. C. Bown of GEC Hirst Research Centre. Part of this paper incorporates work carried out under a CVD contract and is published by permission of the Ministry of Defence (Procurement Executive).

10 References

1. Laurent, T., 'Frequency Filter Methods' (Wiley, New York, 1963).
2. Herrero, J. L. and Willoner, W., 'Synthesis of Filters' (Prentice-Hall, Englewood Cliffs, N.J., 1966).
3. Bown, G. C., 'The Design of Narrow Band Crystal Filters', GEC Telecommunications Research Laboratories Report 14,040R, December 1961.
4. Bode, H. W., 'Network Analysis and Feedback Amplifier Design' (Van Nostrand, New York, 1945).
5. Stevenson, J. K., 'Synthesis of Quartz Crystal Band-Pass Lattice Filters from a Low-Pass Analogue', Ph.D. Thesis, University of London, 1971.

Table 8. Computer output from analysis of 6th-order filters

FREQ(HZ)	ATTEN(DB)	PHASE(DEG)
49950000.	64.920	139.515
49952500.	61.437	142.624
49955000.	57.711	146.191
49957500.	53.700	150.336
49960000.	49.351	155.229
49962500.	44.594	161.125
49965000.	39.325	168.423
49967500.	33.396	177.812
49970000.	26.561	190.634
49972500.	18.394	210.131
49975000.	8.297	247.373
49977500.	0.311	330.998
49980000.	0.157	402.350
49982500.	0.056	453.385
49985000.	0.000	498.750
49987500.	0.000	539.972
49990000.	0.031	578.762
49992500.	0.125	615.443
49995000.	0.155	650.368
49997500.	0.066	684.910
50000000.	0.000	719.981
50002500.	0.067	755.048
50005000.	0.155	789.586
50007500.	0.125	824.512
50010000.	0.031	861.197
50012500.	0.000	899.989
50015000.	0.000	941.211
50017500.	0.056	986.580
50020000.	0.158	1037.615
50022500.	0.310	1108.968
50025000.	8.299	1192.621
50027500.	18.399	1229.849
50030000.	26.566	1249.334
50032500.	33.402	1262.147
50035000.	39.331	1271.530
50037500.	44.599	1278.824
50040000.	49.357	1284.716
50042500.	53.705	1289.606
50045000.	57.715	1293.748
50047500.	61.442	1297.313
50050000.	64.925	1300.421

(a) Single Jaumann lattice network

FREQ(HZ)	ATTEN(DB)	PHASE(DEG)
49950000.	64.966	139.529
49952500.	61.473	142.638
49955000.	57.738	146.204
49957500.	53.720	150.349
49960000.	49.366	155.241
49962500.	44.604	161.136
49965000.	39.333	168.434
49967500.	33.400	177.322
49970000.	26.563	190.642
49972500.	18.396	210.135
49975000.	8.297	247.375
49977500.	0.311	331.003
49980000.	0.158	402.352
49982500.	0.056	453.382
49985000.	0.000	498.745
49987500.	0.000	539.967
49990000.	0.032	578.756
49992500.	0.126	615.437
49995000.	0.156	650.361
49997500.	0.067	684.901
50000000.	0.000	719.972
50002500.	0.066	755.043
50005000.	0.155	789.585
50007500.	0.125	824.512
50010000.	0.031	861.198
50012500.	0.000	899.989
50015000.	0.000	941.211
50017500.	0.056	986.578
50020000.	0.158	1037.615
50022500.	0.310	1108.970
50025000.	8.300	1192.619
50027500.	18.401	1229.852
50030000.	26.570	1249.339
50032500.	33.407	1262.155
50035000.	39.340	1271.539
50037500.	44.612	1278.834
50040000.	49.374	1284.727
50042500.	53.729	1289.618
50045000.	57.747	1293.761
50047500.	61.483	1297.326
50050000.	64.976	1300.434

(b) Double Jaumann lattice network

6. 'Reference Data for Radio Engineers', International Telephone and Telegraph Corporation, 4th edition, 1956.

7. Stevenson, J. K. and Redwood, M., 'The motional reactance of a piezoelectric resonator—a more accurate and simpler representation for use in filter design', *IEEE Trans. on Circuit Theory*, **CT-16**, No. 4, pp. 568–72, November 1969.

8. Kosowsky, D. I., 'Synthesis and Realisation of Crystal Filters', MIT Research Laboratory of Electronics, Technical Report 298, June 1955.

Manuscript first received by the Institution on 29th August 1974, in revised form on 13th March 1975, and in final form on 21st October 1975. (Paper No. 1713/CC 249).

IERE News and Commentary

Design Council Design Consultancy Scheme

In 1973 the Design Council, with the support of the CEI, launched a scheme to use experienced designers on a consulting basis in the mechanical and electrical fields. It was believed that industry could derive benefit from the short-term service of visiting consultant designers, either during project design, in the detail design phase, or to give judgment in the pre-launch phase of a new engineering product. In the event, the scheme was well received and blended in well with the development by the Design Council of a Field Officer Service and a Record of Engineering Design Expertise.

The function of these Field Officers is to diagnose difficulties in industry which are susceptible to specialist design treatment. The Record of Engineering Design Expertise, which contains information on national sources of expertise, exists to support the Field Officers in locating the most appropriate specialized expertise for their particular problem.

One of the most important sources of expertise is the older, retired Designer or Engineer of experience and achievement. There is a need for many more design specialists in this category to be included in the 'Record', particularly those with relevant experience in the fields of Mechanisms, Gears, Drives, Precision Instrument Engineering and Overall Application of Plastics. Normal contractual arrangements and fees are negotiated directly between the specialist and the company in question.

Engineers wishing to consider taking part in the scheme should write in the first place and in confidence to Mr. H. G. Conway, at the Design Council, 28 Haymarket, London SW1Y 4SU.

Sir Stanley Hooker Awarded 1975 John Smeaton Medal

The 1975 John Smeaton Medal for outstanding achievement in engineering has been awarded to Sir Stanley Hooker, Technical Director of Rolls-Royce (1971) Limited.

The Medal, established in 1974 by CEI in conjunction with the Smeatonian Society to mark the 250th anniversary of the birth of the eminent engineer John Smeaton, has been presented to Sir Stanley—a household name in aviation circles—in recognition of his 40 years in aeronautical engineering, during which he pioneered improvements in superchargers for piston engines and in the design and development of aviation gas turbines. Sir Stanley joined Rolls-Royce, Derby, in 1938. The culmination of his work on superchargers was the two-stage intercooled *Merlin* supercharger which had a dramatic effect on the performance of the *Spitfire* at high altitudes. More recently he has had overall responsibility for engines powering the *Britannia*, the RAF *Vulcan* bomber, the Hawker Siddeley *Harrier* VSTOL fighter and the *Concorde*.

CONFERENCES IN 1976-77

International Broadcasting Convention 1976

More than sixty papers will be presented during the fourteen sessions of the Technical Programme of IBC 76 (to be held at Grosvenor House, London, 20th–24th September 1976). They cover new techniques, systems, developments and trends which will be of interest to engineers concerned with all aspects of broadcasting.

In addition to conventional broadcasting techniques there will be two sessions concerned with new information systems utilizing the domestic television receiver for information display. Papers on Teletext, which is already in use in the UK (BBC Ceefax and IBA Oracle programmes) and undergoing tests in various other countries, will be presented. Other papers will relate to Viewdata, the system being developed by the British Post Office for use in conjunction with the telephone network, and to Text Television, the experimental system of NHK in Japan.

A special session will highlight Electronic Journalism (or Electronic News Gathering) using lightweight camera, recording and transmission equipment specially designed for this purpose and now being produced by many manufacturers for increasing use around the world to cover news events for television.

The exhibition at IBC 76, at which leading manufacturers will display and demonstrate an extensive range of professional broadcasting equipment, will complement the technical sessions and enable delegates to get up-to-date information and firsthand experience of the latest equipment.

The interest now being shown in IBC 76, the biennial International Broadcasting Convention, points to a record attendance in September. Over 2000 delegates from 44 countries attended IBC 74.

Sponsored by the Electronic Engineering Association (EEA), the Institution of Electrical Engineers (IEE), the Institute of Electrical and Electronics Engineers (IEEE), the Institution of Electronic and Radio Engineers (IERE), the Royal Television Society (RTS), and the Society of Motion Picture and Television Engineers (SMPTE), IBC is now established as the international forum for new techniques covering the entire field of broadcasting and allied services and is the shop window for the latest professional equipment.

Further information and registration forms can be obtained from The Secretariat, International Broadcasting Convention, IEE, Savoy Place, London WC2R 0BL, United Kingdom.

International Conference on Displays for Man-Machine Systems

'Displays for Man-Machine Systems' is the title of an international conference which will take place at the University of Lancaster between 4th and 7th April 1977.

The conference is being organized by the Control and Automation and the Electronics Divisions of the Institution of Electrical Engineers in association with the Biological Engineering Society, the British Computer Society, the British Psychological Society (Occupational Psychology Section), the Ergonomics Research Society, the Institute of Electrical and Electronics Engineers (Systems, Man and Cybernetics Society), the Institute of Physics, the Institution of Electronic

and Radio Engineers, the Ministry of Defence and the Society for Information Display.

The conference aims to review new research and applications, both in engineering and in behavioural and related human sciences, and will include discussion of the design of software appropriate to the needs both of the engineering system and of the human user. In addition it is proposed to arrange a small exhibition associated with the conference.

The topics to be covered in the programme will include the following:

Man/Display Interaction

Uses of displays:
- data entry and retrieval devices
- memory and decision making aids
- alerting devices, etc.

The human as an information retriever

The use of various sensory channels:
- visual, auditory, tactile, etc.

Advantages and problems of man in the loop:
- enhancing display efficiency
- limiting data rates, etc.

Special requirements of systems for the disabled

Social consequences of new machines

How technical innovation influences human methods

Display Systems

System considerations:
- contexts of use
- compatibility (technical and human factors)
- remote terminal working
- distributed systems, etc.

Problems in various types of systems:
- computer driven displays
- air traffic control systems
- plant control room display
- real time, multiple function information systems
- head up display systems, etc.

Display Hardware and Software

New developments in equipment and software:
- techniques for overlaying information (e.g. ported displays and mixing techniques)
- large scale and high resolution display techniques
- solid state displays
- lasers and other optical techniques
- picture storage
- real time displays and animation
- non-visual information (e.g. tactile, acoustic methods)
- colour and 3D methods, etc.

Reliability problems of displays

Manufacturing problems of displays

Software organization

Interactive languages

Offers of contributions should be submitted in synopsis form (approximately 250 words) to the IEE Conference Department on or before 1st June 1976. The synopsis should include the main points of the paper and, where possible, indicate where the emphasis will be placed. The authors whose synopses are selected for development will be requested to provide a typescript of not more than 3200 words of text, correspondingly less if illustrations are included, for assessment by 19th November 1976.

Requests for further information and offers of papers should be sent to the Conference Department, IEE, Savoy Place, London WC2R 0BL.

Eurocon '77—International Conference on Communications

An international conference on communications—EUROCON '77— will be held in Venice from 3rd to 6th May, 1977. The conference will cover communications in large electric power systems, new developments in communications, communications and computers and communications and signal processing in medicine. A special session will deal with communications problems in developing countries.

This meeting follows the successful EUROCON '74 which was held in Amsterdam. It is being organized by the Institute of Electrical and Electronics Engineers (IEEE) Region 8, and by EUREL (The Convention of National Societies of Electrical Engineers of Western Europe), of which the Institution of Electrical Engineers and the Institution of Electronic and Radio Engineers are the UK members. Local organization is being carried out by the Associazione Elettrotecnica ed Elettronica Italiana (AEI) and the N. and M. & S. Italy Sections of IEEE.

Further details are available from EUROCON '77, c/o AEI, Viale Monza 259, 20126 Milan, Italy, or from the IERE or IEE, or other national associations in membership of EUREL.

Standard Frequency Transmissions—February 1976

(Communication from the National Physical Laboratory)

February 1976	Deviation from nominal frequency in parts in 10^{10} (24-hour mean centred on 0300 UT)	Relative phase readings in microseconds NPL—Station (Readings at 1500 UT)	
	Droitwich 200 kHz	*GBR 16 kHz	†MSF 60 kHz
1	−0·1	700·6	612·9
2	−0·1	701·0	612·9
3	−0·1	699·5	613·2
4	−0·1	700·0	613·4
5	−0·1	699·5	613·4
6	−0·1	699·5	613·4
7	−0·1	699·3	613·2
8	−0·2	699·7	613·1
9	−0·1	698·0	613·2
10	−0·2	697·3	613·1
11	−0·2	698·9	613·1
12	−0·2	698·3	613·2
13	−0·2	697·3	613·2
14	−0·2	696·9	613·2
15	−0·2	696·0	613·1
16	−0·2	697·2	612·9
17	−0·2	699·7	612·9
18	−0·2	697·5	612·9
19	−0·2	697·9	612·9
20	−0·2	697·5	612·9
21	−0·2	699·0	612·9
22	−0·3	697·3	612·9
23	−0·3	698·0	612·9
24	−0·1	697·3	612·9
25	−0·1	696·7	612·9
26	−0·1	696·0	612·9
27	−0·1	697·0	612·8
28	−0·1	697·6	612·5
29	−0·1	696·7	612·5

All measurements in terms of H-P Caesium Standard No. 344, agrees with the NPL Caesium Standard to 1 part in 10^{11}.

* Relative to UTC Scale; $(UTC_{NPL}-Station)$ = +500 at 1500 UT 31 December 1968.

† Relative to AT Scale; $(AT_{NPL}-Station)$ = +468·6 at 1500 UT 31 December 1968.

Tropospheric Telephone and Data Links to North Sea Platforms

The first of the many North Sea oil and gas platforms off the British coast is now linked to the public telephone network with direct dialling throughout the UK and to many places abroad. The new service was inaugurated on 15th January to Mobil's Beryl platform, which is 150 km east of the Shetlands, and it now has an automatic public telephone service with Aberdeen telephone numbers.

Because the oil and gas production platforms are well out of sight of land—their locations stretch from 150 to 300 km (100 to 200 miles) from the mainland—they are linked to the British telecommunications network by trans-horizon microwave radio or tropospheric scatter propagation. Focal points of the new off-shore network are two radio stations, built from scratch in just over a year. They are strategically sited to serve almost the entire British sector of the northern North Sea gas and oil field areas. One station—the control centre—is sited near Fraserburgh, Aberdeenshire; the other is on South Shetland. Aerials, transmitters, receivers and other equipment for both stations were supplied by Marconi Communication Systems Ltd. and cost of the project so far is nearly £3M.

High reliability for the North Sea trans-horizon systems is ensured by quadruple diversity, using two transmitters and four receivers connected to two aerials at the receiving end. The received signals are continuously combined to give constant output compared with the fluctuating signal received over a single trans-horizon path, which is subject to severe fading. Each shore station has pairs of either 18 m or 12 m parabolic 'billboard' aerials operating in the 2 GHz band, which radiate an equivalent power of 100–180 MW. The transmitters—both on-shore and off-shore—have output powers of 1 kW.

Transmissions from the on-shore antennae are concentrated in 1° beams. The part of the troposphere 'visible' to both transmitting and receiving aerials lies about 1 km above sea level. Attenuation of the signal is typically in excess of 200 dB. Tropospheric turbulence causes almost continual fluctuations with rapid fading of the received signal level, which is about 110 dB below 1 watt on average. One of each pair of transmitter aerials transmits on vertical polarization, the other is horizontally polarized. Each of the two receiving aerials receives the vertically polarized signals and also the horizontally polarized signals, and feeds them to two separate receivers.

The system aims at giving a signal/noise ratio on telephone calls exceeding 40 dB for 99·9% of the time and a data error rate less than 1 in 10^5 at 2400 bits/s for 99·98% of the time. This is a higher order of service contingency than many private systems, which are usually designed to give an error rate for 2400 baud data of better than 1 in 10^5 for 99·90% of the worst month. Transmission bandwidth is 3 MHz for 72 telephone channels, transmitted by frequency modulation; some links may be expanded to 132 voice circuits if required.

Operational as well as reserve communication equipment on each platform is monitored and any failure is automatically signalled as a change-of-state to the Post Office control station on land. Here, master receivers, which scan sequentially the supervisory signals received from the platforms, sound an alarm and at the same time identify the platform where the failure has occurred. This can then be interrogated to determine which equipment has failed. In addition, a telephone circuit is available at all stations throughout the system for telecommunication engineers who need to carry out tests on the various items of equipment.

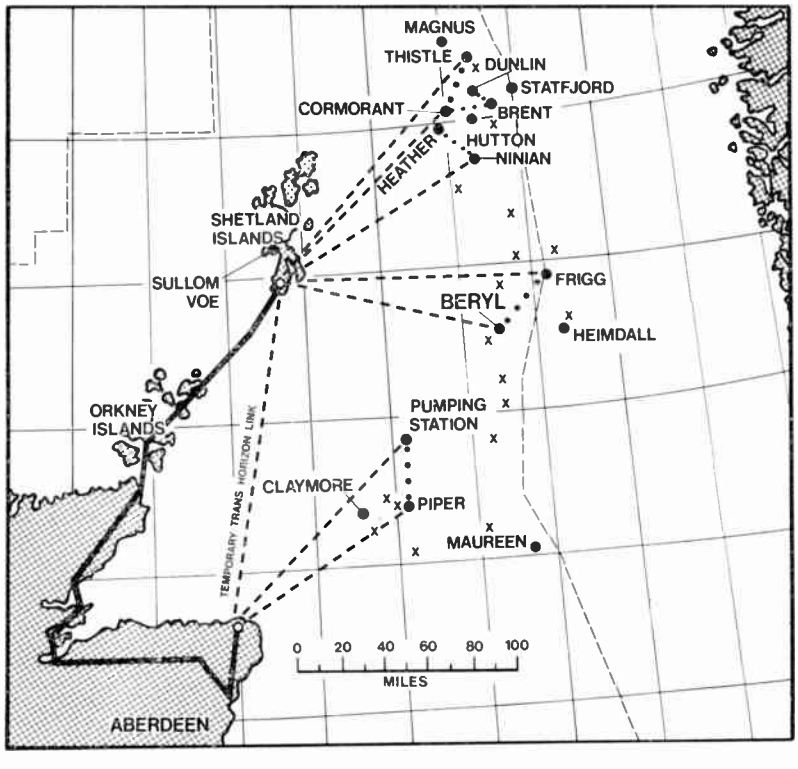

INLAND RADIO NETWORK

•• ALTERNATE PATH LINE-OF-SIGHT RADIO LINKS

•• OTHER LINE-OF-SIGHT RADIO LINKS

-- TRANS-HORIZON LINK

– – INTERNATIONAL BOUNDARY

x EXPLORATIONS

● PRODUCTION PLATFORM

○ TRANS-HORIZON RADIO STATION

Post Office communications for oil and gas production platforms in the UK sector of the North Sea.

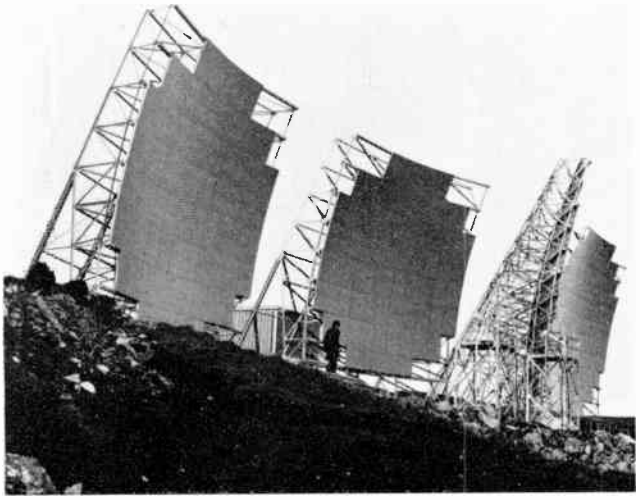

The tropo-scatter 'billboard' aerials at the new radio station on South Shetland. The left-hand pair of aerials—12 m high—are for the trans-horizon radio link to Mobil Oil's Beryl platform; the right-hand pair—18 m high—will serve Total's Frigg platform.

Additional security of operation is obtained by adopting where possible alternate routing of trans-horizon links. Two separate paths are set up from land to a pair of platforms separated by between 20 and 50 km (12–30 miles); these are then linked to each other by line-of-sight microwave radio. Both platforms are served over one path at a time, which is alternated with the other week and week about, with the working tropo-path terminal relaying communications to the other platform over the line-of-sight link.

Mobil's Beryl platform is linked by tropospheric scatter to the South Shetland station. From there the signals are relayed by a second over-the-horizon link to the Fraserburgh station, where they are fed into Britain's inland network. The Shetland–Fraserburgh tropo-link is a temporary arrangement which will eventually be replaced by a series of line-of-sight microwave links routed through the Orkneys to the mainland. These will be provided as part of the expansion of the inland network undertaken to keep ahead of increasing demand for telecommunications services.

As the production phase of the oil industry gathers pace, more and more platforms will be linked into the network. Indeed, studies by the Post Office into the likely requirements for tropospheric scatter links to oil and gas production platforms in the northern sector of the North Sea and to the north of Scotland envisage that up to 20 links could be required in the area. To avoid the proliferation of individual systems for each offshore platform, the Post Office selected the two shore terminal sites from which it will be possible to serve almost the entire British sector of the North Sea in this area. Thus the station on South Shetland will serve as the terminal for links planned for the Thistle, Cormorant, Ninian, Heather and Frigg Fields, as well as the Beryl Field, while that near Fraserburgh will be the shore end of links to the Frigg pipeline intermediate platforms and the Piper Field. This latter will soon be linked directly to Occidental's Piper platform, also equipped by Marconi, 110 miles north-east of Aberdeen. Similarly, Total's Marconi-equipped Frigg gas field platform and mid-pipeline pumping platform are also expected to be connected to the system this year.

On 3rd March the Institution's Communications Group held a Colloquium in London on Tropospheric Scatter Communications at which six papers by speakers from Government, industry and users discussed how the communications problems with the North Sea platforms were being overcome. It is hoped to publish a report on the meeting shortly and subsequently to include at least some of the papers in full.

Police Mobile Communications Study

The Home Office Directorate of Telecommunications has awarded the Marconi Research Laboratories a £½M contract as part of Stage 2 of the Mobile Automatic Data Experiment (MADE). In July 1976, the Police Forces of West Mercia and West Midlands will employ automatic data transmission and processing equipment in fully operational conditions. The Home Office will supervise the trials and benefit assessment.

During MADE Stage 1, Marconi successfully developed and demonstrated experimental equipment for use in police cars in co-operation with a study group consisting of representatives from West Mercia, West Midlands, Staffordshire and Warwickshire police forces and the Home Office. Stage 2 of the project will equip 56 vehicles of West Mercia and West Midlands police and the two control rooms and will allow transmission of numeric codes, alpha-numeric messages and will permit semi-automatic vehicle location.

Each of the vehicles will be equipped with mobile radpue oi special modem controller together with some or all of the peripheral devices; alpha-numeric printer (Spectronics TP40), alpha-numeric keyboard and display, a numeric code display and keyboard unit, and touch map unit. The Force control rooms will be equipped with video data terminals with their associated keyboards and a receive-only high speed printer for presenting hard copy output of the message traffic. The whole system operation will be controlled by a small communications processor system.

The experiment, the first phase of which began in 1971, became necessary because of the ever-increasing demands placed on the police service. Police communications requirements continue to expand and it is unlikely that sufficient speech channels could be made available to meet the foreseeable demand. Digital data transmission would allow the existing channels to carry about forty times as much information as they do at present.

Equipment installed in the car will allow personnel to transmit status and location and extended message information back to control. The extended message information originating either from the vehicle or from the Force Headquarters is reproduced as a hard copy output on the teleprinter installed in the vehicle. This eliminates the need for transcription by the operators in the mobile.

The manufacture and supply of equipment, which is due for completion by mid-June 1976, is to be carried out jointly by the Marconi Research Laboratories and the GEC Mobile Radio Division of Marconi Communication Systems Limited.

An Integrated Channel Selector for V.H.F/U.H.F.

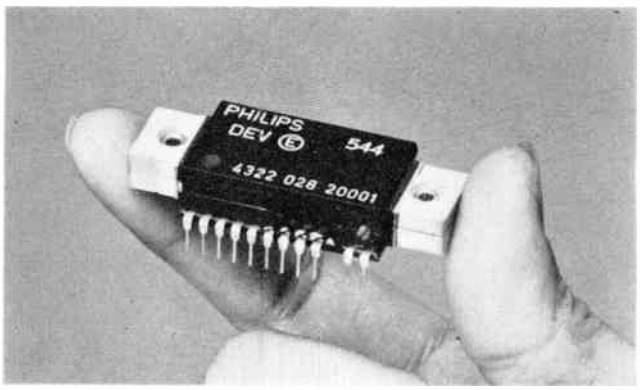

Fig. 1. This small channel selector covers, without switching, the entire television band in the v.h.f./u.h.f. region from 40–950 MHz.

A fully integrated wide-band channel selector embracing the entire v.h.f./u.h.f. region (40–950 MHz) has been developed by Philips research and development laboratories, Eindhoven. For this purpose a new series of silicon integrated circuits has been produced capable of resolving the problems arising in integrated circuits handling these very high frequencies. The substantial integration of the channel selector has led to a more compact and greatly simplified construction (see Fig. 1).

Electronically as well, this tuner offers some remarkable advantages. Whereas two tuners are currently required for the complete television band, this integrated channel selector covers on its own, without switchover, the v.h.f. and u.h.f. region up to 950 MHz. In the wide-band system being employed, the selector is extremely versatile and takes account of the latest proposals in the sphere of cable television, among them the use of S-channels, non-standard frequency regions, etc. Excellent signal-processing and signal-to-noise properties render the tuner usable in those situations in which, due to an abnormal strength or weakness of the signals to be received, special tuners were hitherto required.

The new integrated circuits specially developed for this tuner includes:

a wide-band amplifier based on four u.h.f. transistors and a number of resistors (Fig. 2);

an attenuator, consisting of seven p-i-n diodes and seven resistors;

two double balanced mixing stages, one comprising four and the other eight Schottky diodes;

a tuning circuit consisting of two varicap diodes.

The integrated u.h.f. diodes and transistors are manufactured using diffusion techniques employed in the manufacture of discrete u.h.f. devices but adapted to the integrated version and the further processing steps entailed in the construction of the channel selector.

With integration employing current planar silicon techniques, the devices could not operate satisfactorily at the very high frequencies here desired, and an air insulation technique was chosen. The advantage of this is that the parasitic coupling effects between the components of the circuit are greatly reduced. Furthermore, the parasitic capacitance of the wiring on the i.c.s is considerably lessened by the employment of multi-level wiring.

The circuits are mounted together with the other components, such as oscillators, on a substrate of aluminium oxide provided with a pattern of strip conductors. The chips have beam leads of gold giving reproducible mounting of high yield.

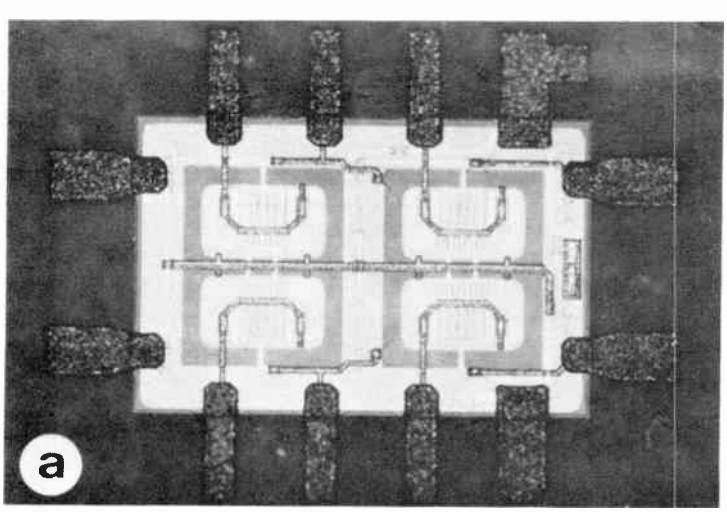

(a) Wide-band amplifier with air isolation and beam leads.

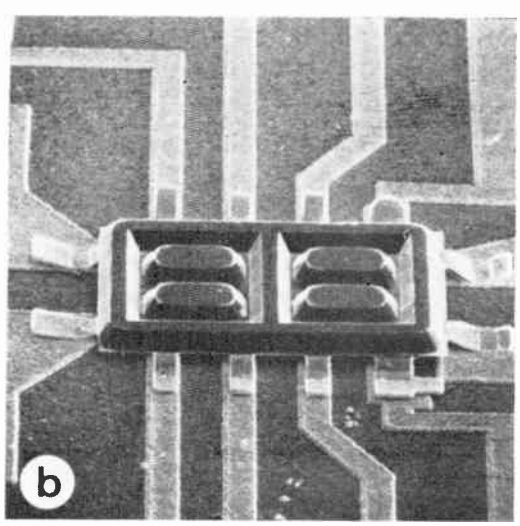

(b) Amplifier mounted upside-down on ceramic substrate.

Fig. 2. Micrographs of the wide-band amplifier.

IERE Golden Jubilee Convention

'ELECTRONICS IN SOCIETY'

University of Cambridge, 28th June—1st July 1976

Outline Programme

Monday, 28th June

The Convention will be opened by Sir LEONARD ATKINSON (Past President). His opening speech will be followed by a Keynote Address by Professor Sir HERMANN BONDI (Chief Scientific Adviser to the Ministry of Defence); this will be the first of four Keynote Addresses to be given, one on each day of the Convention, by leading authorities from Government and Industry on different aspects of the overall theme of the Convention. Other speakers will include Sir IEUAN MADDOCK, (Immediate Past President and Chief Scientist, Department of Industry) and the Hon. CHRISTOPHER LAYTON (EEC).

Following the first Keynote Address, the Convention Session Chairman will join Professor BONDI in a Panel Discussion led by Professor W. GOSLING, Chairman of the Convention Committee.

Tuesday, 29th June

SESSION 1—COGNITIVE SCIENCE AND SIGNAL PROCESSING

Chairman: Prof. W. A. GAMBLING (*University of Southampton*)

'Present and possible future for intelligent machines'
By Dr. J. R. PARKS (*Department of Industry*)

'Application of pattern recognition and scene analysis to the electronics industry'
By J. A. WEAVER (*Mullard Research Laboratories*)

'Some applications of digital signal processing'
By Prof. J. W. R. GRIFFITHS (*University of Loughborough*)

SESSION 2—COMMUNICATIONS

Chairman: Prof. J. W. R. GRIFFITHS (*University of Loughborough*)

'Future telecommunication services'
By Dr. A. A. L. REID (*Post Office*)

'Broadcast and wired teletext systems'
By P. L. MOTHERSOLE (*Mullard*)

'Optical fibres—the new transmission line'
By Prof. W. A. GAMBLING (*University of Southampton*)

'Computer communication networks'
By D. W. DAVIES (*National Physical Laboratory*)

HISTORICAL LECTURES (delivered in parallel sessions)

'A history of control'
By Prof. K. A. HAYES (*Royal Military College of Science*)

'Hunting for Hertzian waves—a history of early radio detectors'
By Dr. V. J. PHILLIPS (*University College of Swansea*)

Wednesday, 30th June

SESSION 3—ADVANCES IN DATA PROCESSING

Chairman: Prof. D. W. LEWIN (*Brunel University*)

'Microprocessor applications'
By P. H. HAMMOND (*Warren Spring Laboratory*)

'Microprocessor technology and architecture'
By L. A. CRAPNELL (*Ferranti*)

'Towards nanosecond digital data processing'
By P. M. THOMPSON (*Thompson Foss*)

SESSION 4—MEDICAL ELECTRONICS

Chairman: I. D. JEFFERIES (*Cossor Electronics*)

'Seeing inside the human body by computer'
By G. HOUNSFIELD (*EMI*)

'Aids for the handicapped—rehabilitation engineering'
By K. COPELAND (*University College London*)

'The 8-bit medicine man'
By Dr. G. H. BYFORD (*RAF Institute of Aviation Medicine*)

THE NINTH CLERK MAXWELL MEMORIAL LECTURE

to be given by Dr. H. B. G. CASIMIR (*Philips*)

Thursday, 1st July

SESSION 5—MICROELECTRONICS

Chairman: Prof. D. S. CAMPBELL (*University of Loughborough*)

'A new linear integrated circuit'
By C. S. DEN BRINKER (*Mackintosh Consultants Co.*)

'The present and future of microelectronics'
By W. HOLT (*Plessey*)

'LSI realization of digital filters for signal processing'
By Dr. G. P. EDWARDS (*Pye-TMC*)

SESSION 6—CONTROL AND AUTOMATION

Chairman: Brig. R. KNOWLES (*Institute of Quality Assurance*)

'An overview of control'
By Prof. D. R. TOWILL (*UWIST*)

'Aircraft landing systems'
By G. C. HOWELL (*Royal Aircraft Establishment, Bedford*)

'Automated design of control systems'
By P. ATKINSON (*University of Reading*)

'Future electronic control and communications in guided land transport systems'
By M. S. BIRKIN (*British Rail*)

Convention Banquet

The programme of addresses and papers will be supported by an Exhibition. Residential accommodation has been arranged at King's College and several social events will take place there and elsewhere. Fuller details of the programme may be obtained from the Conference Department, IERE, 9 Bedford Square, London WC1B 3RG.

INSTITUTION OF ELECTRONIC AND RADIO ENGINEERS

Applicants for Election and Transfer

THE MEMBERSHIP COMMITTEE at its meeting on 16th March 1976 recommended to the Council the election and transfer of the following candidates. In accordance with Bye-law 23, the Council has directed that the names of the following candidates shall be published under the grade of membership to which election or transfer is proposed by the Council. Any communication from Corporate Members concerning the proposed elections must be addressed by letter to the Secretary within twenty-eight days after publication of these details.

Meeting: 16th March 1976 (Membership Approval List No. 219)

GREAT BRITAIN AND IRELAND

CORPORATE MEMBERS

Transfer from Member to Fellow

LAUDER, Robert P. F. *Edinburgh.*

Transfer from Graduate to Member

BAILLIE, Paul Roger. *Maidstone, Kent.*
BERRY, Paul Morgan. *Bristol.*
ECKERT, Paul Michael. *Dereham, Norfolk.*
OBORNE, Kenneth Wyndham. *London.*

Direct Election to Member

CROSS, Anthony Robert. *London.*
DONNINGTON, Jerrold Howard. *Surbiton, Surrey.*
REES, Huw. *Lyneham, Wiltshire.*

NON-CORPORATE MEMBERS

Direct Election to Graduate

CLAY, Malcolm Nicholas. *Cowplain, Hampshire.*
HASSAN, Iahola Acmad K. *Bolton, Lancashire.*
SHOBBROOK, David Edmund. *London.*
STEWART, Andrew Alexander. *Chelmsford, Essex.*

Transfer from Graduate to Associate Member

GLOVER, Jeffrey Edward. *Shrewsbury, Salop.*

Direct Election to Associate Member

AGUH, Jude B. Anozie. *Battersea, London.*
DAVISON, John. *Middlesbrough, Cleveland.*
KIRKWOOD, William. *Busby, Glasgow.*
KONG, Sian Fua. *London.*
MARSH, Robert. *BFPO 26.*
REES, Gareth John. *HMS Ark Royal.*

Direct Election to Associate

FRASER, Thomas. *Leven, Fife, Scotland.*
KEMMETT, Edwin James. *Cheltenham, Gloucestershire.*

STUDENTS REGISTERED

BROOKER, Graham John. *St. Leonards-on-Sea, Sussex.*
FU, Hay Yau. *London.*
GOTHEL, Hitesh. *London.*
KALEJAIYE, Abayomi Adegboyega. *Middlesbrough, Cleveland.*
NICHOLS, Martin John. *Bristol.*
WONG, Tai. *London.*

OVERSEAS

CORPORATE MEMBERS

Transfer from Member to Fellow

COCKBAINE, David Robinson. *Istanbul, Turkey.*

Transfer from Graduate to Member

FADAHUNSI, Kehinde Ayoola. *Lagos, Nigeria.*

Direct Election to Member

AXISA, Grazio Francis. *Fgura, Malta.*
LAMDAN-LERNER, Tuvia. *Rehovot, Israel.*
LAWSON, Barrie Forster. *Santiago, Chile.*
NAYLOR, John Antony. *Hong Kong.*
SAYLE, Joseph. *Voorburg, Holland.*
STRASZEWICZ, Jacek Bohdan. *Warsaw, Poland.*

NON-CORPORATE MEMBERS

Direct Election to Graduate

CHAN, Hai-Ping. *Hong Kong.*
OKPOLI, Felix Uzor. *Benin, Nigeria.*

Direct Election to Associate Member

JOLLIFFE, Anthony, *Mbabane, Swaziland.*
CHAN, Kin Chung Stanley. *Hong Kong.*
WONG, Yeang Kiat. *Singapore.*

STUDENTS REGISTERED

AYODELE, Mojeed Adeniyi. *Ile-Ife, Nigeria.*
CHAN, Shui Lun. *Hong Kong.*
LAM, Chiew Kuen. *Singapore.*
TAN, Sing Hoon. *Singapore.*
TING, Kwai Meng. *Singapore.*
YEUNG, Hoi Wan. *Hong Kong.*
YUEN, Siu Nin. *Hong Kong.*

Addenda to Earlier Meetings

13th February 1975 (List No. 206)

OVERSEAS

CORPORATE MEMBERS

Transfer from Associate Member to Member

JUSTIN, John A. *San Diego, California.*

17th June 1975 (List No. 210)

OVERSEAS

CORPORATE MEMBERS

Transfer from Graduate to Member

FERREIRA, Ronald Charles A. *Paris.*

6th November 1975 (List No. 214)

GREAT BRITAIN AND IRELAND

NON-CORPORATE MEMBERS

Direct Election to Graduate

AKINHANMI, James Ayodeni. *London.*

FORTHCOMING INSTITUTION MEETINGS

London Meetings

Wednesday, 12th May

EDUCATION AND TRAINING GROUP

Colloquium on TRAINING OF ELECTRONICS ENGINEERS AND TECHNICIANS IN THE ARMED SERVICES

School of Electronic Engineering, Arborfield, Reading, 10.25 a.m.

Advance registration necessary. For further details and registration forms, apply to Meetings Secretary, IERE.

Thursday, 13th May

AUTOMATION AND CONTROL SYSTEMS GROUP

Computer Control Systems for Automatic Warehouses

By A. St. Johnston (*Vaughan Systems and Programming*).

IERE Lecture Room, 6 p.m.
(Tea 5.30 p.m.).

Tuesday, 18th May

AEROSPACE, MARITIME AND MILITARY SYSTEMS GROUP

Advances in Earth Station Technology and Satellite Communications

By R. I. Harris and D. Longhurst (*RSRE*)
IERE Lecture Room, 6 p.m.
(Tea 5.30 p.m.).

Wednesday, 19th May

MEASUREMENTS AND INSTRUMENTS GROUP

Colloquium on DYNAMIC ANALYSIS INSTRUMENTATION

IERE Lecture Room, 11 a.m.

Advance registration necessary. For further details and registration forms, apply to Meetings Secretary, IERE.

Wednesday, 26th May

COMPONENTS AND CIRCUITS GROUP

Colloquium on INDUSTRIAL CATHODE RAY TUBES

Cancelled.